arXiv:1209.2803v1 [hep-ph] 13 Sep 2012

The Spin Structure of the Nucleon

Christine A. Aidala*

Physics Department,
University of Michigan,
450 Church Street,
Ann Arbor, MI 48109-1040,
U.S.A.

Steven D. Bass†

Institute for Theoretical Physics,
University of Innsbruck,
Technikerstrasse 25,
A-6020 Innsbruck,
Austria

Delia Hasch‡

INFN-Frascati, via E. Fermi 40,
00044 Frascati (Rm),
Italy

Gerhard K. Mallot§

CERN, CH-1211 Genève 23,
Switzerland

(Dated: 24 August 2012)

This article reviews our present understanding of QCD spin physics: the proton spin puzzle and new developments aimed at understanding the transverse structure of the nucleon. We discuss present experimental investigations of the nucleon's internal spin structure, the theoretical interpretation of the different measurements and the open questions and challenges for future investigation.

CONTENTS

I. Introduction 2

II. Spin Structure Functions and Parton Distributions 3

III. Experiments 5
- A. SLAC experiments 6
- B. CERN experiments 6
  - 1. The EMC and SMC experiments 6
  - 2. The COMPASS experiment 7
- C. The HERMES experiment at DESY 8
- D. JLab experiments 9
- E. Hadronic scattering experiments 9
  - 1. The Relativistic Heavy Ion Collider 9
  - 2. RHIC as a polarized $p + p$ collider 10
  - 3. RHIC experiments 11

IV. The Proton Spin Puzzle 11
- A. Spin sum-rules 13
- B. Proton spin puzzles 14
- C. Spin and the singlet axial-charge 14

V. Quark and Gluon Polarization from Data 15
- A. Valence and sea polarization 15
- B. Gluon polarization 18
- C. NLO QCD motivated fits to spin data 20

VI. Theoretical Understanding 21

VII. Transverse Nucleon Structure and Orbital Angular Momentum 24
- A. Generalized parton distributions 25
  - 1. Deeply virtual Compton scattering 26
  - 2. The quest for orbital angular momentum and GPD parametrizations 28
- B. Transversity, transverse-momentum-dependent distributions and fragmentation functions 29
  - 1. The Sivers and Boer-Mulders TMD distributions 30
  - 2. The Collins TMD fragmentation function 32
  - 3. Probing transversity 33
  - 4. Current status and recent progress with TMD distributions 34
  - 5. Proton-proton asymmetries and TMD-factorization breaking 34

VIII. Future Projects 35

IX. Conclusions and Outlook 36

Acknowledgments 37

References 37

---

* caidala@bnl.gov
† Steven.Bass@uibk.ac.at
‡ Delia.Hasch@lnf.infn.it
§ Gerhard.Mallot@cern.ch

I. INTRODUCTION

There has been a vigorous and global program of experiments and theoretical developments in the last 25 years aimed at understanding the internal spin structure of the proton. How is the proton's spin built up from the spin and orbital angular momentum of the quarks and gluons inside? Tremendous progress has been made with unraveling the proton's spin structure with advances in experimental techniques, theoretical models, perturbative QCD, non-perturbative QCD and lattice calculations.

This activity was inspired by the initial European Muon Collaboration (EMC) data which suggested the puzzling result that quark intrinsic spin contributes little to the proton's spin (Ashman *et al.*, 1988). Today there is good convergence of the theoretical and experimental understanding the proton's longitudinal spin structure. Further puzzling data in measurements of transverse single-spin asymmetries revealed up to 40% asymmetries in proton-proton collisions (and 5–10% in lepton-nucleon collisions with unpolarized leptons and transversely polarized nucleons) which persist to high energies. These single-spin asymmetries indicate significant spin-orbit coupling in the nucleon associated with quark transverse momentum and the bound state structure of the nucleon. The study of transverse momentum and associated orbital angular-momentum processes has spawned new programs to map out the three-dimensional structure of the nucleon. In this article we review these developments highlighting the considerable and exciting developments in QCD spin physics in recent years, together with an outlook to the future: What are the main open questions and the planned experiments to help answer them?

In 1988 EMC published their polarized deep inelastic measurement of the proton's g_1 spin dependent structure function and the flavor-singlet axial-charge $g_A^{(0)}$ (the nucleon's "quark spin content") suggesting that quark spins summed over up, down and strange quark flavors contribute only a small fraction of the proton's spin. This result inspired considerable theoretical activity and new experiments at CERN, SLAC, DESY, Jefferson Laboratory (JLab) and the Relativistic Heavy Ion Collider (RHIC) at Brookhaven National Laboratory (BNL) to understand the spin structure of the nucleon. The first task was to check the initial curious result from EMC and second to resolve the spin-flavor structure of the proton. How is the spin content of the proton distributed among the valence and sea quarks and gluons? What about orbital angular momentum in the nucleon?

We now know that the nucleon's flavor-singlet axial-charge measured in polarized deep inelastic scattering is $g_A^{(0)} \sim 0.35$. This value was surprising from the viewpoint of early quark models. In the static quark model – the eightfold way picture of Gell-Mann – before inclusion of quark motion, quark spin contributes 100% of the proton's spin. Relativistic quark models without gluonic or pion cloud degrees of freedom generally predict about 60% of the proton's spin should be carried by the quarks, with the remaining 40% in quark orbital angular momentum. Today data and theory point to a consistent picture where the proton spin puzzle is a valence quark effect. Valence quark contributions to $g_A^{(0)}$ approximately saturate the measured value. While polarized glue may contribute a significant fraction of the proton's spin (perhaps up to 50% at the scale of present experiments), sea quark and QCD gluon corrections to the singlet axial-charge are small and within the expectations of quark models. The pion cloud of the nucleon acts to shift angular momentum from spin to orbital angular momentum and induces SU(3) breaking in the nucleon's axial-charges. There is also a fascinating theoretical possibility that the valence quarks may polarize the QCD vacuum in a nucleon through gluon topological effects so that some fraction of the proton's singlet axial-charge resides at zero parton momentum (or Bjorken x). Non-zero orbital angular momentum of the valence quarks is expected, induced also by confinement which introduces a transverse scale in the physics. This orbital angular momentum through spin-orbit coupling is a prime candidate to explain the large single spin asymmetries observed in proton-proton collisions. Information about quark total angular momentum in the proton can be extracted from deeply virtual Compton scattering and high-energy single spin asymmetry data in model-dependent analyses. The results are consistent with QCD lattice calculations.

This Review is organized as follows. In the first part (Sections II–III) we give a brief introduction to nucleon spin physics and the experiments that have been performed to investigate it. Then, in Section IV, we discuss the proton spin puzzle and the small value of $g_A^{(0)}$ extracted from polarized deep inelastic scattering. In Section V we give an overview of the present global program aimed at disentangling the spin-flavor structure of the proton. Section VI covers the theoretical interpretation of longitudinal spin data and understanding of the proton spin puzzle. We next turn our attention to the transverse structure of the nucleon and manifestations of orbital angular momentum in the nucleon in Section VII. This discussion introduces generalized parton distributions (GPDs), which describe hard exclusive reaction processes, and transverse momentum dependent distributions (TMDs), which describe spin-momentum correlations and spin-orbit couplings in the nucleon. The TMDs are manifest in high-energy single-spin and azimuthal asymmetries. A summary of key issues and challenging questions for the next generation of experiments is given in Section VIII and IX.

Earlier review articles on the spin structure of the proton as well as complementary more recent reviews, each with a different emphasis, are given in Anselmino *et al.* (1995), Ellis and Karliner (1995), Cheng (1996), Altarelli *et al.* (1998), Shore (1998), Lampe and Reya (2000), Filippone and Ji (2001), Jaffe (2001), Bass (2005), Kuhn *et al.* (2009), Barone *et al.* (2010a), Burkardt *et al.* (2010), Myhrer and Thomas (2010) and the monograph Bass (2007b).

II. SPIN STRUCTURE FUNCTIONS AND PARTON DISTRIBUTIONS

Our knowledge about the high-energy spin structure of the nucleon comes from both polarized deep inelastic scattering (DIS) experiments and high-energy polarized proton-proton collisions. Polarized deep inelastic scattering (pDIS) experiments involve scattering a longitudinally polarized high-energy lepton beam from a longitudinally or transversely polarized nucleon at large momentum transfer. Inclusive measurements, where only the scattered lepton is observed in the final state, and semi-inclusive measurements, where one tags on at least one high-energy final state hadron in coincidence with the scattered lepton, have been performed. The experiments were performed with an electron beam at SLAC and JLAB, with electron and positron beams at DESY and with muon beams at CERN. In proton-proton scattering the protons are either longitudinally or transversely polarized. Polarized deep inelastic scattering experiments have so far all been performed using a fixed target. A future polarized electron-ion collider is in planning. Details of the experiments are given in Section III. Historically, information about the proton's internal spin structure came first from measuring the proton's g_1 and g_2 spin structure functions in inclusive deep inelastic scattering and, more recently, from semi-inclusive reactions in both lepton-nucleon and proton-proton collisions and hard exclusive processes in lepton-nucleon scattering.

Measurements with longitudinally polarized targets and beams tell us about the helicity distributions of quarks and gluons in the nucleon, which at leading order can be thought of as the difference in probability of finding a parton with longitudinal polarization parallel or anti-parallel to that of the nucleon. Measurements with transversely polarized targets are particularly sensitive to quark and gluon transverse and orbital angular momentum. Studies of transverse degrees of freedom in the nucleon and in fragmentation processes are a current subject of experimental investigation with sensitivity to spin-orbit couplings in QCD.

For polarized lepton-proton scattering, specialize to the target rest frame and let E denote the energy of the incident lepton which is scattered through an angle θ to emerge in the final state with energy E'. Let $\uparrow\downarrow$ denote the longitudinal polarization of the lepton beam. In photon-nucleon scattering the spin dependent structure functions g_1 and g_2 are defined through the imaginary part of the forward Compton scattering amplitude. The structure functions contain all of the target-dependent information in the deep inelastic process. Consider the amplitude for forward scattering of a photon carrying momentum q_μ ($q^2 = -Q^2 \leq 0$) from a polarized nucleon with momentum p_μ, mass M and spin s_μ. We work with the kinematic Bjorken variable $x = Q^2/2p\cdot q = Q^2/2M\nu$ where $\nu = p\cdot q/M = E - E'$, and let $y = p\cdot q/p\cdot k = \nu/E$. For a longitudinally polarized proton target (with spin denoted $\Uparrow\Downarrow$) the unpolarized and polarized differential cross-sections are

$$\frac{d^2\sigma\uparrow\Downarrow}{dxdy}+\frac{d^2\sigma\uparrow\Uparrow}{dxdy}= \frac{2\pi\alpha^2}{MEx^2y^2}\left[\left(1-y-\frac{Mxy}{2E}\right)F_2(x,Q^2)+xy^2F_1(x,Q^2)\right] \tag{1}$$

and

$$\frac{d^2\sigma\uparrow\Downarrow}{dxdy}-\frac{d^2\sigma\uparrow\Uparrow}{dxdy}= \frac{4\alpha^2}{MExy}\left[\left(2-y-\frac{Mxy}{E}\right)g_1(x,Q^2)-\frac{2Mx}{E}g_2(x,Q^2)\right] \tag{2}$$

where the mass of the lepton is neglected. The relation between the structure functions in deep inelastic lepton-nucleon scattering and the virtual-photon nucleon cross-sections is discussed and derived in various textbooks, *e.g.* Roberts (1990). One finds

$$A_1 = \frac{\sigma_{\frac{1}{2}} - \sigma_{\frac{3}{2}}}{\sigma_{\frac{1}{2}} + \sigma_{\frac{3}{2}}} = \frac{g_1 - \frac{Q^2}{\nu^2}\, g_2}{F_1} \to \frac{g_1}{F_1} \tag{3}$$

where $\sigma_{\frac{3}{2}}$ and $\sigma_{\frac{1}{2}}$ are the cross-sections for the absorption of a transversely polarized photon with spin polarized parallel and anti-parallel to the spin of the longitudinally polarized nucleon. For a longitudinal polarized target the g_2 contribution to the differential cross-section and the longitudinal spin asymmetry is suppressed relative to the g_1 contribution by the kinematic factor $M/E \ll 1$. For a transverse polarized target this kinematic suppression factor for g_2 is missing implying that transverse polarization is vital to measure g_2. We refer to Roberts (1990) and Windmolders (2002) for the procedure how the spin dependent structure functions are extracted from the spin asymmetries measured in polarized deep inelastic scattering.

In high-Q^2 deep inelastic scattering the structure functions F_1, F_2, g_1 and g_2 exhibit approximate scaling. They are to a very good approximation independent of Q^2 and depend *only* on Bjorken x. (The small Q^2 dependence which is present in these structure functions is logarithmic and determined by perturbative QCD evolution.)

In the (pre-QCD) parton model the deep inelastic structure functions F_1 and F_2 are written as

$$F_1(x) = \frac{1}{2x} F_2(x) = \frac{1}{2} \sum_q e_q^2 \{q + \bar{q}\}(x) \tag{4}$$

and the polarized structure function g_1 is

$$g_1(x) = \frac{1}{2} \sum_q e_q^2 \Delta q(x). \tag{5}$$

Here e_q denotes the electric charge of the struck quark and

$$\begin{aligned} \{q + \bar{q}\}(x) &= (q^\uparrow + \bar{q}^\uparrow)(x) + (q^\downarrow + \bar{q}^\downarrow)(x) \\ \Delta q(x) &= (q^\uparrow + \bar{q}^\uparrow)(x) - (q^\downarrow + \bar{q}^\downarrow)(x) \end{aligned} \tag{6}$$

denote the spin-independent (unpolarized) and spin-dependent quark parton distributions which measure the distribution of quark momentum and spin in the proton. For example, $\bar{q}^\uparrow(x)$ is interpreted as the probability to find an anti-quark of flavor q with plus component of momentum xp_+ ($p_+ = p_0 + p_3$ is the plus component of the target proton's momentum) and spin polarized in the same direction as the spin of the target proton. When we integrate out the momentum fraction x the quantity $\Delta q = \int_0^1 dx\ \Delta q(x)$ is interpreted as the fraction of the proton's spin which is carried by quarks (and anti-quarks) of flavor q. Hence summing over the up, down and strange quark Δq contributions gives the total fraction of the proton's spin carried by the spins of these quarks.

What values should we expect for the Δq? First, consider the static quark model. The simple SU(6) proton wavefunction

$$\begin{aligned} |p \uparrow\rangle = &\frac{1}{\sqrt{2}} |u \uparrow (ud)_{S=0}\rangle + \frac{1}{\sqrt{18}} |u \uparrow (ud)_{S=1}\rangle \\ &- \frac{1}{3} |u \downarrow (ud)_{S=1}\rangle - \frac{1}{3} |d \uparrow (uu)_{S=1}\rangle \\ &+ \frac{\sqrt{2}}{3} |d \downarrow (uu)_{S=1}\rangle \end{aligned} \tag{7}$$

yields the values $\Delta u - \Delta d = \frac{5}{3}$ and $\Delta u + \Delta d = 1$. In relativistic quark models one has to take into account the four-component Dirac spinor $\psi \sim \begin{pmatrix} f \\ i\sigma \cdot \hat{r} g \end{pmatrix}$. The lower component of the Dirac spinor is p-wave with intrinsic spin primarily pointing in the opposite direction to the spin of the proton (Jaffe and Manohar, 1990). Relativistic effects renormalize the axial charges by the depolarization factor 0.65 with a net transfer of angular momentum from intrinsic spin to orbital angular momentum. In QCD and in more sophisticated models further depolarization is induced by gluonic and pion-cloud degrees of freedom – see Section VI.

In QCD the flavor-singlet combination of the $\Delta q(x)$ quark parton distributions mixes with the spin-dependent gluon distribution under Q^2 evolution (Altarelli and Parisi, 1977). This spin dependent gluon distribution measures the momentum and spin dependence of glue in the proton. The second spin structure function g_2 vanishes without the effect of quark transverse momentum and has a non-trivial parton interpretation (Jaffe, 1990; Roberts, 1990).

The parton model description of polarized deep inelastic scattering involves writing the deep inelastic structure functions as the sum over the convolution of "soft" quark and gluon parton distributions with "hard" photon-parton scattering coefficients

$$\begin{aligned} g_1^p(x) = &\left\{ \frac{1}{12}(\Delta u - \Delta d) + \frac{1}{36}(\Delta u + \Delta d - 2\Delta s) \right\} \otimes C_{ns}^q \\ &+ \frac{1}{9} \left\{ (\Delta u + \Delta d + \Delta s) \otimes C_s^q + f \Delta g(z, \mu^2) \otimes C^g \right\}. \end{aligned} \tag{8}$$

Here $\Delta q(x)$ and $\Delta g(x)$ denote the polarized quark and gluon parton distributions, C^q and C^g denote the corresponding hard-scattering coefficients, and f is the number of quark flavors liberated into the final state ($f = 3$ below the charm production threshold). The parton distributions contain all the target-dependent information and describe a flux of quark and gluon partons into the (target independent) interaction between the hard photon and the parton which is described by the coefficients C^q and C^g. These coefficients are calculated using perturbative QCD via the cross-section for the hard photon scattering from a quark or gluon parton "target". They are independent of infra-red mass singularities (terms involving the quark mass or virtuality of the parton in the photon-parton collision) which are absorbed into the parton distributions (and softened by confinement related physics). If the same recipe ("factorization scheme") for separating hard and soft parts of the parton phase space is applied consistently to all hard processes then the factorization theorem asserts that the parton distributions that one extracts from different experiments are process independent. In other words, the same polarized quark and gluon distributions should be obtained from experiments involving polarized hard QCD processes in polarized proton-proton collisions and polarized deep inelastic scattering experiments. For example, colliding longitudinally polarized proton beams provides sensitivity to the gluon-helicity distribution function at leading order. For hadron production with transverse momentum p_T, the helicity-dependent difference in hadron production is defined as

$$\frac{d\Delta\sigma}{dp_T} \equiv \frac{1}{2} \left[\frac{d\sigma^{++}}{dp_T} - \frac{d\sigma^{+-}}{dp_T} \right] \tag{9}$$

where the superscripts ++ and +− refer to same and opposite helicity combinations of the colliding protons. Factorization allows this to be written as a convolution of the long- and short-distance terms summed over all possible flavors for the partonic interaction $a+b \to jet + X$

$$\frac{d\Delta\sigma}{dp_T} = \sum_{ab} \int dx_a dx_b \Delta f_a(x_a,\mu) \Delta f_b(x_b,\mu) \times \frac{d\Delta\hat{\sigma}^{ab\to jet+X}}{dp_T}(x_a P_a, x_b P_b, \mu). \tag{10}$$

Here P_a and P_b denote the momenta of the incident protons; $f(x,\mu)$ are the polarized parton distributions of the colliding partons carrying light-cone momentum fraction x evaluated at factorization and renormalization scale μ. The helicity-dependent difference in the cross-section of the hard partonic scattering $a+b \to jet + X$ is denoted by $d\Delta\hat{\sigma}$ and is calculable in perturbative QCD. Partonic cross-section calculations are carried out to finite order in α_s and have a dependence on factorization and renormalization scales, denoted μ. The final hadronic cross-section is independent of the factorization and renormalization scales and the scheme used. The QCD parton model treatment readily generalizes to the production of high-energy hadrons in the final state, with the produced "fast" hadron carrying a significant fraction of the momentum of a "parent" parton. The parton-to-hadron process is parametrized by fragmentation functions which also obey process-independent factorization in perturbative QCD calculations.

Analogous to the helicity distributions measured with longitudinal polarization, transversity distributions describe the density of transversely polarized quarks inside a transversely polarized proton, see e.g. Barone *et al.* (2002). The transversity distributions, which were introduced in Ralston and Soper (1979), Artru and Mekhfi (1990) and Jaffe and Ji (1992), are interpreted in parton language as follows. Consider a nucleon moving with (infinite) momentum in the $\hat{e}_3$-direction, but polarized transverse to $\hat{e}_3$. Then $\delta q(x)$ (also denoted $\Delta_T q(x)$ and $h_1^q(x)$ in the literature) counts the quarks with flavor q, momentum fraction x and their spin parallel to the spin of a nucleon minus the number anti-parallel. That is, in analogy with Eq. (6), $\delta q(x)$ measures the distribution of partons with transverse polarization in a transversely polarized nucleon, *viz.*

$$\delta q(x) = q^{\uparrow}(x) + \bar{q}^{\uparrow}(x) - q^{\downarrow}(x) - \bar{q}^{\downarrow}(x). \tag{11}$$

In a helicity basis transversity corresponds to helicity-flip making it a probe of chiral symmetry breaking (Collins, 1993). There is no gluon analogue of transversity in the nucleon so δq evolves in Q^2 like a valence or non-singlet quark distribution, without mixing with glue. If quarks moved non-relativistically in the nucleon δq and Δq would be identical since rotations and Euclidean boosts commute and a series of boosts and rotations can convert a longitudinally polarized nucleon into a transversely polarized nucleon at infinite momentum. The difference between the transversity and helicity distributions reflects the relativistic character of quark motion in the nucleon.

Following the discovery that the quark spin contribution to the proton's spin is small, there has been a vigorous program to measure the separate contributions of up, down and strange quark flavors as well as the gluon spin and the orbital contributions. This has inspired dedicated spin programs in semi-inclusive deep inelastic scattering (SIDIS) and polarized proton-proton collisions to measure the separate valence and sea quark as well as gluon polarization. As efforts to investigate nucleon spin in more detail intensified and various experimental programs were being developed in the 1990s, new theoretical ideas arose as well. TMD distributions, describing spin-momentum correlations in the nucleon, were initially proposed (Sivers, 1990) to explain the very large transverse single spin asymmetries involved in polarized hadronic scattering that were first observed in the 1970s by Klem *et al.* (1976) and Dragoset *et al.* (1978). The GPDs introduced in Mueller *et al.* (1994), Ji (1997b) and Radyushkin (1997) to describe hard exclusive reactions provided for the first time a means of describing the radial position distributions of partons at a specific longitudinal momentum within the nucleon. Both TMD distributions and GPDs offer links to the orbital angular momentum contributions to the nucleon's spin. These processes and the present status of experimental and theoretical investigation are described in Section VII.

III. EXPERIMENTS

Experiments that have probed the nucleon spin structure are outlined in Table I. This includes both polarized deep inelastic lepton-nucleon scattering and proton-proton collision experiments. Considerable effort was invested in developing polarized beam and target technology, yielding physics results with ever increasing precision. The first experiments focused on inclusive deep inelastic measurements of nucleon spin structure. More recent experiments, described in detail below, were able to detect and identify hadrons in the final state leading to new probes of the nucleon in semi-inclusive and hard exclusive reactions. Future experimental programs (COMPASS-II, the 12 GeV upgrade of JLab and experiments at Fermilab and RHIC) with high luminosity and acceptance are planned to explore the three-dimensional structure of the nucleon in spatial and transverse momentum degrees of freedom. We discuss these future programs in Section VIII.

TABLE I High energy spin experiments: the kinematic ranges in x and Q^2 correspond to the average kinematic values of the highest statistics measurement of each experiment, which is typically the inclusive spin asymmetry; x denotes Bjorken x unless specified.

Experiment	Year	Beam	Target	Energy (GeV)	Q^2 (GeV^2)	x
Completed experiments						
SLAC – E80, E130	1976–1983	e^-	H-butanol	$\lesssim$23	1–10	0.1–0.6
SLAC – E142/3	1992–1993	e^-	NH_3, ND_3	$\lesssim$ 30	1–10	0.03–0.8
SLAC – E154/5	1995–1999	e^-	NH_3, ^{6}LiD, ^{3}He	$\lesssim$ 50	1–35	0.01–0.8
CERN – EMC	1985	μ^+	NH_3	100, 190	1–30	0.01–0.5
CERN – SMC	1992–1996	μ^+	H/D-butanol, NH_3	100, 190	1–60	0.004–0.5
FNAL E581/E704	1988–1997	p	p	200	$\sim$ 1	$0.1 < x_F < 0.8$
Analyzing and/or Running						
DESY – HERMES	1995–2007	e^+, e^-	H, D, ^{3}He	$\sim$ 30	1–15	0.02–0.7
CERN – COMPASS	2002–2012	μ^+	NH_3, ^{6}LiD	160, 200	1–70	0.003–0.6
JLab6 – Hall A	1999–2012	e^-	^{3}He	$\lesssim$ 6	1–2.5	0.1–0.6
JLab6 – Hall B	1999–2012	e^-	NH_3, ND_3	$\lesssim$ 6	1.-5	0.05–0.6
RHIC – BRAHMS	2002–2006	p	p (beam)	2× (31–100)	$\sim$ 1–6	$-0.6 < x_F < 0.6$
RHIC – PHENIX, STAR	2002+	p	p (beam)	2× (31–250)	$\sim$ 1–400	$\sim$ 0.02–0.4
Approved future experiments (in preparation)						
CERN – COMPASS–II	2014+	μ^+, μ^-	unpolarized H_2	160	$\sim$ 1–15	$\sim$ 0.005–0.2
		π^-	NH_3	190		$-0.2 < x_F < 0.8$
JLab12 – HallA/B/C	2014+	e^-	HD, NH_3, ND_3, ^{3}He	$\lesssim$12	$\sim$ 1–10	$\sim$ 0.05–0.8

A. SLAC experiments

SLAC experiments pioneered polarized DIS measurements and set many standards in polarized beam and target technologies. Their spin program focused on high statistics measurements of the inclusive asymmetries. The first measurements of the proton spin structure were performed by the experiments E80 (Alguard *et al.*, 1976, 1978) and E130 (Baum *et al.*, 1980, 1983), followed by a series of high precision experiments E142 (Anthony *et al.*, 1996), E143 (Abe *et al.*, 1998), E154 (Abe *et al.*, 1997) and E155 (Anthony *et al.*, 1999, 2000) a decade later. These experiments utilized polarized electrons which were produced by laser photoemission and subsequently accelerated. The longitudinal polarization of the beam was frequently inverted and the polarization measured using Møller scattering. A rapid cycling of the beam and/or target polarization reduces systematic uncertainties in the measured spin asymmetries related to the stability of the experimental setup. Polarized target materials involved solid-state butanol and ammonia (NH_3) for the proton and D-butanol, ND_3 as well as ^{6}LiD for the deuteron. The target material, doped with a paramagnetic substance or irradiated with electron beams, was polarized using dynamic nuclear polarization, which requires temperatures of about 1 K and strong magnetic holding fields. Such targets contain a considerable amount of non-polarizable nucleons, which is parametrized by the so-called dilution factor. This factor depends on all kinematic variables relevant for the process under study and needs, in principle, to be determined for each type of measurement. Typical values for polarized solid state targets range between 0.1 and 0.2 with the exception of ^{6}LiD (0.4-0.5) and represent an important factor in the extraction of physical observables from the measured ones. Information on the neutron structure was obtained either from the combination of measurements with proton and deuteron targets or by using a polarized ^{3}He target which is dominated by the neutron since the two proton spins in ^{3}He are anti-aligned. Here, polarization was obtained from optical pumping and adiabatic spin exchange. The target polarization was measured using the NMR technique. Scattered electrons were detected with magnetic spectrometers optimized for high-momentum-resolution and good electron identification.

B. CERN experiments

1. The EMC and SMC experiments

Following the early measurements at SLAC, the European Muon Collaboration (EMC) experiment performed at CERN in 1985 the first polarized DIS measurements at $x < 0.1$ down to $x = 0.01$ after a series of measurements of unpolarized nucleon and nuclear structure functions. The experiment used the polarized CERN muon beam up to momenta of 200 GeV and a solid-state irradiated ammonia target. Their low-x measurements, accessible due to the high energy of the muons, suggested the breakdown of the naive parton picture that quarks provide essentially all of the spin of the nucleon (Ashman *et al.*, 1988, 1989).

This triggered more detailed and precise measurements by the Spin Muon Collaboration (SMC) in 1992–1996, and by COMPASS (since 2002). The beam line and the principal ideas of the CERN muon experiments are described in the COMPASS Section III.B.2.

After 1987 the focus was on the region $x < 0.1$ and the flavor-singlet axial-charge (Ellis–Jaffe sum-rule) for the neutron. The latter must deviate from the naive prediction in a similar way as for the proton in order to preserve the fundamental isovector Bjorken sum-rule for $g_1^p - g_1^n$. (These sum-rules are discussed below.) The SMC experiment could extend the measured x-range down to $x = 0.004$ (for $Q^2 > 1$ GeV^2) and established the validity of the Bjorken sum-rule with measurements using polarized proton (butanol and ammonia) and deuteron (D-butanol) targets (Adeva *et al.*, 1993, 1998b). The large acceptance of the SMC spectrometer in the forward direction allowed them to present the first determination of individual quark distributions for different flavors (Adeva *et al.*, 1996, 1998a) from semi-inclusive DIS. A dedicated polarimeter confirmed the validity of the beam polarization obtained from Monte Carlo simulations (Adams *et al.*, 2000; Adeva *et al.*, 1994) used in the EMC, SMC and COMPASS analyses.

2. The COMPASS experiment

The COMPASS spectrometer (Abbon *et al.*, 2007) is installed at the muon beam line of the CERN SPS accelerator. A polarized muon beam of energy 160–200 GeV and with a polarization of about 80% impinges on a solid-state polarized target consisting of two or three cells with proton or deuteron target material polarized in opposite directions. The usable beam intensity is typically 2×10^7/s during a 9.6 s long spill. The repetition rate varies and is typically about 1/40 s. The muon polarization arises naturally from the weak decay of the parent pions produced by the primary proton beam of 400 GeV. The momentum of each beam muon is measured in the beam momentum station. Downstream of the target, the scattered muon and produced hadrons are detected in a two-stage magnetic spectrometer with the two dipole magnets.

Charged particles are tracked in the beam regions by scintillating fiber stations and by silicon detectors. In the inner region close to the beam, gaseous detectors of the micromegas and gas-electron-multiplier (GEM) types with high rate capabilities are deployed. The backbone of tracking in the intermediate region is multiwire proportional chambers (MWPCs). Finally, the large area tracking away from the beam region is covered by drift chambers and drift tubes.

The velocity of charged particles is measured in a ring-imaging Cherenkov detector (RICH), which can separate pions and kaons from 9 GeV up to 50 GeV. The inner quarter of the photon detector is made of multianode-photomultiplier tubes, while the outer part relies on MWPCs with a photosensitive CsI cathode.

The energy of charged particles is measured in sampling hadron calorimeters, while neutral particles, in particular high-energy photons, are detected in electromagnetic calorimeters. They comprise lead glass modules as well as scintillator/lead "shashlik" modules in the inner high-radiation region.

Event recording is triggered by the scattered muon, which is "identified" by its ability to traverse thick hadron absorbers, located just upstream of the Muon Wall detectors. The event selection is based on various systems of scintillator hodoscopes and logic modules applying selection criteria like target pointing and energy loss in the scattering. The patterns causing a trigger were optimized by Monte Carlo simulations. The spectrometer has about 250k read-out channels, which can be recorded with a frequency of 20 kHz for an event size of the order of 40 kByte.

The heart of the experiment is the polarized target system. While the muon beam comes naturally polarized due to the parity violation in the decay of the parent pions, polarizing protons and deuterons is very difficult. Gas targets can not be used with the muon beam due to the low beam intensity compared to electron beams. An advantage of muon beams is the high muon energy, which presently can not be reached by electron beams. The polarized target system comprises a 2.5 T solenoid magnet, a 0.6 T dipole magnet, a ^{3}He/^{4}He dilution refrigerator, a 70 GHz microwave system and an NMR system to measure the target polarization. The target material is cooled down to about 60 mK in frozen spin mode. The nucleons/nuclei are polarized by dynamic nuclear polarization which only is applicable for particular materials. In COMPASS irradiated ammonia (NH_3) and lithium-6 deuteride (^{6}LiD) were selected as proton and deuteron targets, respectively. Lithium-6 is very close to a system of a free deuteron and a helium-4 core and has essentially the same magnetic moment as the deuteron. Thus ^{6}LiD corresponds to two deuterons plus a helium nucleus. Typically, polarizations of 85% for protons and 50% for deuterons were reached. A key feature of COMPASS is that both target polarizations are present simultaneously in separate target cells along the beam, e.g. "$\rightarrow, \leftarrow$" for the two-cell configuration until 2004 and "$\rightarrow, \leftarrow, \rightarrow$" for the three-cell configuration from 2006 onward. In the former configuration the length of the cells was twice

60 cm while in the latter it was 30 cm, 60 cm, 30 cm, respectively. Thus in an asymmetry measurement most systematic uncertainties cancel. Using the dipole and solenoid magnet, the magnetic field can be rotated from *e.g.* pointing downstream to transverse to upstream. The spin follows the magnetic field adiabatically and thus the spin orientations can be changed within 30 min. Such a field rotation is performed typically once per day for the longitudinal polarization in order to cancel potentially remaining systematic effects. The field can also be kept transverse for measurements with transverse target polarization. Here the polarization is inverted by repolarizing typically once per week. In the shutdown year 2005 the superconducting target magnet was replaced by a new one, increasing the angular acceptance from ±70 mrad to ±180 mrad.

The experiment is taking data since 2002. The years 2008–2009 were dedicated to the hadron spectroscopy program of COMPASS with pion, kaon and proton beams. In 2012 the pion polarizability will be measured using a negative pion beam and a thin nickel target. A pilot run for deeply virtual Compton scattering and hard exclusive meson production is also planned for 2012.

C. The HERMES experiment at DESY

The HERMES experiment employed an innovative technique for the polarized target, which is very different from all other polarized DIS experiments. Gas targets of pure nuclear-polarized atoms of hydrogen or deuterium were used, which permit essentially background-free measurements from highly polarized nucleons with little or no dilution of the signal from unpolarized nucleons in the target. This choice eliminates one of the main systematic sources in polarized DIS, the uncertainty in the determination of the dilution factor.

The HERMES gas targets were highly longitudinally ($\sim 85\%$) or transversely (75%) polarized with the ability to invert the direction of the spin of the nucleons within milliseconds. Due to the low densities, however, such targets are only practicable in the high currents of storage rings. HERMES was operating from 1995 to 2007 at the HERA lepton storage ring, which provided electron or positron beams of typically 40 mA and with an energy of 27.5 GeV. In order to enhance the target density, the novel technique of a storage cell was used. Here, the gas was fed into a T-shaped open-ended elliptical cell coaxial to the lepton beam. The gas atoms underwent several hundred wall bounces before escaping from the ends where they were differentially pumped away by a large system of turbo-pumps. This increased the density by a factor of about 100 compared to free gas jet targets.

The polarized atoms were injected into the cell from an atomic beam source based on Stern-Gerlach polarization filtering and radio-frequency transitions between atomic substates in a magnetic field (Airapetian *et al.*, 2005c). A small sample gas diffused from the middle of the cell into a Breit-Rabi polarimeter which measured the atomic polarization, or into a target gas analyzer which measured the atomic and the molecular content of the sample. A magnet surrounding the storage cell provided a holding field defining the polarization axis and prevented spin relaxation via spin exchange or wall collisions. The cell temperature was kept at about 100 K, the value for which atomic recombination and spin relaxation during wall collisions are minimal.

Stored high energy electron beams may become spontaneously transversely polarized via a small polarization asymmetry in the emission of synchrotron radiation by the beam particles as they are deflected by the magnetic fields of the ring (Sokolov-Ternov effect) (Sokolov and Ternov, 1964). The beam polarization grows and approaches asymptotically an equilibrium value with a time constant depending on the characteristics of the ring, for HERA typically 1/2 hour. Polarizations as large as 60% were achieved. Spin rotators and polarimeters were essential components of the HERA lepton beam (Barber *et al.*, 1994, 1993; Beckmann *et al.*, 2002; Buon and Steffen, 1986). Spin rotators in front of and behind the experiment provided longitudinal polarization at the interaction point and at one of the two beam polarimeters. The two beam polarimeters were based on Compton back-scattering of circularly polarized laser light. They continuously monitored the transverse and longitudinal polarization of the lepton beam.

The HERMES spectrometer was designed to detect the scattered lepton and produced hadrons within a wide angular acceptance and with good momentum resolution. Particular emphasis was given to the particle identification capabilities which allowed for pion, kaon and proton separation over almost the whole momentum range. The HERA beam lines passed through the non-instrumented horizontal mid-plane of the spectrometer. A horizontal iron plate shielded the beam lines from the 1.5 Tm dipole field of the spectrometer magnet, thus dividing the spectrometer in two identical halves. The geometrical acceptance of ±170 mrad horizontally and $\pm(40-140)$ mrad vertically resulted in detected scattering angles ranging from 40 to 220 mrad. Tracking was provided by several stages of drift chambers before and after the spectrometer magnet. The combination of signals from a lead-glass calorimeter, a preshower detector, a transition radiation detector and a ring-imaging Cherenkov provided lepton identification with very high efficiency and purity better than 99% as well as pion, kaon and proton separation over almost the whole momentum range of 2–15 GeV. All components are described in detail in Ackerstaff *et al.* (1999a).

A recoil detector was installed in the target region for the last 1.5 years of HERMES data taking with unpolarized hydrogen and deuterium targets in order to enhance access to hard exclusive processes, in particular to deeply virtual Compton scattering.

D. JLab experiments

Experiments at Jefferson Lab utilized the highest polarization electron beams (85%) with energy ranging from 0.8 GeV close to 6 GeV. The technologies of polarizing beam and target follow those pioneered and further developed at SLAC.

The beam was provided by the Continuous Electron Beam Accelerator Facility (CEBAF), which used polarized electron guns based on a "superlattice" of a thin gallium arsenide (GaAs) layer on top of GaAs-phosphide bulk matter illuminated by circularly polarized photons from high intensity lasers. Subsequently, the polarized electrons passed up to five times the two linear accelerators based on superconducting radio frequency technology and connected by two recirculation arcs. The spin direction of the electrons was manipulated using the crossed electric and magnetic fields of Wien filters, which allow for rapid spin rotation. Their direction was inverted every about 30 ms. Beam polarimetry was employed at several stages of the acceleration process. CEBAF delivered polarized beams simultaneously to the three experimental halls (Hall A, B and C) with the option to independently dial the energy and intensity. Typical beam intensities ranged from a few nA in Hall B to over 100 μA in the other two halls.

Longitudinal polarized solid state ammonia (NH_3) targets for the proton and ND_3 for the deuteron were employed at Hall B. These targets are based on similar techniques as discussed before for the SLAC and CERN experiments for both polarization and polarimetry. Hall A used a polarized ^{3}He target. The target polarization was measured by both the NMR technique of adiabatic fast passage and a technique based on electron paramagnetic resonance (Romalis *et al.*, 1998). Average target polarizations of about 55% were obtained.

Hall A and C were both instrumented with small acceptance but high resolution spectrometers that could cope with the highest beam intensities but measured at fixed scattering angles. These spectrometers are equipped for high resolution tracking, precise time-of-flight measurements and lepton/hadron separation (Alcorn *et al.*, 2004).

Hall B was instrumented with the CEBAF Large Acceptance Spectrometer (CLAS) (Mecking *et al.*, 2003). The CLAS design was based on a toroidal field, generated by six superconducting coils arranged around the beam line. The six coils naturally divided the detector into six independent spectrometers, each of them containing a set of drift chambers for tracking, a gas Cerenkov counter for electron/pion separation, an array of scintillator counters for particle identification using time of flight measurements, and electromagnetic calorimeters for neutral particle identification. For charged particles, CLAS covered polar angles between 8° and 142° in the laboratory frame and between 60% and 80% of the azimuthal angles.

E. Hadronic scattering experiments

While deep-inelastic lepton-nucleon scattering has long been a standard tool of the trade in the study of unpolarized and polarized nucleon structure, much has been learned from polarized hadronic scattering as well. The first high-energy primary polarized proton beams were achieved at the Zero-Gradient Synchrotron at Argonne National Laboratory in 1973. Proton beams there were initially accelerated to 6 GeV with a polarization of about 60%, and shortly thereafter polarized beams up to 12 GeV were achieved. In the 1990s at Fermilab, secondary beams of polarized protons or antiprotons from lambda or antilambda decays opened up new kinematic regions for polarized hadronic scattering, with polarized beams of up to 200 GeV ($\sqrt{s} = 19$ GeV). Polarized hadronic scattering experiments at center-of-mass energies more than an order of magnitude higher were achieved with the inauguration of the Relativistic Heavy Ion Collider for polarized protons in 2001.

1. The Relativistic Heavy Ion Collider

RHIC is located at Brookhaven National Laboratory in New York. RHIC was built to collide heavy ions at center-of-mass energies of up to 200 GeV per colliding nucleon pair and polarized protons at center-of-mass energies ranging from 50 to 500 GeV. Collision of asymmetric species, *i.e.* different species in the two beams, is also possible due to independent rings with independent steering magnets. The first polarized proton collisions were achieved at a center-of-mass energy of 200 GeV in December 2001.

The RHIC storage ring is 3.83 km in circumference and is designed with six interaction points (IPs) at which beam collisions are possible. Up to 112 particle bunches per ring can be injected, in which case the time between bunch crossings at the IPs is 106 ns. Polarizations of up to 65% for 100 GeV proton beams and about 60% for 255 GeV beams have been achieved. The maximum luminosities achieved thus far are 5×10^{31} cm^{-2} s^{-1} at $\sqrt{s} = 200$ GeV and 2×10^{32} cm^{-2} s^{-1} at $\sqrt{s} = 510$ GeV.

Three experiments have studied polarized proton collisions at RHIC. There are two ongoing large experiments, STAR (Ackermann *et al.*, 2003) and PHENIX (Adcox *et al.*, 2003), each of which have more than 500 collaborators total working on both the heavy ion and polarized proton programs, and the smaller BRAHMS (Adamczyk *et al.*, 2003) experiment, with fewer than 100 collaborators, which took data through 2006. In additional to the program of proton spin structure measurements, the transverse single-spin asymmetry in elastic proton-proton scattering has also been measured to constrain the hadronic spin-flip amplitude in this reaction (Adamczyk *et al.*, 2012b).

2. RHIC as a polarized $p + p$ collider

RHIC is the first and only high-energy polarized proton-proton collider in the world. A number of technological developments and advances over the past several decades have made it possible to create a high-current polarized proton source, maintain the beam polarization throughout acceleration and storage, and obtain accurate measurements of the degree of beam polarization at various stages from the source to full-energy beams in RHIC. For an overview of RHIC as a polarized-proton collider see Alekseev *et al.* (2003). In the case of polarized-proton running at RHIC, a pulse of polarized H^- ions from the source is accelerated to 200 MeV in the linac, then stripped of its electrons as it is injected and captured as a single bunch of polarized protons in the Booster, which accelerates the protons to 1.5 GeV. The bunch of polarized protons is then transferred to the Alternating Gradient Synchrotron (AGS) and accelerated to 24 GeV before injection into RHIC. Each bunch is accelerated in the AGS and injected into RHIC independently, with the two RHIC rings being filled one bunch at a time. The direction of the spin vector is selected for each bunch separately. The nominal fill duration is eight hours, after which the beams are dumped and fresh beams are injected into RHIC. The bunch-by-bunch spin patterns in consecutive fills are varied in order to reduce potential systematic effects.

Polarized proton injection uses an optically-pumped polarized H^- ion source (OPPIS) (Zelenski *et al.*, 2002). H^- polarization at the source of 85% has been achieved. There are two principal types of depolarizing resonances that may be encountered during acceleration, imperfection and intrinsic resonances. Imperfection resonances refer to those due to errors in magnet currents or alignments; intrinsic resonances are due to the (desired) beam focusing fields. A depolarizing resonance is encountered whenever the spin precession frequency is equal to the frequency with which a depolarizing field is crossed, leading to additive depolarization effects.

Siberian snakes (Derbenev *et al.*, 1978), a series of spin-rotating dipoles, so named because of the beam trajectory through the magnets and the fact that they were developed at Novosibirsk in Russia, are used to overcome both imperfection and intrinsic resonances in RHIC. There are two snakes installed in each RHIC ring at diametrically opposite points along the rings. The two snakes in each ring rotate the spin vector 180° about perpendicular horizontal axes, without perturbing the stable spin direction and with only local distortion of the beam orbit. In this way, all additive depolarizing effects from resonances are avoided.

For RHIC to provide full-energy polarized beams, the polarization must be measurable at various stages of acceleration in order to identify and address possible origins of depolarization at each step. Only RHIC polarimetry will be discussed here. There are two types of polarimeters installed in RHIC. The proton-carbon (pC) polarimeter takes advantage of a known analyzing power, $A_N^{p\mathrm{C}} \approx 0.01$, in the elastic scattering of polarized protons with carbon atoms ($p^\uparrow + \mathrm{C} \to p^\uparrow + \mathrm{C}$) in order to measure the beam polarization (Nakagawa *et al.*, 2008). This analyzing power originates from interference between electromagnetic and hadronic elastic scattering amplitudes, which are finite due to the anomalous magnetic moment of the proton. Calibration of the pC polarimeter to within an absolute beam polarization of less than 5% can be provided by a polarized hydrogen-jet-target polarimeter (Zelenski *et al.*, 2005). The technique is similar to that of the pC polarimeter in that the left-right transverse single spin asymmetry of elastically scattered protons due to the CNI process is measured. However, the analyzing power for this process of elastic proton-proton scattering at a given energy does not need to be known. Instead, the hydrogen-jet-target polarization, greater than 90%, is known to better than 2% in absolute polarization (Okada *et al.*, 2006). The beam polarization can be obtained by measuring first the asymmetry due to the polarized target, averaging over the spin states of the beam, and then similarly measuring the asymmetry due to the polarized beam, averaging over spin states of the target, which are varied in time. The same (unknown) analyzing power, A_N, applies to both cases, allowing the beam polarization to be calculated. Low rates for this process mean that measurements performed over a long time are necessary. Because of this, the pC polarimeter, which can make measurements in less than ten seconds and provide immediate information on the stability or decay of the beam polarization from a few data points taken over the several hours of a fill, is essential. Results obtained from the two different polarimeters can later be compared in order to calibrate the pC polarimeter at any beam energy.

The naturally stable spin direction through acceleration and storage in RHIC is transverse to the proton's momentum, in the vertical direction. Spin rotator dipole magnets have been used to achieve both radial and longitudinal spin (MacKay *et al.*, 2003). The spin vector is rotated away from vertical immediately before the collision point and then back to vertical immediately afterwards. The rotators are located outside the interaction regions of the PHENIX and STAR experiments, giving both experiments the ability to choose independently whether they want longitudinally or transversely polarized collisions.

The BRAHMS experiment, having no spin rotators available, focused on transverse spin measurements. The local nature of the spin rotator magnets means that the STAR and PHENIX experiments must each have their own way of checking the direction of the spin vector at their respective interaction regions.

Observed azimuthal transverse single spin asymmetries in the production of forward neutrons (Bazilevsky *et al.*, 2003) and forward charged particles can be used to provide local polarimetry. These asymmetries are exploited by PHENIX and STAR to measure the degree to which the beam polarization is vertically transverse, radially transverse, or longitudinal. Maxima and minima of particle production are expected at right angles in ϕ to the spin vector. For longitudinal polarization, no azimuthal asymmetry is expected; a non-zero longitudinal single spin asymmetry would violate parity and is forbidden in particle production via strong and electromagnetic processes. More information on local polarimetry at PHENIX and STAR can be found in Adare *et al.* (2007) and Kiryluk (2005).

3. RHIC experiments

a. The PHENIX detector PHENIX was designed as a large, multi-purpose experiment with fast data acquisition and high granularity over a limited acceptance. There are two central arms with an acceptance covering a pseudorapidity range $|\eta| < 0.35$ and $\Delta\phi = \frac{\pi}{2}$ each in azimuth. The central arms include drift and pad chambers for momentum and position measurements, a ring-imaging Cherenkov detector primarily for electron identification, small-acceptance time-of-flight and aerogel counters for charged hadron identification, and electromagnetic calorimetry. Electronics-level triggering in the central arms uses information from the calorimetry and ring-imaging Cherenkov detector. There are two muon spectrometers covering a pseudorapidity of $1.2 < |\eta| < 2.4$, consisting of tracking chambers and muon identifier panels. Resistive plate chambers were added in 2011 and 2012 to improve triggering on high-momentum muons for W boson measurements. Forward electromagnetic calorimetry covering $3.0 < |\eta| < 3.9$ was added in 2006 and 2007, and silicon vertex detectors for heavy flavor measurements over $|\eta| < 2.4$ were added in 2011 and 2012.

For luminosity measurements, identical zero-degree hadronic calorimeters (ZDCs) are located in the RHIC tunnel at ±18 m from the nominal IP for all RHIC experiments. PHENIX also uses quartz Cherenkov beam-beam counters positioned around the beam pipe at ±1.44 m from the nominal interaction point as a minimum-bias trigger detector and for polarization-averaged as well as spin-dependent luminosity measurements. Collision rates for 500 GeV $p + p$ running reach $\sim$3 MHz, and the electronics-level triggers select events to reduce this rate to approximately 7 kHz of recorded data.

b. The STAR detector The Solenoidal Tracker at RHIC (STAR) was designed as a large, multi-purpose detector with wide acceptance, making it well suited for correlation measurements. The core of STAR is a time-projection chamber, which covers 2π in azimuth and has tracking capabilities over $|\eta| < 1.3$ and good particle identification for $|\eta| < 1$. There is electromagnetic calorimetry for $-1 < \eta < 2$. In the forward direction, there is additional electromagnetic calorimetry for $2.5 < \eta < 4.0$. Recent upgrades include a time-of-flight detector with 100 ps resolution for additional particle identification, and tracking based on GEM detectors for $1 < \eta < 2$ was partially installed for 2012 data-taking to enable charge-sign discrimination of forward electrons from W boson decays.

In addition to the zero-degree hadronic calorimeters identical among the RHIC experiments, STAR has scintillator beam-beam counters positioned around the beam pipe covering $3.4 < |\eta| < 5.0$, which provide a minimum-bias trigger as well as spin-averaged and spin-dependent luminosity measurements along with the ZDCs.

c. The BRAHMS detector The BRAHMS detector was a smaller experiment at RHIC designed for excellent momentum measurement and charged particle identification over a very broad range of rapidities. It consisted of two movable spectrometer arms covering small solid angles, the Forward Spectrometer, which could be positioned as close as 2.3° from the beam pipe, and the Midrapidity Spectrometer, which could be moved to cover an angular range from $30^\circ < \theta < 95^\circ$. The spectrometer arms included five dipole magnets, time-projection chambers, multi-wire drift chambers, time-of-flight hodoscopes, and threshold as well as ring-imaging Cherenkov detectors. Global detectors consisted of a silicon array for multiplicity measurements, threshold Cherenkov beam-beam counters for event vertex and timing determination as well as luminosity measurements, and ZDCs identical to those used by PHENIX and STAR.

IV. THE PROTON SPIN PUZZLE

We begin our discussion of physics results by first describing how the small value of the “quark spin content” $g_A^{(0)}$ is obtained from polarized deep inelastic scattering and the first moment of the g_1 spin structure function.

In QCD the first moment of g_1 is determined from the dispersion relation for polarized photon-nucleon scattering and the light-cone operator product expansion. One finds that the first moment of g_1 is related to the scale-invariant axial charges of the target nucleon by

$$\begin{aligned}&\int_0^1 dx\; g_1^p(x,Q^2) \\ &= \left(\frac{1}{12}g_A^{(3)} + \frac{1}{36}g_A^{(8)}\right)\Bigl\{1+\sum_{\ell\geq 1} c_{\mathrm{NS}\ell}\,\alpha_s^\ell(Q)\Bigr\} \\ &+\frac{1}{9}g_A^{(0)}|_{\mathrm{inv}}\Bigl\{1+\sum_{\ell\geq 1} c_{\mathrm{S}\ell}\,\alpha_s^\ell(Q)\Bigr\} + \mathcal{O}(\frac{1}{Q^2}) + \ \beta_\infty .\end{aligned} \tag{12}$$

Here $g_A^{(3)}$, $g_A^{(8)}$ and $g_A^{(0)}|_{\mathrm{inv}}$ are the isovector, SU(3) octet and scale-invariant flavor-singlet axial-charges respectively. The flavor non-singlet $c_{\mathrm{NS}\ell}$ and singlet $c_{\mathrm{S}\ell}$ Wilson coefficients are calculable in ℓ-loop perturbative QCD. These perturbative QCD coefficients have been calculated to $O(\alpha_s^3)$ precision (Larin *et al.*, 1997). For $\alpha_s = 0.3$ typical of the deep inelastic experiments one finds $\Bigl\{1 + \sum_{\ell=1}^3 c_{\mathrm{NS}\ell}\,\alpha_s^\ell(Q)\Bigr\} = 0.85$ and $\Bigl\{1 + \sum_{\ell=1}^3 c_{\mathrm{S}\ell}\,\alpha_s^\ell(Q)\Bigr\} = 0.96$. The term β_∞ represents a possible leading-twist subtraction constant from the circle at infinity when one closes the contour in the complex plane in the dispersion relation (Bass, 2005). The subtraction constant affects just the first moment and corresponds to a contribution at Bjorken x equal to zero.

In terms of the flavor-dependent axial-charges

$$2Ms_\mu \Delta q = \langle p,s|\overline{q}\gamma_\mu\gamma_5 q|p,s\rangle \tag{13}$$

the isovector, octet and singlet axial charges are

$$\begin{aligned} g_A^{(3)} &= \Delta u - \Delta d \\ g_A^{(8)} &= \Delta u + \Delta d - 2\Delta s \\ g_A^{(0)}|_{\mathrm{inv}}/E(\alpha_s) \equiv g_A^{(0)} &= \Delta u + \Delta d + \Delta s. \end{aligned} \tag{14}$$

Here

$$E(\alpha_s) = \exp \int_0^{\alpha_s} d\tilde{\alpha}_s\, \gamma(\tilde{\alpha}_s)/\beta(\tilde{\alpha}_s) \tag{15}$$

is a renormalization group factor which corrects for the (two loop) non-zero anomalous dimension $\gamma(\alpha_s)$ of the singlet axial-vector current

$$J_{\mu 5} = \bar{u}\gamma_\mu\gamma_5 u + \bar{d}\gamma_\mu\gamma_5 d + \bar{s}\gamma_\mu\gamma_5 s \tag{16}$$

which is close to one and which goes to one in the limit $Q^2 \to \infty$. The symbol β denotes the QCD beta function $\beta(\alpha_s) = -\biggl(11 - \frac{2}{3}f\biggr)(\alpha_s^2/2\pi) + ...$ and γ is given by $\gamma(\alpha_s) = f(\alpha_s/\pi)^2 + ...$ where f (=3) is the number of active flavors (Kodaira, 1980). The singlet axial charge, $g_A^{(0)}|_{\mathrm{inv}}$, is independent of the renormalization scale μ and corresponds to $g_A^{(0)}(Q^2)$ evaluated in the limit $Q^2 \to \infty$. The flavor non-singlet axial-charges $g_A^{(3)}$ and $g_A^{(8)}$ are renormalization group invariants. We are free to choose the QCD coupling $\alpha_s(\mu)$ at either a hard or a soft scale μ. The perturbative QCD expansion of $E(\alpha_s)$ remains close to one – even for large values of α_s. If we take $\alpha_s \sim 0.6$ as typical of the infra-red then $E(\alpha_s) \simeq 1 - 0.13 - 0.03 + ... = 0.84 + ...$ where -0.13 and -0.03 are the $\mathcal{O}(\alpha_s)$ and $\mathcal{O}(\alpha_s^2)$ corrections respectively.

In the naive parton model $g_A^{(0)}$ is interpreted as the fraction of the proton's spin which is carried by the intrinsic spin of its quark and anti-quark constituents. The experimental value of $g_A^{(0)}$ is obtained through measuring g_1 and combining the first moment integral in Eq.(12) with knowledge of $g_A^{(3)}$ and $g_A^{(8)}$ from other processes plus theoretical calculation of the perturbative QCD Wilson coefficients.

The isovector axial-charge is measured independently in neutron β-decays ($g_A^{(3)} = 1.270 \pm 0.003$ (Beringer *et al.*, 2012)) and the octet axial charge is commonly taken to be the value extracted from hyperon β-decays assuming a 2-parameter SU(3) fit ($g_A^{(8)} = 0.58 \pm 0.03$ (Close and Roberts, 1993)). However, it should be noted the uncertainty quoted for $g_A^{(8)}$ has been a matter of some debate (Jaffe and Manohar, 1990; Ratcliffe, 2004). SU(3) symmetry may be badly broken and some have suggested that the error on $g_A^{(8)}$ should be as large as 25% (Jaffe and Manohar, 1990). A recent re-evaluation of the nucleon's axial-charges in the Cloudy Bag model taking into account the effect of the one-gluon-exchange hyperfine interaction and the pion cloud plus kaon loops led to the value $g_A^{(8)} = 0.46 \pm 0.05$ (Bass and Thomas, 2010). The model reduction of $g_A^{(8)}$ from the SU(3) value comes primarily from the pion cloud with $g_A^{(3)}$ taking its physical value.

Deep inelastic measurements of g_1 have been performed in experiments at CERN, DESY, JLab and SLAC. An overview of the world data on the nucleon's g_1 spin structure function is shown in Fig. 1. This data is published in EMC (Ashman *et al.*, 1989), SMC (Adeva *et al.*, 1998b), E142 (Anthony *et al.*, 1996), E143 (Abe *et al.*, 1998), E154 (Abe *et al.*, 1997), E155 (Anthony *et al.*, 2000), E155 (Anthony *et al.*, 1999), HERMES (Airapetian *et al.*, 2007a), JLab (Dharmawardane *et al.*, 2006; Zheng *et al.*, 2004), and COMPASS (Alekseev *et al.*, 2010d; Alexakhin *et al.*, 2007). There is a general consistency among all data sets. The kinematic reach of the different experiments is visible in Fig. 2. COMPASS have the smallest-x data, down to $x \sim 0.004$.

There are several striking features in the data. COMPASS measurements of the deuteron spin structure function g_1^d show the remarkable feature that g_1^d is consistent with zero in the small-x region between 0.004 and 0.02 (Alexakhin *et al.*, 2007). In contrast, the isovector part of g_1 is observed to rise at small x as $g_1^{p-n} \sim$

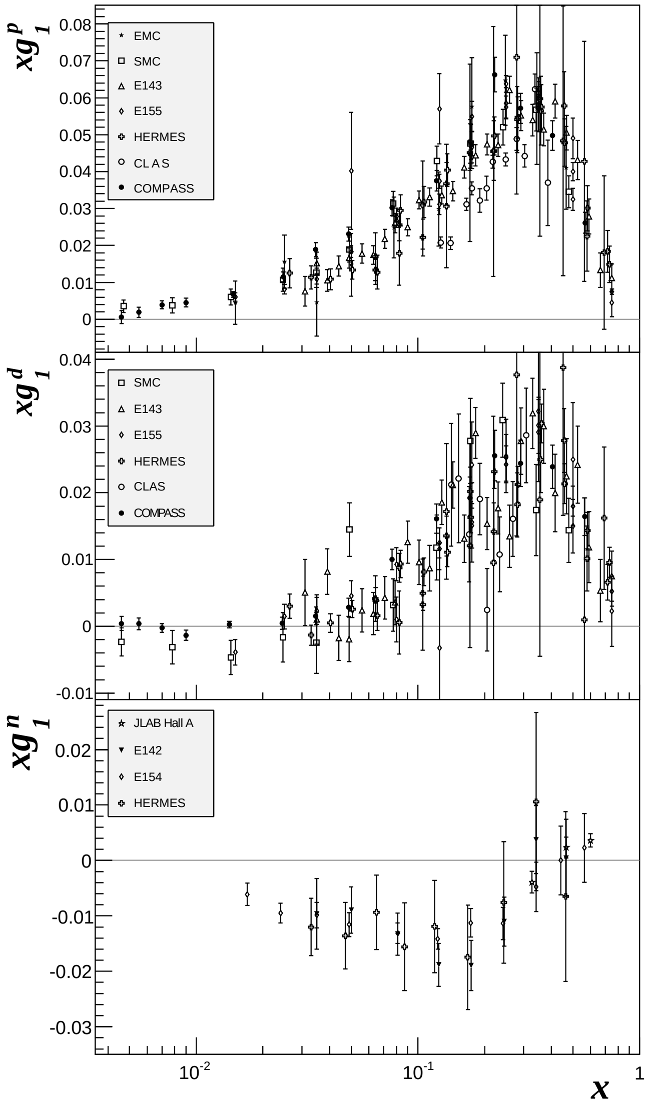

FIG. 1 World data on xg_1 as a function of x for the proton (top), the deuteron (middle) and the neutron (bottom) at the Q^2 of the measurement. Only data points for $Q^2 > 1$ GeV^2 and $W > 2.5$ GeV are shown.

$x^{-0.22\pm0.07}$ (Alekseev *et al.*, 2010d) and is much bigger than the isoscalar g_1^d. This compares to the situation in the unpolarized structure function F_2 where the small-x region is dominated by isoscalar gluonic exchanges.

A. Spin sum-rules

To test deep inelastic sum-rules it is necessary to have all data points at the same value of Q^2. Next-to-leading order (NLO) QCD-motivated fits taking into account the scaling violations associated with perturbative QCD are used to evolve all the data points to the same Q^2. First moment sum-rules are then evaluated by extrapolating these fits to $x = 0$ and to $x = 1$, or using a Regge-motivated extrapolation of the data. Next-to-leading order (NLO) QCD-motivated fits discussed in Section V.C are used to extract from these scaling violations the parton distributions and in particular the gluon polarization.

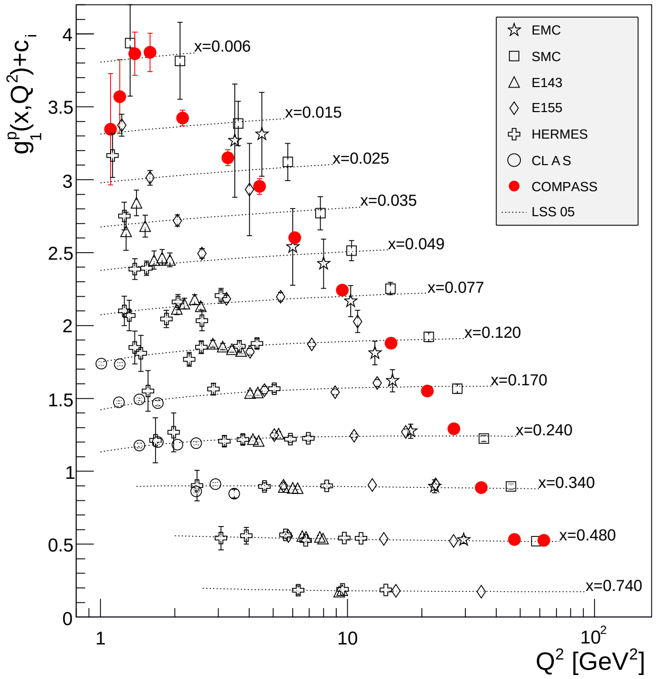

FIG. 2 World data for $g_1(x,Q^2)$ for the proton with $Q^2 > 1$ GeV^2 and $W > 2.5$ GeV. For clarity a constant $c_i = 0.28(11.6 - i)$ has been added to the g_1 values within a particular x bin starting with $i = 0$ for $x = 0.006$. (Also shown is the QCD fit of Leader *et al.* (2006).)

Polarized deep inelastic scattering experiments are interpreted in terms of a small value for the flavor-singlet axial-charge. For example, COMPASS found using the SU(3) value for $g_A^{(8)}$ (Alexakhin *et al.*, 2007) and no leading twist subtraction constant

$$g_A^{(0)}|_{\rm pDIS, Q^2\to\infty} = 0.33 \pm 0.03({\rm stat.}) \pm 0.05({\rm syst.}). \quad (17)$$

(This deep inelastic quantity misses any contribution to $g_A^{(0)}|_{\rm inv}$ from a possible delta function at $x = 0$). When combined with $g_A^{(8)} = 0.58 \pm 0.03$, the value of $g_A^{(0)}|_{\rm pDIS}$ in Eq.(17) corresponds to a negative strange-quark polarization

$$\begin{aligned}\Delta s_{Q^2\to\infty} &= \frac{1}{3}(g_A^{(0)}|_{\rm pDIS, Q^2\to\infty} - g_A^{(8)}) \\ &= -0.08 \pm 0.01({\rm stat.}) \pm 0.02({\rm syst.}) \quad (18)\end{aligned}$$

– that is, polarized in the opposite direction to the spin of the proton. With this Δs, we obtain values for the up and down quark polarizations

$$\begin{aligned}\Delta u_{Q^2\to\infty} &= 0.84 \pm 0.01({\rm stat.}) \pm 0.02({\rm syst.}) \\ \Delta d_{Q^2\to\infty} &= -0.43 \pm 0.01({\rm stat.}) \pm 0.02({\rm syst.}) \quad (19)\end{aligned}$$

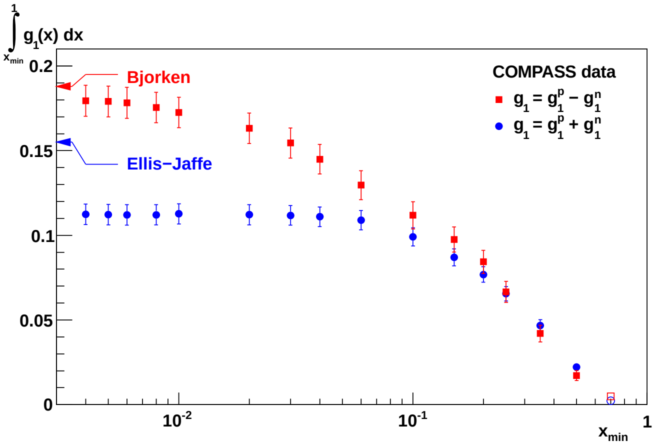

FIG. 3 Convergence of the first moment integral of g_1 as a function of the lower integration limit $x_{\rm min}$ for the Bjorken integral (isospin non-singlet) and the Ellis–Jaffe integral (isosinglet) from the COMPASS proton and deuteron data at $Q^2 = 3$ GeV^2. The arrows indicate the theoretical expectations.

The non-zero value of $\Delta s_{Q^2 \to \infty}$ in Eq.(18) is known as the violation of the Ellis-Jaffe sum-rule (Ellis and Jaffe, 1974).

The extracted value of $g_A^{(0)}|_{\rm pDIS}$ required to be understood by theory, and the corresponding polarized strangeness, depend on the value of $g_A^{(8)}$. If we instead use the value $g_A^{(8)} = 0.46 \pm 0.05$ the corresponding experimental value of $g_A^{(0)}|_{\rm pDIS}$ would increase to $g_A^{(0)}|_{\rm pDIS} = 0.36 \pm 0.03 \pm 0.05$ with

$$\Delta s \sim -0.03 \pm 0.03. \qquad (20)$$

We shall discuss the value of Δs in more detail in Sections V and VI in connection with more direct measurements from semi-inclusive deep inelastic scattering plus global fits to spin data, models and recent lattice calculations with disconnected diagrams (quark sea contributions) included.

The Bjorken sum-rule (Bjorken, 1966, 1970) for the isovector part of g_1 follows from current algebra and is a fundamental prediction of QCD. It has been confirmed in polarized deep inelastic scattering at the level of 5%

$$\int_0^1 dx g_1^{p-n} = \frac{1}{6} g_A^{(3)} \Bigl\{ 1 + \sum_{\ell \geq 1} c_{{\rm NS}\ell} \, \alpha_s^\ell (Q) \Bigr\}. \qquad (21)$$

The value of $g_A^{(3)}$ extracted from the most recent COMPASS data is 1.28 ± 0.07(stat.) ± 0.010(syst.) (Alekseev *et al.*, 2010d) and compares well with the Particle Data Group value 1.270 ± 0.003 deduced from neutron beta-decays (Beringer *et al.*, 2012).

The evolution of the Bjorken integral $\int_{x_{\rm min}}^1 dx g_1^{p-n}$ as a function of x_{min} as well as the isosinglet integral $\int_{x_{\rm min}}^1 dx g_1^{p+n}$ are shown in Fig. 3. The Bjorken sum-rule and isosinglet integral converges in the measured x region. Note that a large contribution, about 50%, of the Bjorken sum-rule comes from $x \lesssim 0.15$. The integral for the first moment of g_1^{p+n} saturates at $x \sim 0.05$: the isosinglet part of g_1 is close to zero in this measured range of small Bjorken x.

The nucleon's second spin structure function g_2 is believed to satisfy the Burkhardt-Cottingham sum-rule $\int_0^1 dx g_2 = 0$ (Burkhardt and Cottingham, 1970). The most precise measurements to date in polarized deep inelastic scattering come from the SLAC E155 and E143 experiments, which report $\int_{0.02}^{0.8} dx \; g_2^p = -0.042 \pm 0.008$ for the proton and $\int_{0.02}^{0.8} dx \; g_2^d = -0.006 \pm 0.011$ for the deuteron at $Q^2 = 5$ GeV^2 (Anthony *et al.*, 2003). E155 estimate a contribution about 0.02 to the first moment of the proton g_2 come from the x range between 0 and 0.02 from the twist-two (Wandzura-Wilczek) part of g_2: $g_2^{\rm WW}(x) = \int_x^1 \frac{dy}{y} g_1(y) - g_1(x)$.

B. Proton spin puzzles

The results from polarized deep inelastic scattering pose the following questions:

- How is the spin $\frac{1}{2}$ of the proton built up from the spin and orbital angular momentum of the quarks and gluons inside?
- Why is the quark spin content $g_A^{(0)}|_{\rm pDIS}$ so small?
- How about $g_A^{(0)} \neq g_A^{(8)}$? What separates the values of the octet and singlet axial-charges? How reliable is the SU(3) value of $g_A^{(8)}$?
- Is the proton spin puzzle a valence quark or sea/glue effect?
- Can we extract information about the quark and gluon orbital angular momentum contributions from experiments, and with minimal model dependence?

We next discuss the theoretical development and experimental work that has been performed to address these questions and the physics interpretation of present measurements.

C. Spin and the singlet axial-charge

There are two key issues involved in understanding the small value of $g_A^{(0)}|_{\rm pDIS}$: the physics interpretation of the flavor-singlet axial-charge $g_A^{(0)}$ and possible SU(3) breaking in the extraction of $g_A^{(8)}$ from hyperon β-decays. How big really is the OZI violation $\Delta s = \frac{1}{3}(g_A^{(0)}|_{\rm pDIS} - g_A^{(8)})$?

Theoretical QCD analysis leads to the formula

$$g_A^{(0)} = \left(\sum_q \Delta q - 3\frac{\alpha_s}{2\pi}\Delta g \right)_{\rm partons} + \mathcal{C}_\infty \tag{22}$$

– see Altarelli and Ross (1988), Efremov and Teryaev (1988), Carlitz *et al.* (1988), Bass *et al.* (1991) and Bass (2005). Here $\Delta g_{\rm partons}$ is the amount of spin carried by polarized gluon partons in the polarized proton with $\alpha_s \Delta g \sim \texttt{constant}$ as $Q^2 \to \infty$ (Altarelli and Ross, 1988; Efremov and Teryaev, 1988)); $\Delta q_{\rm partons}$ measures the spin carried by quarks and anti-quarks carrying "soft" transverse momentum $k_t^2 \sim \mathcal{O}(P^2, m^2)$ where P^2 is a typical gluon virtuality in the nucleon and m is the light quark mass. The polarized gluon term is associated with events in polarized deep inelastic scattering where the hard photon strikes a quark or anti-quark generated from photon-gluon fusion and carrying $k_t^2 \sim Q^2$ (Carlitz *et al.*, 1988). It is associated with the QCD axial anomaly in perturbative QCD. $\mathcal{C}_\infty$ denotes a potential non-perturbative gluon topological contribution with support only at Bjorken $x = 0$ (Bass, 2005). This term is discussed in Section VI on theoretical understanding. It is associated with the possible subtraction constant in the dispersion relation for g_1. If non-zero it would mean that $\lim_{\epsilon \to 0} \int_\epsilon^1 dx g_1$ will measure the difference of the singlet axial-charge and the subtraction constant contribution; that is, polarized deep inelastic scattering measures the combination $g_A^{(0)}|_{\rm pDIS} = g_A^{(0)} - \mathcal{C}_\infty$.

Possible explanations for the small value of $g_A^{(0)}|_{\rm pDIS}$ extracted from polarized deep inelastic experiments that have been suggested in the theoretical literature include screening from positive gluon polarization, possible SU(3) breaking in the isosinglet axial-charges $g_A^{(8)}$ and $g_A^{(0)}$, negative strangeness polarization in the nucleon, a possible topological contribution at $x = 0$ plus connections to axial U(1) dynamics discussed in Fritzsch (1989), Narison *et al.* (1995), Shore (2008) and Bass (1999b).

The two-loop QCD evolution factor $E(\alpha_s)$ in Eq.(15) is associated with the polarized gluon term which carries all the scale dependence. The quark spin contribution $\Delta q_{\rm partons}$ and the subtraction constant in Eq.(22) are QCD scale invariant. The quark spin term $\Delta q_{\rm partons}$ is also known as the JET and chiral scheme (Cheng, 1996; Leader *et al.*, 1998) and AB scheme (Ball *et al.*, 1996) version of quark polarization – see Section VI.C. The growth in the gluon polarization $\Delta g \sim 1/\alpha_s$ at large Q^2 is compensated by growth with opposite sign in the gluon orbital angular momentum.

One would like to understand the dynamics which yield a small value of the singlet axial-charge extracted from polarized deep inelastic scattering and also the sum-rule for the longitudinal spin structure of the nucleon

$$\frac{1}{2} = \frac{1}{2}\sum_q \Delta q + \Delta g + L_q + L_g \tag{23}$$

where L_q and L_g denote the orbital angular momentum contributions. Operator definitions of the different terms or combinations of terms in this equation are discussed in Jaffe and Manohar (1990), Ji (1997b), Shore and White (2000), Bakker *et al.* (2004), Bass (2005), Chen *et al.* (2008), Wakamatsu (2010) and Leader (2011). We discuss orbital angular momentum and attempts to measure it in Sections VI–VII.

There is presently a vigorous global program to disentangle the different contributions. Key experiments include semi-inclusive polarized deep inelastic scattering (COMPASS and HERMES) and polarized proton-proton collisions (PHENIX and STAR), as well as deeply virtual Compton scattering and hard exclusive meson production to learn about total angular momentum (COMPASS, HERMES and JLab). Single spin observables in semi-inclusive scattering from transversely polarized targets is sensitive to orbital angular momentum in the proton.

V. QUARK AND GLUON POLARIZATION FROM DATA

Key observables needed to understand the small value of the singlet axial-charge $g_A^{(0)}|_{\rm pDIS}$ are the polarized strangeness and polarized glue in the nucleon. The search for polarized strangeness has inspired a dedicated experimental program with semi-inclusive deep inelastic scattering. Further, much activity was motivated by the discovery of Altarelli and Ross (1988) and Efremov and Teryaev (1988) that polarized glue makes a scaling contribution to the first moment of g_1, $\alpha_s \Delta g \sim \texttt{constant}$. If there were a large negative contribution $-3\frac{\alpha_s}{2\pi}\Delta g$ with *e.g.* gluon polarization of the order of $\Delta g \simeq 2.5$ at $Q^2 = 10$ GeV^2, then this could reconcile the small measured value of $g_A^{(0)}|_{\rm pDIS}$ with the naive parton model expectation of about 0.6 through Eq. (22). This suggestion sparked a vigorous and ambitious program to measure Δg. Interesting channels include gluon mediated processes in semi-inclusive polarized deep inelastic scattering (COMPASS and HERMES) and hard QCD processes in high-energy polarized proton-proton collisions at RHIC.

A. Valence and sea polarization

Semi-inclusive measurements of fast pions and kaons in the current fragmentation region with final state particle identification can be used to reconstruct the individual up, down and strange quark contributions to the proton's spin. In contrast to inclusive polarized deep inelastic scattering where the g_1 structure function is deduced by detecting only the scattered lepton, the detected particles in the semi-inclusive experiments are high-energy (greater than 20% of the energy of the incident photon)

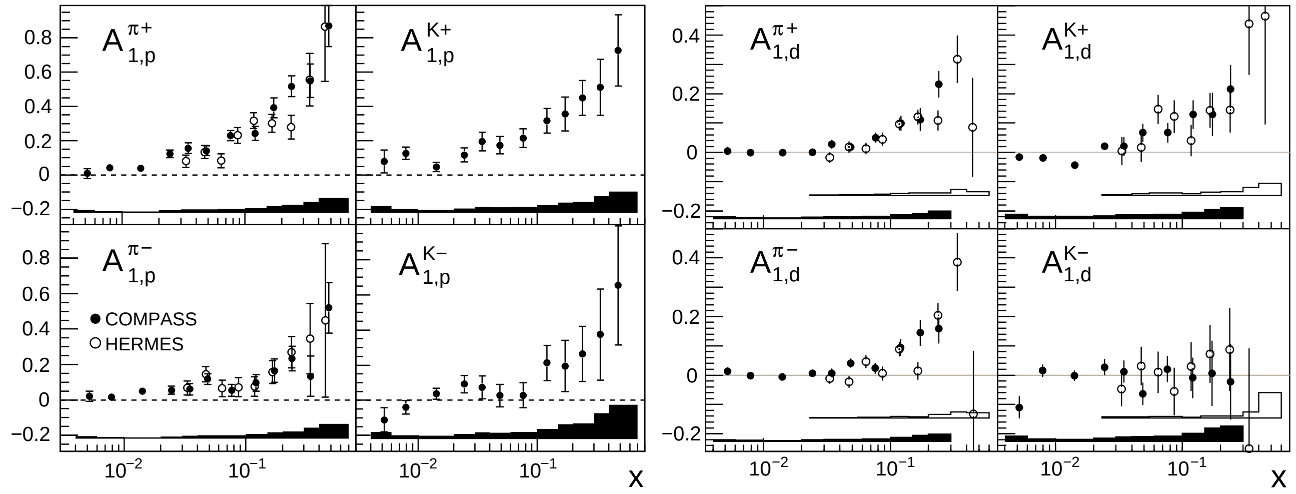

FIG. 4 Semi-inclusive longitudinal double-spin asymmetries for identified pions and kaons from COMPASS (Alekseev *et al.*, 2009b, 2010c) and HERMES (Airapetian *et al.*, 2005a) for the proton (left) and the deuteron (right) as function of x at the Q^2 of the measurements. The error bars and bands indicate the statistical and systematic uncertainties, respectively.

charged pions and kaons in coincidence with the scattered lepton. For large energy fraction $z = E_h/E_\gamma \to 1$ the most probable occurrence is that the detected $\pi^\pm$ and $K^\pm$ contain the struck quark or anti-quark in their valence Fock state. They therefore act as a tag of the flavor of the struck quark (Close, 1979).

In leading order the virtual-photon–proton double-spin (cross-section) asymmetry is

$$A^h_{1p}(x, Q^2) \simeq \frac{\sum_{q,h} e_q^2 \Delta q(x, Q^2) \int_{z_{\min}}^1 dz D_q^h(z, Q^2)}{\sum_{q,h} e_q^2 q(x, Q^2) \int_{z_{\min}}^1 dz D_q^h(z, Q^2)} \quad (24)$$

where $z_{\min} \sim 0.2$. Here $D_q^h(z, Q^2) = \int dp_t^2 D_q^h(z, p_t^2, Q^2)$ is the fragmentation function for the struck quark or anti-quark to produce a hadron h $(= \pi^\pm, K^\pm)$ carrying energy fraction $z = E_h/E_\gamma$ in the target rest frame; $\Delta q(x, Q^2)$ is the quark (or anti-quark) polarized parton distribution and e_q is the quark charge. Note the integration over the transverse momentum p_t (Close and Milner, 1991). Since pions and kaons have spin zero, the fragmentation functions are the same for both polarized and unpolarized leptoproduction. The fragmentation functions for $u \to \pi^+$ and $d \to \pi^-$ are known as "favored" (where the fragmenting quark has the same flavor as a valence quark in the final state hadron); the fragmentation functions for $u \to \pi^-$ and $d \to \pi^+$ are known as "unfavored".

This program for polarized deep inelastic scattering was pioneered by the SMC (Adeva *et al.*, 1996, 1998a) and the HERMES (Ackerstaff *et al.*, 1999b; Airapetian *et al.*, 2004, 2005a) experiments. The most recent measurements from HERMES are reported in Airapetian *et al.* (2008c) and from COMPASS in Alekseev *et al.* (2010c).

The experimental strategy has been to measure the asymmetries A_1^h for charged hadron production and separated charged pion and kaon production from proton and deuteron targets. There is good agreement between the COMPASS and HERMES data in the kinematic region of overlap – see Fig. 4. Flavor-separated polarized quark distributions for valence and sea quarks are then extracted from the data using fragmentation functions that have been fitted to previous hadron production data, with the most accurate taken to be those from the DSS group (de Florian *et al.*, 2007) from a global fit to single-hadron production in e^+e^-, ep and pp collisions.

The polarizations of the up and down quarks are positive and negative respectively, while the extracted sea polarization data are consistent with zero – see Table II which includes measurements from COMPASS (Alekseev *et al.*, 2010c), HERMES (Airapetian *et al.*, 2005a) and SMC (Adeva *et al.*, 1998a).

The COMPASS and HERMES determinations of the sum of strange and anti-strange polarisation $\Delta s(x)$ are shown together in Fig. 5, plotted in the combination $x\Delta s(x)$. There is no evidence in the semi-inclusive data

TABLE II First moments for valence quark and light-sea polarization from SMC, HERMES, and COMPASS. For each experiment the integrated sea is evaluated from data up to $x = 0.3$ and, for SMC, assuming an isospin symmetric polarized sea.

Experiment	x-range	Q^2 (GeV^2)	Δu_v	Δd_v	$\Delta\bar{u}$	$\Delta\bar{d}$
SMC	0.003–0.7	10	$0.73 \pm 0.10 \pm 0.07$	$-0.47 \pm 0.14 \pm 0.08$	$0.01 \pm 0.04 \pm 0.03$	$0.01 \pm 0.04 \pm 0.03$
HERMES	0.023–0.6	2.5	$0.60 \pm 0.07 \pm 0.04$	$-0.17 \pm 0.07 \pm 0.05$	$0.00 \pm 0.04 \pm 0.02$	$-0.05 \pm 0.03 \pm 0.01$
COMPASS	0.006–0.7	10	$0.67 \pm 0.03 \pm 0.03$	$-0.28 \pm 0.06 \pm 0.03$	$0.02 \pm 0.02 \pm 0.01$	$-0.05 \pm 0.03 \pm 0.02$

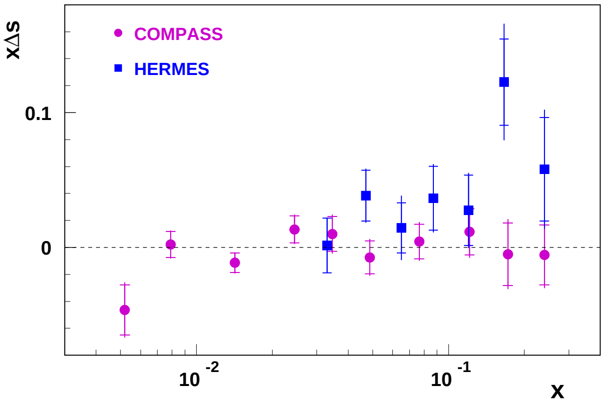

FIG. 5 COMPASS (Alekseev *et al.*, 2010c) and HERMES (Airapetian *et al.*, 2008c) results for the strangeness polarization $x\Delta s(x)$ as function of x. The data are obtained in a leading-order analysis of SIDIS asymmetries (including those for charged kaons) and using the DSS fragmentation functions (de Florian *et al.*, 2007).

for large negative strange quark polarization in the nucleon. The HERMES data covers the region $0.02 < x < 0.6$, where the extracted Δs is consistent with a zero or small positive value. This data integrates to $\int_{0.02}^{0.6} dx \Delta s = 0.037 \pm 0.019 \pm 0.027$ (Airapetian *et al.*, 2008c) in contrast with the negative value for polarized strangeness, Eq.(18), extracted from inclusive measurements of g_1. COMPASS measurements (Alekseev *et al.*, 2009b, 2010c) show no evidence of strangeness polarization in the region $x > 0.004$ with the integrated $\Delta s = -0.02 \pm 0.02 \pm 0.02$.

The precise value of Δs extracted from semi-inclusive scattering may be affected by any possible future improvement in the accuracy of the kaon fragmentation functions $D_q^K(z)$. However a drastic change in the ratio $\int dz D_{\bar{s}}^{K^+} / \int dz D_u^{K^+}$ would be needed to bring the first moment of Δs extracted from semi-inclusive scattering in agreement with the inclusive value, Eq.(18), obtained using the SU(3) value of $g_A^{(8)}$ (Alekseev *et al.*, 2010c). More experimental data, especially on kaon fragmentation processes, are needed for improved precision on strangeness polarization in the nucleon.

Semi-inclusive data are consistent with a small positive or zero isospin asymmetry in the polarized sea $\Delta\bar{u} - \Delta\bar{d}$. For the COMPASS data at 3 GeV^2 one finds $\int_{0.004}^{0.3} dx(\Delta\bar{u} - \Delta\bar{d}) = 0.06 \pm 0.04(\text{stat.}) \pm 0.02(\text{syst.})$. For HERMES data at 2.5 GeV^2 $\int_{0.023}^{0.3} dx(\Delta\bar{u} - \Delta\bar{d}) = 0.048 \pm 0.057(\text{stat.}) \pm 0.028(\text{syst.})$ (Airapetian *et al.*, 2005a). These values compare with the unpolarized sea measurement $\int_0^1 dx(\bar{u} - \bar{d}) = -0.118 \pm 0.012$ from the E866 experiment at FNAL (Towell *et al.*, 2001). A compilation of theoretical predictions is given in Peng (2003). Meson cloud models predict small negative isospin asymmetries in the polarized sea (Cao and Signal, 2001; Kumano and Miyama, 2002) whereas statistical (Bourrely *et al.*, 2002) and chiral quark soliton models (Wakamatsu, 2003) predict positive values. The COMPASS and HERMES results are consistent with these predictions within uncertainties.

The W-boson production program at RHIC (Bunce *et al.*, 2000) will provide additional flavor-separated measurements of polarized up and down quarks and anti-quarks. At RHIC the polarization of the $u, \bar{u}, d$, and $\bar{d}$ quarks in the proton is being measured directly using W boson production in $u\bar{d} \to W^+$ and $d\bar{u} \to W^-$. The charged weak boson is produced through a pure V$-$A coupling and the chirality of the quark and anti-quark in the reaction is fixed. The W is observed through its leptonic decay $W \to l\nu$, and the charged lepton is measured. Measurement of the flavor-separated anti-quark helicity distributions via W production in $p + p$ collisions is complementary to measurements via SIDIS in that there is no dependence on details of the fragmentation process, and the process scale, $Q^2 \approx M_W^2$ is significantly higher than any data from existing fixed-target polarized DIS experiments. A parity-violating asymmetry for W^+ production in $p + p$ collisions at $\sqrt{s} = 500$ GeV consistent with predictions based on anti-quark helicity distributions extracted from SIDIS has already been observed by both PHENIX (Adare *et al.*, 2011b) and STAR (Aggarwal *et al.*, 2011) based on data collected in 2009. Considerably improved results are expected from data taken in 2011 and 2012 with higher luminosities and polarization.

An independent measurement of the strange-quark axial-charge could be made through neutrino-proton elastic scattering. This process measures the combination $(\Delta u - \Delta d - \Delta s)_{\text{inv}} - 0.01 g_A^{(0)}|_{\text{inv}}$, where the small last term is a correction from heavy-quarks which has been calculated to LO (Kaplan and Manohar, 1988) and NLO

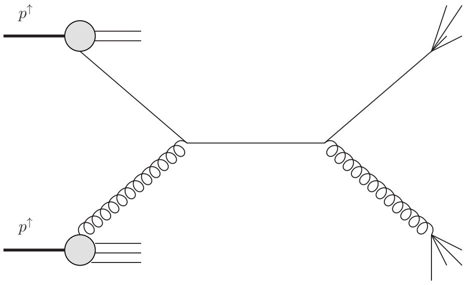

FIG. 6 Jet production from quark-gluon scattering in polarized proton-proton collisions.

(Bass *et al.*, 2002) accuracy. The axial-charge measured in νp elastic scattering is independent of any assumptions about possible SU(3) breaking, the presence or absence of a subtraction at infinity in the dispersion relation for g_1 and the $x \sim 0$ behavior of g_1.

In a recent analysis (Pate *et al.*, 2008) of parity violating quasi-elastic electron and neutrino scattering data between 0.45 and 1 GeV^2 (from the JLab experiments G0 and HAPPEx and the Brookhaven experiment E734), the axial form-factor was extrapolated to $Q^2 = 0$ and favored negative or zero values of Δs with large uncertainty.

B. Gluon polarization

Polarized proton-proton scattering is sensitive to the ratio of polarized to unpolarized glue, $\Delta g/g$, via leading-order interactions of gluons, as illustrated in Fig. 6. The first experimental attempt to look at gluon polarization was made by the FNAL E581/704 Collaboration using a 200 GeV polarized proton beam and a polarized proton target. They measured a longitudinal double-spin asymmetry A_{LL} for inclusive multi-γ and $\pi^0\pi^0$ production consistent with zero within their sensitivities, suggesting that $\Delta g/g$ is not so large in the region of $0.05 \lesssim x_g \lesssim 0.35$ (Adams *et al.*, 1994).

COMPASS was conceived to measure Δg via the study of the photon-gluon fusion process, as shown in Fig. 7. The cross-section for this process is directly related to the (polarized) gluon distribution at the Born level. The experimental technique consists of the reconstruction of charmed mesons (Alekseev *et al.*, 2009c) or high-p_T hadrons (Ageev *et al.*, 2006) in the final state to access Δg. The high-p_T particle method leads to samples with larger statistics, but these have higher background contributions from QCD Compton processes and fragmentation. High-p_T hadron production was also used in early attempts to access gluon polarization by HERMES (Airapetian *et al.*, 2000a) and SMC (Adeva *et al.*, 2004) and the most recent HERMES determination (Airapetian *et al.*, 2010c) and COMPASS measurement (Adolph *et al.*, 2012c).

These measurements in lepton-nucleon scattering are listed in Table III for the ratio of the polarized to unpolarized glue $\Delta g/g$ and shown in Fig. 8 for leading-order (LO) analyses of the data. The data cluster around $x_g \sim 0.1$. There is no evidence in the data for non-zero gluon polarization at this value of x_g.

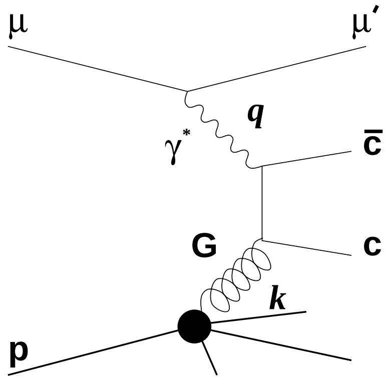

FIG. 7 Production of a $c\bar{c}$ pair in polarized photon gluon fusion is being used to measure gluon polarization in the polarized proton.

The chance to measure Δg was a main physics drive for polarized RHIC. Experiments using the PHENIX and STAR detectors are investigating polarized glue in the proton. Measurements of $\Delta g/g$ from RHIC are sensitive to gluon polarization in the range $0.02 \lesssim x_g \lesssim 0.3$ ($\sqrt{s} = 200$ GeV) and $0.06 \lesssim x_g \lesssim 0.4$ ($\sqrt{s} = 62.4$ GeV) for the neutral pion A_{LL} measured by PHENIX (Adare *et al.*, 2009a,b) and inclusive jet production measured by STAR at 200 GeV center-of-mass energy (Abelev *et al.*, 2008b; Adamczyk *et al.*, 2012a). Additional channels sensitive to Δg at RHIC have been published as well (Abelev *et al.*, 2009; Adare *et al.*, 2011a, 2012).

Preliminary results from PHENIX and STAR using more recent 200 GeV data than those published in Adare *et al.* (2009b) and Abelev *et al.* (2008b) are shown in Figs. 9 and 10. In Fig. 9 the longitudinal double-spin asymmetry in neutral pion production measured by PHENIX based on combined data from 2005, 2006, and 2009 is shown as a function of p_T (Manion, 2011). The data are compared to a calculation using helicity distributions extracted from a global fit to polarized world data from DIS, semi-inclusive DIS, and proton-proton collisions ("DSSV") (de Florian *et al.*, 2008, 2009) and found to be consistent within the ex-

TABLE III Polarized gluon measurements from deep inelastic experiments.

Experiment	process	$\langle x_g \rangle$	$\langle \mu^2 \rangle$ (GeV^2)	$\Delta g/g$
HERMES (Airapetian *et al.*, 2000a)	hadron pairs	0.17	~ 2	$0.41 \pm 0.18 \pm 0.03$
HERMES (Airapetian *et al.*, 2010c)	inclusive hadrons	0.22	1.35	$0.049 \pm 0.034 \pm 0.010^{+0.125}_{-0.099}$
SMC (Adeva *et al.*, 2004)	hadron pairs	0.07		$-0.20 \pm 0.28 \pm 0.10$
COMPASS (Ageev *et al.*, 2006; Procureur, 2006)	hadron pairs, $Q^2 < 1$	0.085	3	$0.016 \pm 0.058 \pm 0.054$
COMPASS (Adolph *et al.*, 2012c)	hadron pairs, $Q^2 > 1$	0.09	3	$0.125 \pm 0.060 \pm 0.063$
COMPASS (Alekseev *et al.*, 2009c; Franco, 2010)	open charm (LO)	0.11	13	$-0.08 \pm 0.21 \pm 0.11$

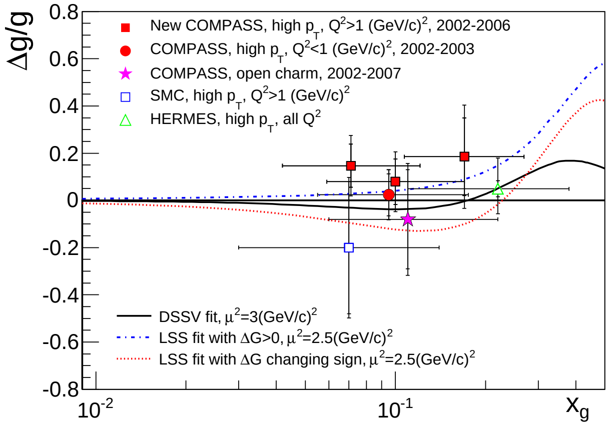

FIG. 8 Gluon polarization $\Delta g/g$ from leading-order analyses of hadron or hadron-pair production as function of the probed gluon momentum fraction x_g. Also shown are NLO fits from de Florian *et al.* (2009) and Leader *et al.* (2010). (Figure taken from Adolph *et al.* (2012c).)

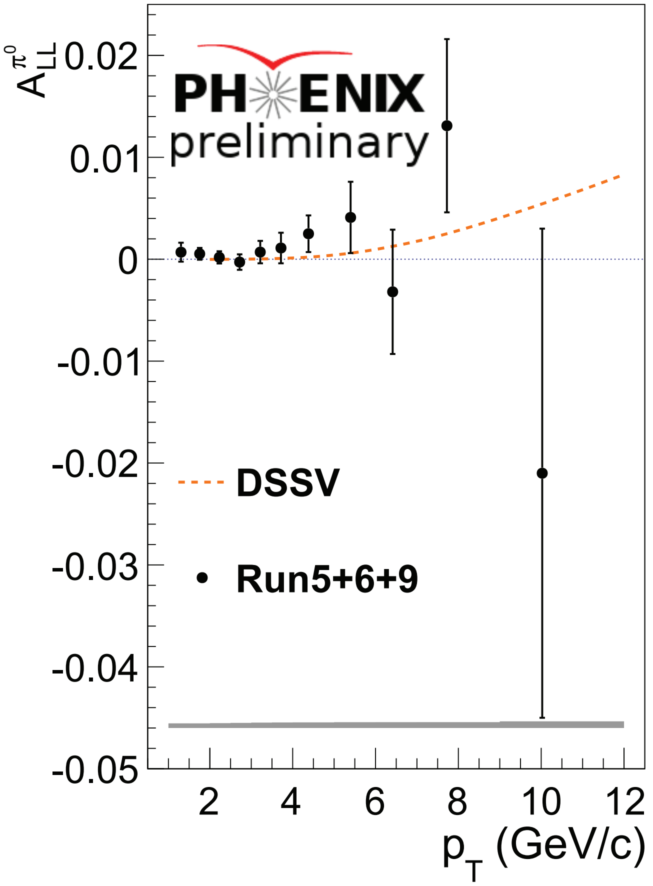

FIG. 9 The longitudinal double-spin asymmetry in π^0 production as measured by PHENIX in 200 GeV polarized pp collisions as a function of the transverse π^0 momentum p_T compared to a calculation using the DSSV polarized parton distributions (Manion, 2011).

perimental uncertainties; these data are also consistent with zero. Figure 10 shows the longitudinal double-spin asymmetry in single-inclusive jet production measured by STAR based on data taken in 2009 (Djawotho, 2011) and provides the first evidence for non-zero gluon polarization in the proton. The results are compared to calculations based on the DSSV helicity distribution function extraction as well as two earlier extractions based only on inclusive DIS data, GRSV-std and GRSV-zero corresponding to $\Delta g \sim 0.4$ and 0.1 at $Q^2 \sim 1$ GeV^2 (Glück *et al.*, 2001). See the following section for more details about fits to helicity distributions. A given p_T bin for single inclusive jet or hadron production generally samples a wide range of x_g values. However, dijet measurements in $p+p$ collisions provide better constraints on the x_g values probed. Preliminary STAR results for dijet production have also been released (Walker, 2011) and confirm the non-zero double-spin asymmetry seen in single jet production.

While there is now evidence in the RHIC data that gluon polarization in the proton is non-zero, the measurements indicate that polarized glue, by itself, is not sufficient to resolve the difference between the small value of $g_A^{(0)}|_{\rm pDIS}$ and the naive constituent quark model prediction, ~ 0.6, through the polarized glue term $-3\frac{\alpha_s}{2\pi}\Delta g$. Note however that gluon polarization $\Delta g \sim 0.2 - 0.3$ would still make a significant contribution to the spin of the proton in Eq.(23).

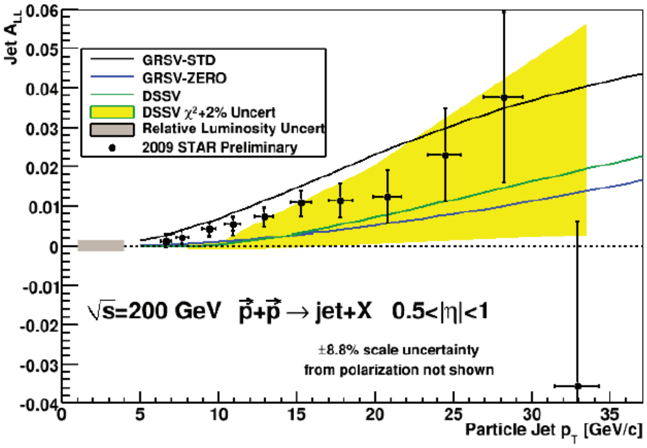

FIG. 10 The longitudinal double-spin asymmetry in inclusive jet production as measured by STAR in 200 GeV polarized pp collisions as a function of the transverse jet momentum p_T compared to a calculations using the DSSV, GRSV-std, and GRSV-zero polarized parton distributions (Djawotho, 2011).

C. NLO QCD motivated fits to spin data

Global NLO perturbative QCD analysis are performed on polarization data sets including both lepton-nucleon and proton-proton collision data. The aim is to extract the polarized quark and gluon parton distributions. These analysis, starting from Ball *et al.* (1996) and Altarelli *et al.* (1997), frequently use DGLAP evolution and are performed in a given factorization scheme. This QCD fit approach has more recently been extended to a global analysis of data from polarized DIS, semi-inclusive polarized DIS and high-energy polarized proton-proton collisions (de Florian *et al.*, 2008, 2009).

The separation of g_1 into "hard" and "soft" contributions is not unique and depends on the choice of "factorization scheme". For example, one might use a kinematic cut-off on the partons' transverse momentum squared ($k_t^2 > \mu^2$) to define the factorization scheme and thus separate the hard and soft parts of the phase space for the photon-parton collision. The cut-off μ^2 is called the factorization scale. The coefficients in Eq.(8) have the perturbative expansion $C^q = \delta(1-x) + \frac{\alpha_s}{2\pi} f^q(x, Q^2/\mu^2)$ and $C^g = \frac{\alpha_s}{2\pi} f^g(x, Q^2/\mu^2)$ where the strongest singularities in the functions f^q and f^g as $x \to 1$ are $\ln(1-x)/(1-x)_+$ and $\ln(1-x)$ respectively, see *e.g.* Lampe and Reya (2000). The deep inelastic structure functions are dependent on Q^2 and independent of the factorization scale μ^2 and the "scheme" used to separate the γ^*-parton cross-section into "hard" and "soft" contributions.

Examples of different "schemes" used in the literature are the modified minimal subtraction ($\overline{\text{MS}}$) (Bodwin and Qiu, 1990; 't Hooft and Veltman, 1972) to regulate the mass singularities which arise in scattering from massless partons, the "AB" (Ball *et al.*, 1996) and "CI" (chiral invariant) (Cheng, 1996) or "JET" (Leader *et al.*, 1998) schemes. In the $\overline{\text{MS}}$ scheme the polarized gluon distribution does not contribute explicitly to the first moment of g_1. In the AB, CI and JET schemes on the other hand the polarized gluon (axial anomaly contribution) $\alpha_s \Delta g$ does contribute explicitly to the first moment since $\int_0^1 dx\ C^{(g)} = -\frac{\alpha_s}{2\pi}$ – see the spin decomposition in Eq.(22).

The μ^2 dependence of the parton distributions is given by the DGLAP equations (Altarelli and Parisi, 1977)

$$\begin{aligned}\frac{d}{dt}\Delta\Sigma(x,t) &= \frac{\alpha_s(t)}{2\pi}\Bigg[\int_x^1 \frac{dy}{y}\Delta P_{qq}(\frac{x}{y})\Delta\Sigma(y,t) \\ &\qquad + 2f\int_x^1 \frac{dy}{y}\Delta P_{qg}(\frac{x}{y})\Delta g(y,t)\Bigg] \\ \frac{d}{dt}\Delta g(x,t) &= \frac{\alpha_s(t)}{2\pi}\Bigg[\int_x^1 \frac{dy}{y}\Delta P_{gq}(\frac{x}{y})\Delta\Sigma(y,t) \\ &\qquad + \int_x^1 \frac{dy}{y}\Delta P_{gg}(\frac{x}{y})\Delta g(y,t)\ \Bigg]\end{aligned} \tag{25}$$

where $\Delta\Sigma(x,t) = \sum_q \Delta q(x,t)$, $t = \ln\mu^2$ and f is the number of active flavors. The splitting functions P_{ij} in Eq.(25) have been calculated at leading order by Altarelli and Parisi (1977) and at next-to-leading order by Zijlstra and van Neerven (1994), Mertig and van Neerven (1996) and Vogelsang (1996).

The largest uncertainties in the QCD fits are associated with the ansatz chosen for the shape of the spin-dependent quark and gluon distributions at a given input scale. Further, the SU(3) value of $g_A^{(8)}$ ($= 0.58 \pm 0.03$) is assumed in present fits though no significant change in the χ^2 quality of the fits should be expected if one instead took a value of $g_A^{(8)}$ with possible 20% SU(3) breaking included.[1] The values for the quark and gluon spin contents ($\Delta\Sigma$ and Δg) obtained in recent NLO fits are listed in Table IV with results quoted from Blümlein and Böttcher (2010) (BB10: DIS data), Nocera *et al.* (2012) (NFRR12: DIS data), Leader *et al.* (2010) (LLS10: DIS and SIDIS data) and Hirai and Kumano (2009) (AAC08: DIS and RHIC data) and de Florian *et al.* (2008, 2009) (DSSV08: DIS, SIDIS and proton-proton collision data).

The most complete fits in terms of maximum included data are from the DSSV group, which take the SU(3) value for $g_A^{(8)}$. One finds need for a large negative contribution to Δs from small x, outside the measured x range when SIDIS data is included. The values obtained in this approach for $\int_{x_{\min}}^1 dx \Delta s(x)$ are $\Delta s = -0.057$ with $x_{\min} = 0$ and about -0.001 with $x_{\min} = 0.001$.

---

[1] We thank S. Taneja and R. Windmolders for discussion on this issue.

TABLE IV First moments of the polarized singlet-quark and gluon distributions at the scale 4 GeV^2 in the $\overline{\mathrm{MS}}$ scheme; values quoted from Nocera *et al.* (2012).

	DSSV08	BB10	LSS10	AAC08	NFRR12
$\Delta\Sigma(Q^2)$	0.25 ± 0.02	0.19 ± 0.08	0.21 ± 0.03	0.24 ± 0.07	0.31 ± 0.10
$\Delta g(Q^2)$	-0.10 ± 0.16	0.46 ± 0.43	0.32 ± 0.19	0.63 ± 0.19	-0.2 ± 1.4

That is, to reproduce the SU(3) value of the octet axial-charge, the negative polarized strangeness obtained from inclusive g_1 measurements gets pushed into the unmeasured small-x range, $x < 0.004$. It is interesting here to note that, historically (before COMPASS, HERMES and RHIC Spin), the proton spin puzzle was assumed to be associated with strangeness/sea/glue polarization in the newly opened kinematics of EMC, SLAC and SMC, x between 0.1 and 0.01. We now have accurate SIDIS measurements down to $x \sim 0.004$ which show no evidence for large sea/glue polarization effects. With the SIDIS measurements of Δs, either one needs SU(3) breaking in the octet axial-charge or strangeness/glue effects at very small x. Without including the most recent data from 2009 or later, de Florian *et al.* (2008, 2009) find a best-fit full first moment $\int_0^1 dx \Delta g(x) = -0.084$ at $Q^2 = 10$ GeV^2. With a very large $\Delta\chi^2/\chi^2 = 2\%$ allowed range, the truncated first moment $\int_{0.001}^1 dx \Delta g = 0.013^{+0.702}_{-0.314}$ was obtained. With these errors Δg is still not precise.

A recent attempt to extract polarized parton distributions from inclusive polarized deep inelastic data using neural network techniques is reported in (Nocera *et al.*, 2012). In this approach no assumption is made about the functional form of the input distributions, greatly reducing the primary (and notoriously difficult to quantify) systematic uncertainty on parton distribution fits. The neural network method has already been used quite successfully in the parametrization of the unpolarized parton distributions, with results published at NLO in 2010 (Ball *et al.*, 2010) and now NNLO in 2012 (Ball *et al.*, 2012). However, in the case of the application of the neural network method in the extraction of polarized parton distributions, thus far only inclusive polarized DIS data has been incorporated, similar to the BB10 fit (Blümlein and Böttcher, 2010).

VI. THEORETICAL UNDERSTANDING

In relativistic quark models some of the proton's spin is carried by quark orbital angular momentum. One has to take into account the four-component Dirac spinor for the quarks $\psi = \frac{N}{\sqrt{4\pi}} \begin{pmatrix} f \\ i\sigma \cdot \hat{r} g \end{pmatrix}$, where f and g are functions of the spatial coordinates and N is a normalization factor. The lower component of the Dirac spinor is p-wave with intrinsic spin primarily pointing in the opposite direction to spin of the nucleon. In the MIT Bag model, where quarks are confined in an infinite square well potential with radius R, one finds the depolarization factor $N^2 \int_0^R drr^2 (f^2 - \frac{1}{3} g^2) = 0.65$ for Δq in the proton with all quarks in the $(1s)$ ground-state (Jaffe and Manohar, 1990). That is, 35% of the proton's spin content is shifted into orbital angular momentum through the confinement potential.

More detailed calculations of non-singlet axial-charges in relativistic constituent quark models are sensitive to the confinement potential, effective color-hyperfine interaction, pion and kaon clouds plus additional wavefunction corrections (associated with center of mass motion) chosen to reproduce the physical value of $g_A^{(3)}$.

This physics was recently investigated within the Cloudy Bag model (Bass and Thomas, 2010; Myhrer and Thomas, 2008; Thomas, 2008). The Cloudy Bag was designed to model confinement and spontaneous chiral symmetry breaking, taking into account pion physics and the manifest breakdown of chiral symmetry at the bag surface in the MIT bag. If we wish to describe proton spin data including matrix elements of $J^3_{\mu 5}$, $J^8_{\mu 5}$ and $J_{\mu 5}$, then we would like to know that the model versions of these currents satisfy the relevant Ward identities (the divergence equations for these currents). For the scale-invariant non-singlet axial-charges $g_A^{(3)}$ and $g_A^{(8)}$, corresponding to the matrix elements of partially conserved currents, the model is well designed to make a solid prediction.

The effective color-hyperfine interaction has the quantum numbers of one-gluon exchange (OGE). In models of hadron spectroscopy this interaction plays an important role in the nucleon-Δ and $\Sigma - \Lambda$ mass differences, as well as the nucleon magnetic moments (Close, 1979) and the spin and flavor dependence of parton distribution functions (Close and Thomas, 1988). It shifts total angular-momentum between spin and orbital contributions and, therefore, also contributes to model calculations of the octet axial-charges (Myhrer and Thomas, 1988). With OGE included (together with a phenomenological wave-function renormalization to ensure $g_A^{(3)}$ takes the physical value), the model is in very good agreement with the SU(3) fit to the nucleon and hyperon axial-charges extracted from β-decays with $g_A^{(8)}$ predicted to be around 0.6.

Next, the pion cloud induces SU(3) breaking in the nucleon's axial-charges. The pion cloud further shifts intrinsic spin into orbital angular momentum (Schreiber and Thomas, 1988; Tsushima *et al.*, 1988). Including pion and kaon cloud corrections gives the model result $g_A^{(8)} = 0.46 \pm 0.05$ (with the corresponding semi-classical singlet axial-charge or spin fraction being 0.42 ± 0.07 before inclusion of gluonic effects) (Bass and Thomas, 2010). With this Cloudy Bag value for $g_A^{(8)}$ the corresponding experimental value of $g_A^{(0)}|_{\rm pDIS}$ would increase to $g_A^{(0)}|_{\rm pDIS} = 0.36 \pm 0.03 \pm 0.05$, considerably reducing the apparent OZI violation $\frac{1}{3}(g_A^{(0)}|_{\rm pDIS} - g_A^{(8)})$ that one needs to explain.

A recent lattice calculation with disconnected diagrams included (Bali *et al.*, 2012) gave $\Delta s = -0.02 \pm 0.01$ in the $\overline{\rm MS}$ scheme at 7.4 GeV^2. This value compares with the Cloudy Bag prediction $\Delta s \sim -0.01$ before gluonic degrees of freedom are included. These numbers are in good agreement with the values extracted from polarized SIDIS data by COMPASS and HERMES with the DSS fragmentation functions.

Gluon polarization has been investigated in bag and light-cone models and in studies of heavy-quark axial-charges. The nucleon's charm-quark axial-charge was interpreted to give an estimate of gluon polarization $|\Delta g(m_c^2)| \lesssim 0.3$ with $\alpha_s(m_c^2) = 0.4$ (Bass *et al.*, 2011). This upper bound corresponds to $|3 \frac{\alpha_s}{2\pi} \Delta g| \lesssim 0.06$. Values of $\Delta g \sim 0.3$ and ~ 0.5 at 1 GeV^2 were obtained in the MIT Bag model (Chen and Ji, 2008) and in a light-cone model (Brodsky *et al.*, 1995) respectively. These theoretical values are consistent with the extractions of gluon polarization from COMPASS, HERMES and RHIC Spin data.

To understand $\mathcal{C}_\infty$,[2] deep inelastic sum-rules are derived using the operator product expansion and the dispersion relation for deeply-virtual photon-nucleon scattering. Two important issues with the dispersion are the convergence of the first moment integral at the highest energies and any contribution from closing the circle in the complex momentum plane. The subtraction constant, if finite, corresponds to a constant real term in the forward Compton scattering amplitude. It affects just the first moment integral and thus behaves like a $\delta(x)$ term with support only at $x = 0$. A subtraction constant yields a finite correction to the sum-rule obtained from integrating only over finite non-zero values of Bjorken x. One can show (Bass, 2005) that non-local gluon topological structure requires consideration of a possible $\delta(x)$ subtraction constant. Whether it has finite value or not is sensitive to the realization of axial U(1) symmetry breaking by instantons (Crewther, 1978; 't Hooft, 1986) and the importance of topological structure in the proton. The QCD vacuum is a Bloch superposition of states characterized by non-vanishing topological winding number and non-trivial chiral properties. When we put a valence quark into this vacuum it can act as a source which polarizes the QCD vacuum with net result that the spin "dissolves". Some fraction of the spin of the constituent quark is shifted from moving partons into the vacuum at $x = 0$. This spin contribution becomes associated with non-local gluon topology with support only at Bjorken $x = 0$.

Valuable information about the spin puzzle also follows from looking at the x dependence of g_1. The small value of $g_A^{(0)}$ or "missing spin" is associated with a "collapse" in the isosinglet part of g_1 to something close to zero instead of a valence-like rise at x less than about 0.05 – see *e.g.* the g_1 data in Fig. 1 and the convergence of $\int_{x_{\rm min}}^1 dx g_1^{p+n}$ and $\int_{x_{\rm min}}^1 dx g_1^{p-n}$ in Fig. 3. This isosinglet part is the sum of SU(3)-flavor singlet and octet contributions. If there were a large positive polarized gluon contribution to the proton's spin, this would act to drive the small x part of the singlet part of g_1 negative (Bass and Thomas, 1993) – that is, acting in the opposite direction to any valence-like rise at small x. However, gluon polarization measurements constrain this spin contribution to be small in measured kinematics meaning that the sum of valence and sea quark contributions is suppressed at small x. Neither the SU(3) flavor-singlet nor octet contribution breaks free in the measured small x region. Hence, the suppression of g_1^{p+n} at small x should be either an isosinglet effect or a delicate cancellation between octet and singlet contributions over an order of magnitude in small Bjorken x.

The g_1^{p-n} data are consistent with quark model and perturbative QCD counting rules predictions in the valence region $x > 0.2$ (Bass, 1999a). The size of $g_A^{(3)}$ forces us to accept a large contribution from small x (a non-perturbative constraint) and the rise in g_1^{p-n} is in excellent agreement with the prediction $g_1^{p-n} \sim x^{-0.22}$ of hard Regge exchange (Bass, 2007a) – in particular a possible a_1 hard-pomeron cut involving the hard-pomeron which seems to play an important role in unpolarized deep inelastic scattering (Cudell *et al.*, 1999) and in the proton-proton total cross-section measured at LHC (Donnachie and Landshoff, 2011). (Soft) Regge theory predicts that the singlet term should behave as $\sim N \ln x$ in the small x limit, with the coefficient N to be determined from experiment (Bass and Landshoff, 1994; Close and Roberts, 1994). From the data, this normalization seems to be close to zero.

---

[2] In the notation of Eq.(12): $\beta_\infty = -\frac{1}{9}\mathcal{C}_\infty \Big\{ 1 + \sum_{\ell \geq 1} c_{S\ell}\, \alpha_s^\ell(Q) \Big\}$.

Where are we in our understanding of the spin structure of the proton and the small value of $g_A^{(0)}|_{\rm pDIS}$? Measurements of valence, gluon and sea polarization suggest that the polarized glue term $-3\frac{\alpha_s}{2\pi}\Delta g$ and the strange quark contribution $\Delta s_{\rm partons}$ in Eq.(22) are unable to resolve the small value of $g_A^{(0)}|_{\rm pDIS}$. Two explanations are suggested within the theoretical and experimental uncertainties depending upon the magnitude of SU(3) breaking in the nucleon and hyperon axial-charges. One is a value of $g_A^{(8)} \sim 0.5$ plus an axial U(1) topological effect at $x = 0$ associated with a finite subtraction constant in the g_1 dispersion relation. The second is a much larger pion cloud reduction of $g_A^{(8)}$ to a value ~ 0.4. Combining the theoretical error on the pion cloud chiral corrections embraces both possibilities. The proton spin puzzle seems to be telling us about the interplay of valence quarks with chiral dynamics and the complex vacuum structure of QCD.

Orbital angular momentum (OAM) in relativistic quark models (for example the MIT and Cloudy bag models) without explicit gluon degrees of freedom has the usual interpretation of relativistic quantum mechanics. For QCD dynamics the definition of OAM is more subtle because of the gauge covariant derivative, meaning that quark orbital momentum is in principle sensitive to the gluon fields in the nucleon that the quarks interact with.

Going beyond spin and helicity to consider also orbital and total angular momentum, several operator decompositions have been proposed. Starting from the relation between angular momentum and the energy-momentum tensor, Ji (1997b) takes

$$\begin{aligned}\vec{J}_q &= \int d^3x \ \vec{x} \times \vec{T}_q \\ &= \int d^3x \ \left[\psi^\dagger \frac{\vec{\Sigma}}{2} \psi + \psi^\dagger \vec{x} \times (-i\vec{D}) \psi \right] , \\ \vec{J}_g &= \int d^3x \ \vec{x} \times (\vec{E} \times \vec{B}). \end{aligned} \qquad (26)$$

The gauge covariant derivative means that L_q is *a priori* sensitive to gluonic degrees of freedom. The J_q and J_g quantities here are amenable to QCD lattice calculations and, in principle, measurable through deeply virtual Compton scattering. In an alternative approach, taking the + light cone component of the QCD angular momentum tensor in $A_+ = 0$ gauge Jaffe and Manohar (1990) proposed the operator decomposition

$$\begin{aligned} M^{+12} = \frac{1}{2} q_+^\dagger \gamma_5 q_+ + q_+^\dagger \left(\vec{x} \times i\vec{\partial} \right)^3 q_+ \\ + 2{\rm Tr} F^{+j} \left(\vec{x} \times i\vec{\partial} \right) A^j + {\rm Tr} \epsilon^{+-ij} F^{+i} A^j \end{aligned} \qquad (27)$$

where the gluon term in the gauge covariant derivative is no longer present through the gauge fixing.

The connection between the quark and gluon total angular momentum contributions J^q and J^g and the QCD energy-momentum tensor allows us to write down their LO QCD evolution equations (Ji *et al.*, 1996). The quark and gluon total angular momenta in the infinite scaling limit are given by $J_q(\infty) = \frac{1}{2}\{3f/(16+3f)\}$ and $J_g(\infty) = \frac{1}{2}\{16/(16+3f)\}$, with f the number of active flavors – that is, the same scaling limit as the quark and gluon momentum contributions at infinite Q^2. The Ji and Jaffe-Manohar definitions of orbital angular momentum satisfy the same (LO) QCD evolution equation, so, at LO, are equal in a model calculation if the glue contribution can be set equal to zero at a low-energy input scale.

To obtain information about the quark "orbital angular momentum" L_q we need to subtract the value of the "intrinsic spin" $S_q = \frac{1}{2}\Delta q$ measured in polarized deep inelastic scattering from the total quark angular momentum J_q. This means that L_q is scheme dependent with different schemes corresponding to different physics content depending on how the scheme handles information about the axial anomaly, large-k_t physics and any possible "subtraction at infinity" in the dispersion relation for g_1. The quark total angular momentum J_q is anomaly free in QCD so that axial anomaly effects occur with equal magnitude and opposite sign in L_q and S_q. When looking at physical observables that are sensitive to OAM and quark spin (with possible axial-anomaly contribution) it will be important to identify which OAM definition and which scheme quantity is most relevant to the observable – for example, in SIDIS the largest k_t events are included in the $\overline{\rm MS}$ version of Δq whereas they are omitted in the JET scheme version (Bass, 2003).

To connect quark model predictions with lattice calculations and fits to data it is necessary to use QCD evolution of the model results from the low-energy scale where the model applies up to the hard scale of deep inelastic scattering. Model calculations (and also lattice calculations without disconnected diagrams) of Δq are commonly understood to refer to the scale invariant version of this quantity, *e. g.* the chiral/JET or AB scheme quark spin contributions in Eq. (22). One chooses a model ansatz for the gluon polarization and total angular momentum, typically $\Delta g = J_g = 0$ at the model input scale. For illustration, Fig. 11 shows the evolution of total and orbital angular momentum contributions in the Cloudy Bag from the model scale up to $Q^2 = 4$ GeV^2. Various phenomenological investigations (Mattingly and Stevenson, 1994; Steffens *et al.*, 1995) found that by going beyond leading order QCD (and including pions in the nucleon wavefunction), the optimal fit to high-energy scattering data involved taking the running coupling α_s about 0.6–0.8 at the low energy input scale. For this range of α_s the scale dependence of

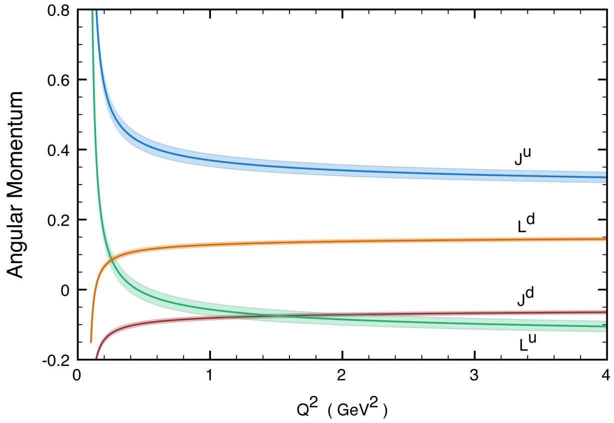

FIG. 11 Calculation of the NLO QCD evolution of J_u, L_d, J_d, L_u in the Cloudy Bag with model input scale $Q_0 = 0.4$ GeV (Thomas *et al.*, 2010).

$\Delta\Sigma$ (in full QCD) through Eq.(15) converges well. (Going to higher orders in the model fits to data and putting in pions raises the model input scale μ_0 needed for the calculations.) Table V compares the results of lattice calculations (Hägler *et al.*, 2008) for up- and down-quark spin and total angular momentum with the Cloudy Bag model results and the values extracted from QCD fits to hard exclusive reaction data, GPDs (Goloskokov and Kroll, 2009), and transverse single spin asymmetries, TMDs (Bacchetta and Radici, 2011). The lattice calculation involves connected diagrams only (no axial-anomaly contribution) plus chiral extrapolation. The QCD fit numbers are central values modulo (possibly large) systematic errors from the model functional forms of distributions used in the fits. There is good convergence of the different theoretical values with "data". Here, one has $L_u \sim -L_d \sim 15\%$ at the scale of typical deep inelastic measurements.

In an alternative approach, the proton spin puzzle has also been addressed in the Skyrme model, where baryons emerge as topological solitons in the meson fields at large number of colors N_c, and in the chiral quark soliton model (ChQSM), where explicit quark degrees of freedom are also present in the model. The nucleon's axial charges in these models are sensitive to which mesons are included in the model and the relative contribution of a quark source and pure meson component. In an early calculation Brodsky *et al.* (1988) found that $g_A^{(0)}$ vanishes in a particular version of the Skyrme model with just pseudoscalar mesons. Finite values of $\Delta s \sim -0.08$, close to the value obtained from inclusive g_1 measurements with good SU(3) assumed for $g_A^{(8)}$ are found in the ChQSM (Wakamatsu, 2007).

TABLE V Model, lattice and fit extractions of angular momentum contributions in the proton, quoted for 4 GeV^2 (except GPD at 2 GeV^2).

	Cloudy Bag	Lattice	GPD	TMD
Δu	0.85 ± 0.06	0.82 ± 0.07		
Δd	-0.42 ± 0.06	-0.41 ± 0.07		
J_u	0.30	0.24 ± 0.05	0.24	0.24
J_d	-0.04	0.00 ± 0.05	0.02	0.02

VII. TRANSVERSE NUCLEON STRUCTURE AND ORBITAL ANGULAR MOMENTUM

Confinement induces transverse hadronic scales in the nucleon with accompanying finite quark orbital angular momentum and finite spin-orbit couplings which can be probed in experiments. The search for orbital angular momentum has motivated new theoretical and experimental investigations of the three dimensional structure of the nucleon. Key observables in deeply virtual Compton scattering (DVCS) and transverse single spin asymmetries in lepton-nucleon and proton-proton scattering, and also the large x limit of the down quark helicity distribution are sensitive to orbital angular momentum in the nucleon.

Hard exclusive reactions such as DVCS are described theoretically using the formalism of generalized parton distributions (GPDs) and probe the three-dimensional spatial structure of the nucleon, as reviewed in Ji (1998), Goeke *et al.* (2001) and Diehl (2003). Ji has derived a sum-rule connecting the forward limit of GPDs to information about the quark and gluon total angular momentum in the proton (Ji, 1997b). Considerable experimental and theoretical effort has and continues to be invested aimed at accessing this information.

Studies of single spin asymmetries for semi-inclusive meson production in high-energy lepton-nucleon and proton-proton collisions are sensitive to possible spin-orbit coupling both in the nucleon and in the final-state hadronization process; for a recent review see Barone *et al.* (2010a). One studies correlations between the transverse momentum (orbital motion) of partons, their spin and the spin polarization of the nucleon. The theoretical tools are transverse momentum dependent (TMD) distributions and fragmentation functions. TMDs probe the three-dimensional transverse momentum structure of the nucleon and are associated, in part, with finite orbital angular momentum.

Experimental studies of three-dimensional nucleon structure have been pioneered at HERMES and JLab for GPDs and at COMPASS, HERMES and RHIC for TMDs in single spin asymmetry measurements. There has also been considerable theoretical effort aimed at model and lattice calculations of these observables.

In the rest of this Section we present the theory and present status of these new GPDs and TMD distributions plus spin-orbit coupling in fragmentation and the prospects for future experiments including key observables that will be studied. The aim for experiments should be to focus on observables that have the cleanest theoretical interpretation with minimal model dependence.

Quark orbital angular momentum in the nucleon may also be manifest in future measurements of the large x behavior of the polarized down-quark distribution $\Delta d/d$ and in the ratio of the proton's spin-flip Pauli form-factor to the Dirac form-factor at large Q^2. These observables can be studied with the 12 GeV upgrade of JLab. Valence Fock states with non-zero orbital angular momentum induce a logarithmic correction to the QCD counting rules predictions for these observables. Perturbative QCD calculations which take into account orbital angular momentum give

$$F_2/F_1 \sim (\log^2 Q^2/\Lambda^2)/Q^2 \tag{28}$$

for the ratio of Pauli to Dirac form-factors at large Q^2 (Belitsky *et al.*, 2003). Form-factor measurements at JLab (Gayou *et al.*, 2002; Jones *et al.*, 2000) are consistent with this behavior and also with $F_2/F_1 \sim 1/\sqrt{Q^2}$ for Q^2 between 4 and 6 GeV^2, in contrast to the counting rules prediction without orbital angular momentum $F_2/F_1 \sim 1/Q^2$ (Lepage and Brodsky, 1980). One also finds a logarithmic correction to the leading large-x behavior of the negative-helicity spin-dependent quark distributions $\sim (1-x)^5 \log^2(1-x)$ (Avakian *et al.*, 2007). An interesting prediction here is that $\Delta d/d$ should cross zero and become positive at a value $x \sim 0.75$ when this term is included, in contrast to the model expectation that crossing occurs at $x \sim 0.5$ when this orbital angular momentum effect is neglected. An accurate measurement of $\Delta d/d$ at x close to unity would be very interesting if this quantity can be extracted free of uncertainties from nuclear effects (Kulagin and Melnitchouk, 2008a,b) in the neutron structure functions measured from deuteron or ^{3}He targets.

A. Generalized parton distributions

Observables in deeply virtual Compton scattering and deeply virtual meson production are sensitive to information about total angular momentum in the nucleon. In these hard exclusive reactions a deeply virtual photon impacts on a nucleon target and a real photon or a meson is liberated from the struck nucleon into the final state, leaving the target nucleon intact. These processes can be described using the formalism of generalized parton distributions (GPDs), involving the Fourier transforms of off-diagonal nucleon matrix elements (Ji, 1997a,b; Mueller *et al.*, 1994; Radyushkin, 1997).

The important kinematic variables are the virtuality of the hard photon Q^2, the momenta $p-\Delta/2$ of the incident proton and $p+\Delta/2$ of the outgoing proton, the invariant four-momentum transferred to the target $t=\Delta^2$, the average nucleon momentum P, the generalized Bjorken variable $k^+ = xP^+$ and the light-cone momentum transferred to the target proton $\xi = -\Delta^+/2p^+$. In the Bjorken limit, ξ is related to Bjorken x_B via $\xi = x_B/(2-x_B)$. The generalized parton distributions are defined as the light-cone Fourier transform of the point-split matrix element[3]

$$\begin{aligned}
&\frac{P_+}{2\pi}\int dy^- e^{-ixP^+y^-}\,\langle p'|\bar\psi_\alpha(y)\psi_\beta(0)|p\rangle_{y^+=y_\perp=0} \\
&= \frac{1}{4}\gamma^-_{\alpha\beta}\Big[H(x,\xi,t)\bar u(p')\gamma^+ u(p) \\
&\qquad\qquad + E(x,\xi,t)\bar u(p')\sigma^{+\mu}\frac{\Delta_\mu}{2M}u(p)\Big] \\
&\quad + \frac{1}{4}(\gamma_5\gamma^-)_{\alpha\beta}\Big[\widetilde H(x,\xi,t)\bar u(p')\gamma^+\gamma_5 u(p) \\
&\qquad\qquad + \widetilde E(x,\xi,t)\bar u(p')\gamma_5\frac{\Delta^+}{2M}u(p)\Big].
\end{aligned} \tag{29}$$

The physical interpretation of the generalized parton distributions (before worrying about possible renormalization effects and higher order corrections) is the following. Expanding out the quark field operators in Eq. (29) in terms of light-cone quantized creation and annihilation operators one finds that for $x > \xi$ ($x < \xi$) the GPD is the amplitude to take a quark (anti-quark) of momentum $k - \Delta/2$ out of the proton and reinsert a quark (anti-quark) of momentum $k+\Delta/2$ into the proton some distance along the light-cone to reform the recoiling proton. In this region the GPD is a simple generalization of the usual parton distributions studied in inclusive and semi-inclusive scattering which are formally defined via light-cone correlation functions – see *e.g.* Bass (2005). In the remaining region $-\xi < x < \xi$ the GPD involves taking out (or inserting) a $q\bar q$ pair with momentum $k-\Delta/2$ and $-k-\Delta/2$ (or $k+\Delta/2$ and $-k+\Delta/2$) respectively. Note that the GPDs are interpreted as probability amplitudes rather than densities. The non-forward matrix elements give access to transverse degrees of freedom in the nucleon.

In the forward limit the GPDs H and $\tilde H$ are related to the parton distributions studied in deep inelastic scattering

$$\begin{aligned}
H(x,\xi,t)|_{\xi=t=0} &= q(x) \\
\widetilde H(x,\xi,t)|_{\xi=t=0} &= \Delta q(x)
\end{aligned} \tag{30}$$

---

[3] We work in the light-cone gauge $A_+ = 0$ (so the path-ordered gauge-link needed for gauge-invariance in the correlation function becomes trivial and set equal to one).

whereas the GPDs E and $\tilde{E}$ have no such analogue. Integrating over x the first moments of the GPDs are related to the nucleon form-factors

$$\begin{aligned}\int_{-1}^{+1} dx H(x,\xi,t) &= F_1(t)\\ \int_{-1}^{+1} dx E(x,\xi,t) &= F_2(t)\\ \int_{-1}^{+1} dx \widetilde{H}(x,\xi,t) &= G_A(t)\\ \int_{-1}^{+1} dx \widetilde{E}(x,\xi,t) &= G_P(t). \qquad (31)\end{aligned}$$

Here F_1 and F_2 are the Dirac and Pauli form-factors of the nucleon, and G_A and G_P are the axial and induced-pseudoscalar form-factors respectively. (The dependence on ξ drops out after integration over x.)

GPDs contain vital information about quark total angular momentum in the nucleon. Ji's sum-rule (Ji, 1997b) relates J_q to the forward limit of the second moment in x of the spin-independent quark GPDs

$$J_q = \frac{1}{2}\int_{-1}^{+1} dx x \Big[H^q(x,\xi,t=0) + E^q(x,\xi,t=0) \Big]. \qquad (32)$$

The gluon "total angular momentum" could then be obtained through the equation

$$\sum_q J_q + J_g = \frac{1}{2}. \qquad (33)$$

In principle, it could be extracted from precision measurements of the Q^2 dependence of DVCS at next-to-leading-order accuracy where the quark GPDs mix with glue under QCD evolution or via $J_g = \frac{1}{2}\int_{-1}^{+1} dx x\{H^g(x,\xi,t=0) + E^g(x,\xi,t=0)\}$ if the gluon GPD can be accurately measured in more direct experiments. In these equations J_q and J_g are defined through the proton matrix elements of the angular momentum operators in Eq.(26). If information about J_q can be extracted from experiments, then the corresponding quark "orbital angular momentum" can be deduced by subtracting the value of the quark spin content Δq extracted from deep inelastic scattering and polarized proton-proton collisions.

Experimental attempts to access J_q *via* Eq.(32) require accurate determination of the two unpolarized GPDs H and E. Measurements from a proton target are more sensitive to J_u, the total angular momentum carried by up quarks, while the neutron (via a deuteron or ^{3}He target) is most sensitive to J_d. The experiments require high luminosity to measure the small exclusive cross-section, plus measurements over a wide range of kinematics in Q^2, x and t (since sum-rule tests and evaluations depend on making reliable extrapolations into unmeasured kinematics). One also needs reliable theoretical technology to extract the GPDs from the measured cross-sections.

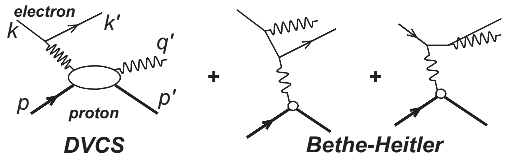

FIG. 12 The leading DVCS and Bethe-Heitler processes.

GPDs appear in the amplitudes for DVCS and hard exclusive meson production as convolutions with the hard scattering coefficient and only these so-called Compton form factors (CFF) are experimentally accessible. Varying the photon or meson in the final state gives access to different flavor combinations of GPDs, like in semi-inclusive DIS. However, meson production is more sensitive to QCD radiative corrections and power corrections in $1/Q$, and reliable theoretical description requires larger values of Q^2 compared to DVCS. Channels particularly sensitive to gluons in the proton are hard exclusive vector meson production where both quark and gluon GPDs appear at lowest order in the strong coupling constant. There is a challenging program to disentangle the GPDs from the formalism and to undo the convolution integrals which relate the GPDs to measured cross-sections. In practice, the approach used is to constrain models of GPDs against experimental data in measured kinematics. These models are then integrated to obtain the Ji moments of J_u and J_d, which may then be compared to the predictions of QCD inspired model plus lattice calculations – see Table V.

In the rest of this discussion we focus on deeply virtual Compton scattering.

1. Deeply virtual Compton scattering

Measurements of hard exclusive processes are much more challenging than traditional inclusive and semi-inclusive scattering experiments. These exclusive processes require a difficult full reconstruction of final state particles and their cross-sections are usually small, demanding high luminosity machines.

DVCS experiments have to be careful to choose the kinematics so as not to be saturated by a large Bethe-Heitler (BH) background where the emitted real photon is radiated from the incident lepton rather than from the proton target – see Fig. 12.

Most of the DVCS program so far has focused on the DVCS-BH interference term. Use of different combinations of beam and target polarization plus changing the electric charge of the incident lepton beam gives maximum access to most combinations of DVCS observables. Measurement of the DVCS-BH interference term – see Eq.(34) below – allows one to measure not only the size of the DVCS amplitude but also its phase – that is, it gives separate information about the real and imaginary parts of the Compton form factors.

Pioneering measurements of DVCS have been performed at DESY (HERMES, H1 and ZEUS) and JLab (Hall A and Hall B), which complement each other in the covered kinematic phase space and the extracted observables.

The experiments use different measurement techniques to access exclusive reactions. The HERA collider experiments at DESY, H1 and ZEUS, as well as CLAS (Hall B at JLab) have the advantage of nearly hermetic spectrometers, whereas the fixed target experiments HERMES and JLab Hall A had to deal with the restrictions caused by incomplete event reconstruction due to their forward spectrometers. Hall A and HERMES successfully employed the so-called missing mass technique together with careful background subtraction (Airapetian *et al.*, 2008b; Camacho *et al.*, 2006). For Hall A the low beam energy and high resolution spectrometer allowed one to resolve pure elastic scattering from associated production with an excited nucleon in the final state. The latter contribution was treated as part of the signal in HERMES results. Very recently, beam-spin asymmetries for a pure DVCS sample have also been reported by HERMES (Airapetian *et al.*, 2012c). In the fixed target experiments the spin-dependent DVCS cross-sections have been explored using longitudinally polarized lepton beams with longitudinally (JLab and HERMES) and transversely (HERMES) polarized targets. HERMES also took advantage of the available different beam charges.

JLab experiments focus on kinematics dominated by valence quarks. Data from Hall A suggest leading twist-2 dominance of DVCS even at the relatively low Q^2 of 1.5–2.3 GeV^2 (Camacho *et al.*, 2006).

The HERA collider experiments H1 and ZEUS measured the DVCS cross-section close to the forward direction with $\xi < 10^{-2}$, integrated over its azimuthal dependence, in an x_B range where two-gluon exchange plays a major role in addition to the leading order quark-photon scattering process. Figure 13 shows the cross-section differential in t for different ranges in Q^2 measured by H1 (Aaron *et al.*, 2008) and ZEUS (Chekanov *et al.*, 2009). The data are well described by the exponential behavior $d\sigma/dt \propto e^{-b|t|}$. The distribution of partons in the transverse plane is then obtained from this dependence by a Fourier transform with respect to Δ_T (the transverse momentum shift in Eq. (29)) $F(b, x, Q^2) \propto \int d^2\Delta_T \exp^{-ib\Delta_T} \sqrt{d\sigma/dt}$ (Burkardt, 2003; Diehl, 2002). The impact parameter provides an estimate of the transverse extension of the partons probed during the hard process. While DVCS data provide information about the transverse distribution of quarks in the proton, data on exclusive heavy vector meson production (J/Ψ or Υ) describe the transverse distribution of glue at specific values of x.

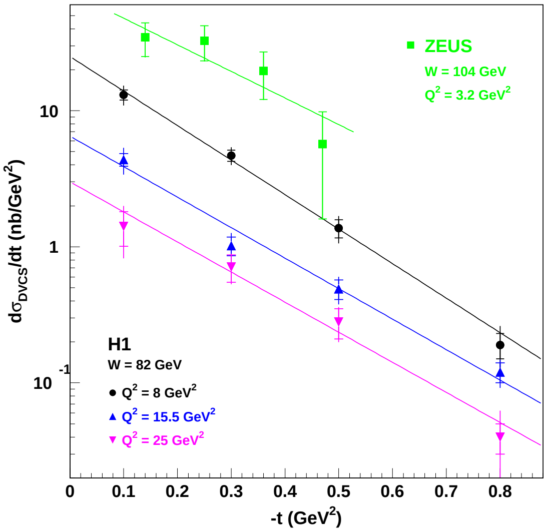

FIG. 13 The t dependence of the DVCS cross-section for several values of Q^2 as measured by H1 and ZEUS. The curves are results of fits of the form $e^{-b|t|}$ with b being related to the transverse extension of partons in the proton at a given x and Q^2 (see text).

The full DVCS cross-section reads (Diehl and Sapeta, 2005)

$$
\begin{array}{lll}
\multicolumn{3}{l}{d\sigma(\ell p \to \ell \gamma p) \sim} \\
d\sigma_{UU}^{BH} & + e_\ell \, d\sigma_{UU}^{I} & + d\sigma_{UU}^{DVCS} \\
+ P_\ell S_L \, d\sigma_{LL}^{BH} & + e_\ell P_\ell S_L \, d\sigma_{LL}^{I} & + P_\ell S_L \, d\sigma_{LL}^{DVCS} \\
+ P_\ell S_T \, d\sigma_{LT}^{BH} & + e_\ell P_\ell S_T \, d\sigma_{LT}^{I} & + P_\ell S_T \, d\sigma_{LT}^{DVCS} \\
 & + e_\ell P_\ell \, d\sigma_{LU}^{I} & + P_\ell \, d\sigma_{LU}^{DVCS} \\
 & + e_\ell S_L \, d\sigma_{UL}^{I} & + S_L \, d\sigma_{UL}^{DVCS} \\
 & + e_\ell S_T \, d\sigma_{UT}^{I} & + S_T \, d\sigma_{UT}^{DVCS} .
\end{array}
\tag{34}
$$

Here the first subscript U, L on $d\sigma$ indicates an unpolarized or longitudinally polarized lepton beam and the second subscript U, L, T denotes an unpolarized, longitudinally or transversely polarized proton target; P_ℓ is the lepton beam polarization; S_L and S_T denote longitudinal and transverse proton polarization. The various cross-section terms depend on the azimuthal angle ϕ between the lepton scattering plane and the photon production plane, and, in case of a transversely polarized proton target, also on the azimuthal angle ϕ_S between the lepton plane and the transverse target spin vector. Equation (34) indicates the large variety of observables accessible with polarized beams and/or targets.

Of particular interest is also the dependence on the sign of the charge of the beam lepton e_ℓ, which allows one to disentangle contributions from the pure interference term and the DVCS term as pioneered in Airapetian *et al.* (2007b, 2008b).

TABLE VI Linear combinations of Compton form factors (CFF) in the DVCS-BH interference terms. Here, F_1 and F_2 are the electromagnetic form factors. Subleading terms not shown are suppressed in a wide range of kinematics.

Target polarization	CFF combination
unpolarized / charge	$F_1 H + \xi(F_1 + F_2)\widetilde{H} - \frac{t}{4m^2} F_2\, E$
longitudinal	$F_1 \widetilde{H} + \xi(F_1 + F_2) H - \ldots$
transverse $\propto \sin(\phi - \phi_S)$	$F_2 H - F_1\, E + \ldots$
transverse $\propto \cos(\phi - \phi_S)$	$F_2 \widetilde{H} - F_1\, \xi \widetilde{E} + \ldots$

As an example for the azimuthal dependence of the cross-section we give the expression for the interference term for the case of an unpolarized target and polarized beam (Belitsky *et al.*, 2002)

$$I \propto -e_\ell \left(\sum_{n=0}^{3} c_n^I \cos(n\phi) + \lambda \sum_{n=1}^{2} s_n^I \sin(n\phi) \right) . \quad (35)$$

The proportionality involves a kinematic factor and the lepton propagators of the BH process; λ is the helicity of the incoming lepton. The Fourier coefficients c_n^I provide an experimental constraint on the real part of the Compton form factor and s_n^I on the imaginary part. Their relation to linear combinations of Compton form factors and hence to the respective GPDs is listed in Table VI. A specific Fourier coefficient can be accessed experimentally by weighting the cross-section with the respective azimuthal modulation.

The DVCS-BH interference term was extracted by varying the electric charge of the incident lepton (HERMES) and studying polarization observables, varying the beam or target helicity (JLab and HERMES). JLab experiments have focused on studying their accessible observables fully differentially. HERMES explored the advantages of using simultaneously polarization and charge observables to cleanly isolate the interference term and obtained the most complete set of DVCS observables measured so far providing access to all interference terms listed in Eq. (34).

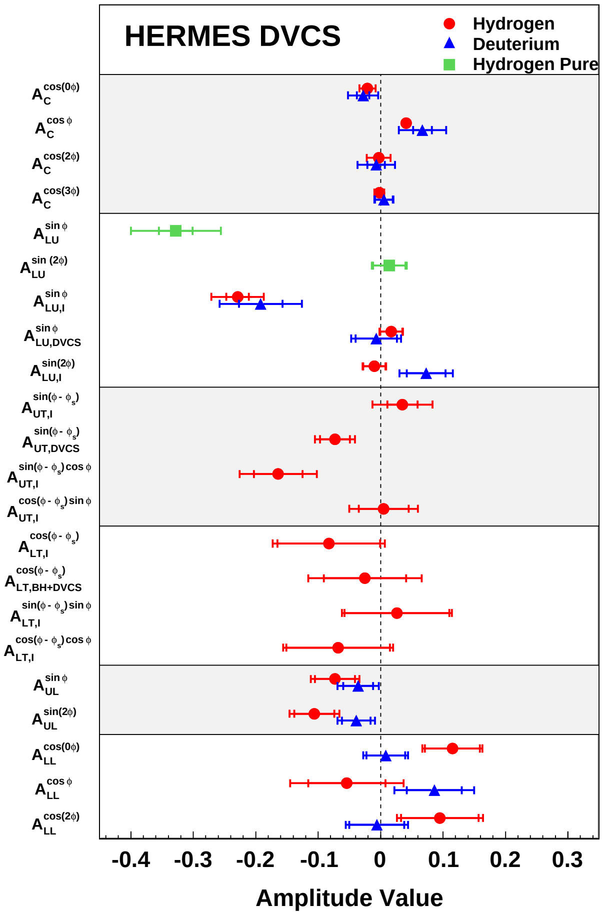

FIG. 14 Overview of all DVCS azimuthal asymmetry amplitudes measured at HERMES with proton and deuterium targets, given at the average kinematics.

Figure 14 shows a summary of the HERMES DVCS measurements with polarized proton and deuterium targets at their average kinematics (Airapetian *et al.*, 2008b, 2009c, 2010b,d, 2011a,b, 2012b,c). Here, A_C is the charge asymmetry and A_{XY} are the polarization-dependent asymmetries with X and Y indicating the beam and target polarization, respectively, which could be longitudinal (L) or transverse (T). The subscript I indicates an extraction of the pure interference term. The measured asymmetries are subject to a harmonic expansion with respect to the azimuthal angle(s) as given by the superscript of A_{XY} in the Figure. These data denoted by squares in Fig. 14 show results extracted from a DVCS sample with kinematically complete event reconstruction (Airapetian *et al.*, 2012c). The dependence on the kinematic variables t, Q^2, and x_B was explored for each observable.

An example of the high statistics data from JLab is shown in Fig. 15 for the beam-spin asymmetry A_{LU} measured fully differentially by CLAS (Girod *et al.*, 2008). The presented data contain an admixture of the $A_{LU,I}^{\sin\phi}$ and $A_{LU,DVCS}^{\sin\phi}$ contributions from the interference and pure DVCS terms, which cannot be separated here. CLAS also provides measurements of $A_{UL}^{\sin\phi}$ and $A_{UL}^{\sin 2\phi}$ (Chen *et al.*, 2006).

2. The quest for orbital angular momentum and GPD parametrizations

Of the two GPDs H and E entering Ji's sum-rule, Eq.(32), measurements with unpolarized targets but longitudinally polarized beams and also beam-charge asymmetries are mainly sensitive to H. As indicated

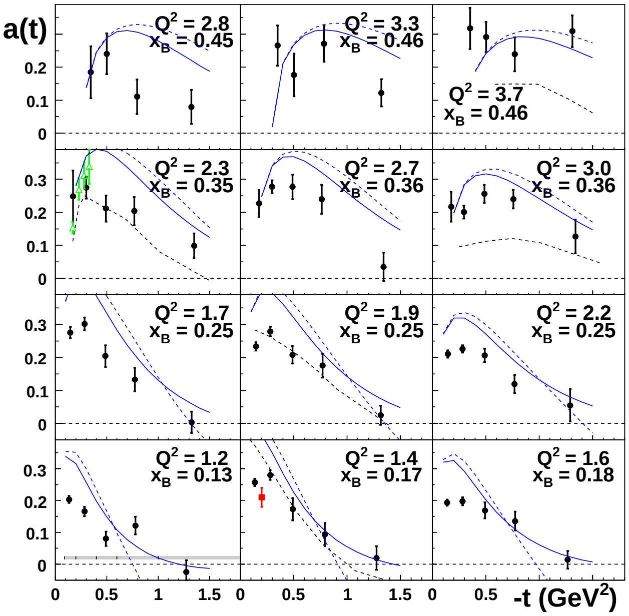

FIG. 15 The leading beam-spin asymmetry amplitude $a(t) = A_{LU}^{sin\phi}$ differential in t, x and Q^2 as measured by CLAS (Girod *et al.*, 2008). An earlier CLAS measurement (Stepanyan *et al.*, 2001) is indicated by the red square. The open green triangles represent the cross-section data from Hall A (Camacho *et al.*, 2006).

in Table VI, transverse target polarization provides kinematics-wise unsuppressed access to E. The GPD E is essentially unknown. In contrast to H, it is not related to a deep inelastic parton distribution in the forward limit; E describes helicity flip at the proton vertex and requires finite orbital angular momentum in the nucleon. Contributions from E to most DVCS observables are damped by kinematic factors $\sim |t|/M_p^2$, with the average $|t|$ value generally much smaller than 1 GeV^2 in the experiments. To access E requires DVCS and/or vector meson production asymmetry measurements with transversely polarized nucleon targets. It may also be accessed through the beam polarization dependence of DVCS with a neutron target because of the different size of the form-factors for the neutron (Belitsky *et al.*, 2002). Measurements have been performed already for all channels (Airapetian *et al.*, 2008b, 2009a; Mazouz *et al.*, 2007). Despite the lack of precision for these observables, attempts to extract information about quark total angular momentum have been performed by fitting theoretical models of GPDs to the DVCS measurements (Airapetian *et al.*, 2008b; Mazouz *et al.*, 2007). Although this analysis is very model dependent, the results agree (surprisingly) well with model and lattice expectations, *e.g.* the calculations reported in Table V. For example, within the model of Vanderhaeghen *et al.* (1999) JLab Hall A DVCS measurements from the neutron were interpreted to give $J_d + J_u/5.0 = 0.18 \pm 0.14(\text{expt.})$ (Mazouz *et al.*, 2007) whereas HERMES results from the proton gave $J_u + J_d/2.8 = 0.49 \pm 0.17(\text{expt.})$ (Airapetian *et al.*, 2008b) in the same model.

To go further and perform global fits of GPDs to hard exclusive observables one faces several challenging theoretical issues. Parameterizations of GPDs have to deal with two longitudinal variables instead of one plus the t dependence of DVCS. It is also not yet known whether relatively simple and smooth functions like those used in QCD fits to deep inelastic data are sufficient to describe GPDs. A reliable parameterization of GPDs might therefore require a larger number of moments than employed in usual QCD parton descriptions. In addition, the dependence of the functions on the variable x is not directly accessible, as x represents a mute variable which is integrated over. In the interpretation of DVCS observables one has to deal with complex amplitudes; the GPDs are embedded in the Compton form factors which relate to the measured cross-sections. Despite these complications and the early stage of global fitting for GPDs, many results have been obtained in recent years fitting to different hard exclusive scattering data. Interested readers are referred to the original literature in Vanderhaeghen *et al.* (1999), Goloskokov and Kroll (2008), Guidal (2010) Kumericki and Mueller (2010) and Goldstein *et al.* (2011). This phenomenology is complemented by progress in lattice QCD calculations of GPD moments (Brommel *et al.*, 2007; Göckeler *et al.*, 2007; Hägler *et al.*, 2008).

B. Transversity, transverse-momentum-dependent distributions and fragmentation functions

Striking single spin asymmetries associated with spin-momentum correlations (expected with parton orbital angular momentum) were first observed in the 1970s. Using a 12 GeV polarized proton beam from the Argonne National Laboratory Zero Gradient Synchrotron on a fixed target, up to 40% more positive pions were produced left of the beam when the beam was polarized up, and up to 20% more negative pions were produced to the right of the beam (Klem *et al.*, 1976). These measurements were confirmed by similar experiments (Antille *et al.*, 1980; Apokin *et al.*, 1990; Dragoset *et al.*, 1978; Saroff *et al.*, 1990), but it was not until the 1990s that a theoretical framework was developed to attempt interpreting them.

Single-spin asymmetries have now also been observed in proton-proton collisions at RHIC, where they reach up to ∼ 40%, and in lepton-nucleon collisions at COMPASS, HERMES and JLab, where they are typically $5 - 10\%$. Single-spin asymmetries for hadron production from transversely polarized targets tell us about spin-orbit coupling in the nucleon and/or in the fragmentation process. Transverse-momentum-dependent distributions simultaneously describe the dependence on longitudinal momentum fraction of the parton within the parent hadron as well as the parton's transverse momentum. Similarly, transverse-momentum-dependent fragmentation functions describe the dependence on longitudinal momentum fraction of the produced hadron with respect to the scattering parton as well as the hadronic transverse momentum with respect to the jet axis.

We next introduce these distributions and fragmentation functions, and discuss their phenomenology. In QCD there are eight leading-twist quark TMDs. These are listed in Table VII and discussed in Mulders and Tangerman (1996) and Bacchetta *et al.* (2007). The three distributions highlighted in boldface survive integration over transverse momentum k_t. These yield the unpolarized parton distribution, $f_1(x, k_t)$, the spin-dependent parton distribution $g_1(x, k_t)$ and the transversity distribution $h_1(x, k_t)$. The other five distributions do not survive integration over k_t. They describe correlations between the quark transverse momentum with the spin of the quark and/or the spin of the parent nucleon, *viz.* spin-orbit correlations. The three TMDs denoted by h describe the distribution of transversely polarized partons. They are chiral-odd distributions and appear only in observables involving two chiral-odd partners, such as Drell-Yan processes (two chiral-odd parton distributions) or SIDIS (chiral-odd parton distribution and the Collins fragmentation function discussed below). The three distributions $f_{1T}^{\perp}$ (the Sivers distribution), $h_1^{\perp}$ (the Boer-Mulders distribution) and $h_{1T}^{\perp}$ (pretzelosity) require orbital angular momentum in the nucleon since they involve a transition between initial and final nucleon states whose orbital angular momentum differ by $\Delta L_z^q = \pm 1$ (Sivers and Boer-Mulders) or $\Delta L_z^q = \pm 2$ (pretzelosity). The "worm-gear" functions $h_{1L}^{\perp}$ and $g_{1T}^{\perp}$ link two perpendicular spin directions and are also connected to quark orbital motion inside nucleons.

TABLE VII Leading-twist transverse-momentum dependent parton distributions. U, L, and T stand for unpolarized, longitudinally polarized, and transversely polarized nucleons (rows) and quarks (columns) respectively.

N \ q	U	L	T
U	$\mathbf{f_1}$		$h_1^{\perp}$
L		$\mathbf{g_1}$	$h_{1L}^{\perp}$
T	$f_{1T}^{\perp}$	g_{1T}	$\mathbf{h_1}$ $h_{1T}^{\perp}$

Transverse momentum distributions have been studied most in semi-inclusive DIS experiments where they appear in combination with the usual unpolarized fragmentation function $D(z, p_t)$ or, in case of the chiral-odd TMD distributions, with a chiral-odd Collins fragmentation function $H_1^{\perp}(z, p_t)$ discussed in Section VII.B.2. One measures the azimuthal distribution of the produced final-state hadron with respect to the virtual-photon axis. Each species of TMD comes with a different angular modulation in the semi-inclusive cross-section allowing it to be projected out to yield information about the different spin-momentum correlations (Bacchetta *et al.*, 2004). All these leading-twist TMDs have been measured in semi-inclusive DIS over the last decade. However, several have been the focus of more intense studies and we focus on those here.

The different modulation combinations are listed in Table VIII together with present experimental measurements. Results quoted at $\sqrt{s} = 18$ GeV are from COMPASS, 7.4 GeV from HERMES and 3.5 GeV from JLab. Here ϕ is the angle between the lepton direction and the plane spanned by the exchanged photon and tagged final-state hadron, *e.g.* a high-energy meson; ϕ_S is the angle between the lepton direction and the transverse nucleon target spin. The convolution is taken over the involved transverse momenta of the quark and the hadron produced in the fragmentation process.

When one projects out the terms with different azimuthal angular dependence summarized in Table VIII, the COMPASS, HERMES and JLab data suggest that the Sivers, Collins and Boer-Mulders effects are all present in the proton target data – see below. JLab data from CLAS reveal a clear signal for the worm-gear-1 distribution; there is some hint for a non-zero worm-gear-2 distribution (with low significance) and (so far) no significant signal for pretzolosity in the proton. For the deuteron target, there is evidence for a Boer-Mulders effect from COMPASS and HERMES. The Sivers, Collins, worm-gear and pretzelosity effects are all consistent with zero in the deuteron target data. The Collins and Sivers effects observed in the proton data therefore contain a predominant isovector contribution.

We next focus on the Sivers, Boer-Mulders and Collins effects.

1. The Sivers and Boer-Mulders TMD distributions

The Sivers distribution was first proposed in Sivers (1990) in an attempt to explain the large transverse single spin asymmetries observed in the 1970s and 1980s. It describes the correlation between the transverse momentum k_t of the struck quark and the spin S and momentum

TABLE VIII Experimental access to the leading twist TMD distributions in SIDIS with unpolarized (U), longitudinally (L) or transversely polarized (T) beam (modulation first subscript) and/or target (modulation second subscript).

Modulation	Combination Distribution name	$\sqrt{s}$ GeV	Target type	Observed hadron types	Measurement
$\sin(\phi+\phi_S)_{UT}$	$h_1 \otimes H_1^\perp$	18	d	$h^\pm, \pi^\pm, K^\pm, K^0$	Ageev *et al.* (2007) and Alekseev *et al.* (2009a)
	Transversity		p	$h^\pm$	Adolph *et al.* (2012a) and Alekseev *et al.* (2010b)
			p	$\pi^\pm, K^\pm$	prelim. Pesaro (2011)
		7.4	p	$\pi^\pm, \pi^0, K^\pm$	Airapetian *et al.* (2005b, 2010a)
		3.5	n	$\pi^\pm$	Qian *et al.* (2011)
$\sin(\phi-\phi_S)_{UT}$	$f_{1T}^\perp \otimes D$	18	d	$h^\pm, \pi^\pm, K^\pm, K^0$	Ageev *et al.* (2007) and Alekseev *et al.* (2009a)
	Sivers		p	$h^\pm$	Adolph *et al.* (2012b) and Alekseev *et al.* (2010b)
			p	$\pi^\pm, K^\pm$	prelim. Pesaro (2011)
		7.4	p	$\pi^\pm, \pi^0, K^\pm$	Airapetian *et al.* (2005b, 2009b)
		3.5	n	$\pi^\pm$	Qian *et al.* (2011)
$\cos(2\phi)_{UU}$	$h_1^\perp \otimes H_1^\perp$	18	d	$h^\pm$	prelim. Sbrizzai (2011)
	Boer-Mulders	7.4	p	$\pi^\pm, K^\pm$	Airapetian *et al.* (2012a)
		3.5	n	π^+	Osipenko *et al.* (2009)
$\sin(3\phi-\phi_S)_{UT}$	$h_{1T}^\perp \otimes H_1^\perp$	18	d	$h^\pm$	prelim. Kotzinian (2007)
	Pretzelosity	18	p	$h^\pm$	prelim.Parsamyan (2011)
		7.4	p	$\pi^\pm, K^\pm$	prelim. Pappalardo (2010)
$\sin(2\phi)_{UL}$	$h_{1L}^\perp \otimes H_1^\perp$	18	d	$h^\pm$	Alekseev *et al.* (2010a)
	Worm-gear 1	7.4	p	$\pi^\pm, \pi^0$	Airapetian *et al.* (2000b, 2001)
			d	$\pi^\pm, \pi^0, K^+$	Airapetian *et al.* (2003)
		3.5	n	$\pi^\pm, \pi^0$	Avakian *et al.* (2010)
$\cos(\phi-\phi_S)_{LT}$	$g_{1T}^\perp \otimes D$	18	d	$h^\pm$	prelim. Kotzinian (2007)
	Worm-gear 2	18	p	$h^\pm$	prelim.Parsamyan (2011)
		7.4	p	$\pi^\pm, \pi^0, K^\pm$	prelim. Pappalardo and Diefenthaler (2011)
		3.5	n	$\pi^\pm$	Qian (2012)

p of its parent nucleon

$$f_{q/p^\uparrow}(x, k_t) = f_1^q(x, k_t^2) - f_{1t}^{\perp q}(x, k_t)\frac{\mathbf{S}\cdot(\mathbf{k_t}\times\hat{\mathbf{p}})}{M}. \quad (36)$$

The k_t dependence means that the Sivers distribution is sensitive to non-zero parton orbital angular momentum in the nucleon, though the mapping from Sivers observables to quark (and gluon) orbital angular momentum is (so far) model dependent with present theoretical technology.

The Sivers distribution has the interesting property that it is odd under time reversal. Due to this feature, such a correlation was believed to be forbidden for more than a decade. Then Brodsky *et al.* (2002a,b) showed that, with initial- or final-state interactions, the Sivers effect could be non-zero in QCD processes. Final-state interactions in SIDIS can generate the azimuthal asymmetry before the quark fragments into hadrons. Shortly afterwards, Collins (2002) realized that initial-state color interactions in the case of Drell-Yan and final-state interactions in the case of SIDIS would lead to a process-dependent sign difference in the Sivers distribution. SIDIS measurements (Adolph *et al.*, 2012b; Airapetian *et al.*, 2005b, 2009b; Alekseev *et al.*, 2010b; Pesaro, 2011; Qian *et al.*, 2011), suggest sizable asymmetries at the level of about 5 – 10% for a proton and a neutron target, while Drell-Yan measurements are planned for the future.

A qualitative picture of the Sivers distribution can al-

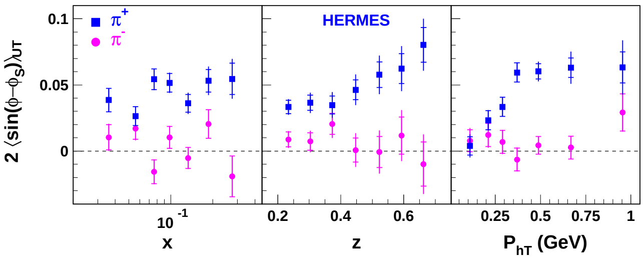

FIG. 16 Sivers amplitudes for charged pions measured by HERMES with a proton target (Airapetian *et al.*, 2009b). The Sivers amplitudes for K^+ (not shown here) appear to be nearly twice as large as those for π^+.

ready be deduced from SIDIS measurements. The nonzero amplitudes shown in Figs. 16 and 17 were obtained with a proton target. For HERMES the amplitude includes a kinematic factor depending on the ratio of transverse-to-longitudinal photon flux, which in the COMPASS data is divided out. Since scattering off u quarks dominates these data due to the quark charge factor, the positive Sivers amplitudes for π^+ (and h^+, which is dominated by the pion yield), suggest a large and negative Sivers function for up quarks. The vanishing amplitudes for π^- (h^-) require cancellation effects, *e.g.* from a d quark Sivers distribution opposite in sign to the u quark Sivers distribution. These cancellation effects between Sivers distributions for up and down quarks are supported by the vanishing Sivers amplitudes extracted from deuteron data by the COMPASS Collaboration (Ageev *et al.*, 2007; Alekseev *et al.*, 2009a). An interesting facet of the HERMES data is the magnitude of the K^+ amplitude, which is nearly twice as large as that of π^+ (Airapetian *et al.*, 2009b). Again, on the basis of u quark dominance, one might naively expect that the π^+ and K^+ amplitudes should be similar. Their difference in size may thus point to a significant role of other quark flavors, *e.g.* sea quarks. A sizable Sivers amplitude for π^+ was also recently reported by JLab Hall A (Qian *et al.*, 2011) for measurements with a ^{3}He (neutron) target. In that data a negative Sivers amplitude for π^+ was found which independently supports a d-quark Sivers distribution opposite in sign to the u-quark one.

The Boer-Mulders distribution (Boer and Mulders, 1998) describes the correlation between transversely polarized quarks in an unpolarized nucleon and the quarks' transverse momentum, $\mathbf{s_q} \cdot (\mathbf{k_t} \times \hat{\mathbf{p}})$, where s_q denotes the spin of the quark and might hence yield unexpected spin effects even in an unpolarized nucleon. It is similar to the Sivers distribution in that it is T-odd. However, it is also chiral-odd and hence must be probed in conjunction with a second chiral-odd function. For Drell-Yan production, the second function is a Boer-Mulders distribution in the second incident hadron. For SIDIS, the Collins fragmentation function described below is involved. Like the T-odd Sivers distribution, the Boer-Mulders distribution is also expected to change sign between Drell-Yan production and SIDIS. Future experimental effort is planned to test this QCD prediction.

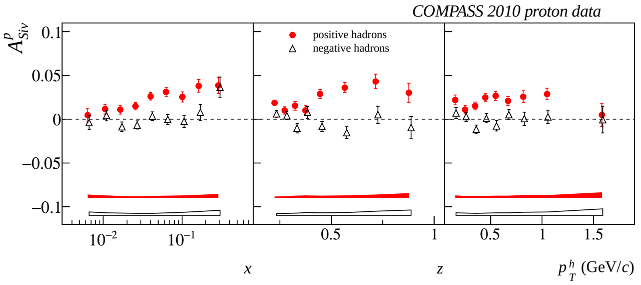

FIG. 17 Sivers amplitudes for unidentified charged hadrons measured by COMPASS with a proton target (Adolph *et al.*, 2012b). The hadron yield is dominated by pions.

Azimuthal distributions sensitive to the Boer-Mulders distribution were originally measured in Drell-Yan experiments (Conway *et al.*, 1989; Falciano *et al.*, 1986; Guanziroli *et al.*, 1988; Zhu *et al.*, 2007, 2009). The SeaQuest fixed-target Drell-Yan experiment currently underway at Fermilab (Reimer, 2007) expects to be sensitive to the Boer-Mulders distribution at high x. In SIDIS the distinctive pattern of Boer-Mulders modulations for oppositely charged pions and for pions and kaons was recently reported by HERMES (Airapetian *et al.*, 2012a). The amplitudes for kaons are larger in magnitude than the amplitudes for pions. The amplitudes for the negative pions have the opposite sign to the amplitudes for negative kaons. This hints at a significant contribution from sea quarks, in particular from strange quarks. Measurements of the Boer-Mulders amplitudes were also reported by COMPASS for unidentified hadrons (Sbrizzai, 2011) and by CLAS for pions (Osipenko *et al.*, 2009). The interpretation of the SIDIS amplitudes for the Boer-Mulders distribution, is, however, complicated by contributions from the twist-4 Cahn effect (Cahn, 1978, 1989) which have been estimated to be sizable even at COMPASS kinematics (Anselmino *et al.*, 2007b). The Cahn effect accounts for the parton intrinsic transverse momenta in the target nucleon and the fact that produced hadrons might acquire transverse momenta during the fragmentation process. Theoretical estimates of the Boer-Mulders effect are still plagued by large uncertainties, mainly related to the insufficient knowledge of the transverse-momentum dependence of the unpolarized distribution $f_1(x, k_t)$ and fragmentation function $D(z, p_t)$.

2. The Collins TMD fragmentation function

The Collins TMD fragmentation function describes a spin-momentum correlation in the hadronization process, $\mathbf{s_q} \cdot (\mathbf{k_q} \times \mathbf{p_t})$, with a hadron produced in fragmentation having some transverse momentum p_t with respect to the momentum direction k of a transversely polarized fragmenting quark with spin s_q (Collins, 1993; Collins *et al.*, 1994). The Collins fragmentation function has been investigated in semi-inclusive lepton-nucleon scattering and e^+e^- annihilation. The magnitude of the effect is approximately 5–10%, like that found for the Sivers asymmetries.

For e^+e^- annihilation the chiral-odd Collins fragmentation function enters with a second Collins function in the opposing jet. The Collins function has been measured to be non-zero for the production of charged pions in

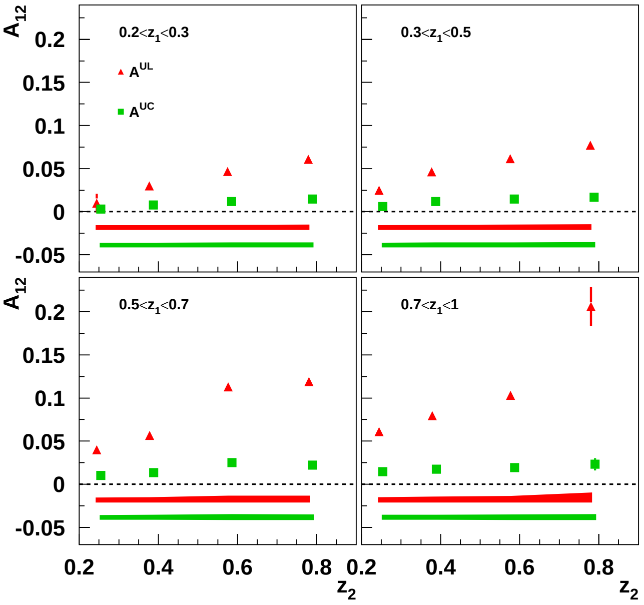

FIG. 18 Collins asymmetry for the double ratios of like-sign (L), unlike-sign (U) and any charged (C) pion pairs from Belle (Seidl *et al.*, 2008). A^{UL} and A^{UC} are sensitive to different combinations of the favored and unfavored Collins fragmentation functions.

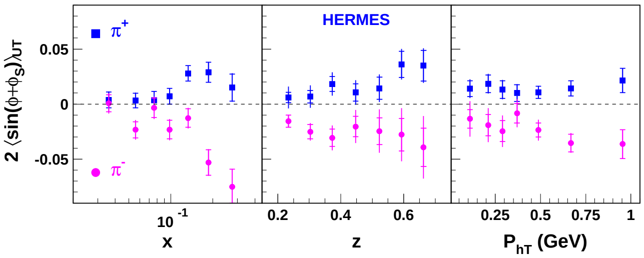

FIG. 19 Collins amplitudes for charged pions measured by HERMES with a proton target (Airapetian *et al.*, 2010a).

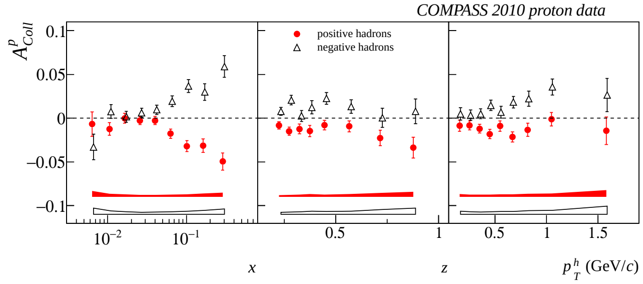

FIG. 20 Collins amplitudes for unidentified charged hadrons measured by COMPASS with a proton target (Adolph *et al.*, 2012b). The hadron yield is dominated by pions. Note that a different definition of the Collins angle results in amplitudes with the opposite sign compared to other measurements.

e^+e^- annihilation at Belle (Abe *et al.*, 2005; Seidl *et al.*, 2008), as shown in Fig. 18, and in recent preliminary data from BABAR (Garzia, 2012).

In SIDIS the second chiral-odd function is the transversity distribution introduced in Section II and discussed further below (or the Boer-Mulders distribution). The HERMES (Airapetian *et al.*, 2005b, 2010a), COMPASS (Adolph *et al.*, 2012a; Ageev *et al.*, 2007; Alekseev *et al.*, 2009a, 2010b; Pesaro, 2011) and JLab Hall A (Qian *et al.*, 2011) experiments have performed SIDIS measurements of the Collins effect. The measurements for a proton target are shown in Figs. 19 and 20 for HERMES and COMPASS respectively. (Note that COMPASS uses a definition of the Collins angle which results in Collins amplitudes with opposite sign to the "Trento convention" of Bacchetta *et al.* (2004) used by HERMES, JLab and commonly in theoretical papers). There is excellent agreement between the measurements in similar kinematics. One finds the striking observation that the Collins amplitude for π^- is of similar size to π^+ production but comes with opposite sign. This hints at an unfavored Collins function of similar size and opposite sign than the favored one, a situation very different from that observed with unpolarized fragmentation functions.

3. Probing transversity

The transversity distribution introduced in Section II describes the transverse polarization of quarks within a transversely polarized nucleon. Along with the unpolarized and helicity distributions, it survives integration over partonic transverse momentum and is thus a collinear distribution.

The first moment of the transversity distribution is proportional to the nucleon's C-odd tensor charge, *viz.* $\delta q = \int_0^1 dx h_1^q(x)$ with

$$\langle p, s|\; \bar{q} i \sigma_{\mu\nu} \gamma_5 q \;|p, s\rangle = (1/M)(s_\mu p_\nu - s_\nu p_\mu)\delta q. \quad (37)$$

The difference between the transversity and helicity spin distributions reflects the relativistic character of quark motion in the nucleon. In Bag models this effect is manifest as follows. The lower component of the Dirac spinor enters the relativistic spin depolarization factor with the opposite sign to Δq because of the extra factor of γ_μ in the tensor charge (Jaffe and Ji, 1992). The relativistic Bag depolarization factor mentioned in Section VI becomes 0.83 for transversity in contrast to 0.65 for helicity and the nucleon's axial-charges. In leading order QCD the transversity distributions are bound by Soffer's inequality $|h_1^q(x,Q^2)| \leq \frac{1}{2}[\{q+\bar{q}\}(x,Q^2) + \Delta q(x,Q^2)]$, Soffer (1995). QCD motivated fits to transversity observables are reported in Anselmino *et al.* (2009b), which also reviews the comparison to model predictions.

Transversity is measured through the Collins effect and also in in dihadron production, where the chiral-odd partner of h_1^q is given by the dihadron fragmentation function $H_1^{\sphericalangle q}$ (Bacchetta *et al.*, 2011; Bianconi *et al.*, 2000; Collins *et al.*, 1994). This describes how the transverse spin of the fragmenting quark is transferred to the relative orbital angular momentum of the hadron pair. Consequently, this mechanism does not require transverse momentum of the produced hadron pair. Standard collinear factorization applies allowing one to study the transversity distribution without having to worry about solving convolution integrals over transverse momentum or issues of TMD factorization and evolution.

Pioneering measurements of two-pion production in polarized semi-inclusive DIS by HERMES (Airapetian *et al.*, 2008a) and COMPASS (Adolph *et al.*, 2012d) reveal a sizable effect and have already been employed for an extraction of transversity (Courtoy *et al.*, 2012a). First measurements of azimuthal correlations of two pion pairs in back-to-back jets in e^+e^- annihilation related to the dihadron fragmentation function have just become available from Belle (Vossen *et al.*, 2011) and a first extraction of the dihadron fragmentation function from these data was performed in Courtoy *et al.* (2012b).

4. Current status and recent progress with TMD distributions

There has been considerable progress in the understanding of intrinsic transverse momentum and spin-momentum correlations in QCD over the past decade, motivated by the theoretical breakthroughs regarding T-odd TMD distributions (Brodsky *et al.*, 2002a,b; Collins, 2002) and by a vast program of theoretical and experimental activity.

A recent monograph, Collins (2011) gives definitions of TMD distributions which allow QCD evolution to be applied rigorously for the first time with separately identifiable TMD distributions and fragmentation functions. Building upon this progress, the evolution of previously unevolved models and fits has now been published for unpolarized TMD distributions and fragmentation functions (Aybat and Rogers, 2011b) and the Sivers distribution (Aybat *et al.*, 2012). QCD evolution is just starting to be applied to phenomenological studies (Aybat *et al.*, 2011), which will be a major step forward in interpreting and comparing results from different experiments. The new definitions of TMD distributions also recently made possible a determination of the hard parts for SIDIS and Drell-Yan at next-to-leading order (Aybat and Rogers, 2011a), which should lead to improved phenomenology.

Much effort has been dedicated to phenomenological extractions of TMDs and parameterizations of the Sivers distribution from SIDIS data, see e.g. Anselmino *et al.* (2009a) and Anselmino *et al.* (2011), with QCD evolution now starting to be considered (Anselmino *et al.*, 2012). One parameterization of the Sivers function includes both semi-inclusive deep inelastic and proton-proton data (Kang and Prokudin, 2012), modulo issues related to factorization breaking (Rogers and Mulders, 2010) discussed below. Fits to the Collins TMD fragmentation function have been performed using both e^+e^- and SIDIS data as input (Anselmino *et al.*, 2007a; Efremov *et al.*, 2006). The Boer-Mulders distribution has been extracted based on Drell-Yan (Lu and Schmidt, 2010; Zhang *et al.*, 2008) as well as SIDIS data (Barone *et al.*, 2010b).

These first phenomenological fits to TMD observables have been performed using a simple Gaussian ansatz for the transverse momentum dependence of quarks in the nucleon and fragmentation functions. For example, the Sivers function in Eq.(36) was parametrized in the fits by the product of the unpolarized distribution $f_{q/p^\uparrow}(x, k_t)$ with an x dependent factor and an x-independent Gaussian $\sim \frac{k_t}{M_1} e^{-k_t^2/M_1^2}$ containing all the k_t dependence. While the Gaussian ansatz is unstable with respect to QCD evolution with increasing Q^2, the method does provide a reasonable fit to present data with values $\langle k_t^2 \rangle = 0.25\text{GeV}^2$ and $\langle p_t^2 \rangle = 0.20\text{GeV}^2$ taken from fits to the Cahn effect in unpolarized scattering (Anselmino *et al.*, 2005). A longer term goal for TMD experiments is to observe deviation from Gaussian behavior for transverse momentum dependence. With extensive unpolarized Drell-Yan and weak boson production data available over scales from ~ 4 GeV^2 to M_Z^2, new fits of unpolarized TMD distributions are quite promising as a means to test the Q^2 evolution of TMD distributions as well as to learn more about the shape of the distributions in k_t.

Lattice calculations of the Sivers and Boer-Mulders distributions have been performed (Göckeler *et al.*, 2007; Hägler *et al.*, 2009; Musch *et al.*, 2012). There have also been efforts in recent years to implement TMDs in Monte Carlo event generators (Bianconi, 2011; Hautmann *et al.*, 2012). Models can provide helpful insight into TMD distributions, and a wealth of different model calculations have been explored and published. We refer to Avakian *et al.* (2009), Bacchetta (2012), Lorce and Pasquini (2011), and Pasquini and Schweitzer (2011) for recent discussion of models related to TMD distributions, including attempts to address the relationship between TMD distributions and orbital angular momentum in the nucleon

5. Proton-proton asymmetries and TMD-factorization breaking

Despite the fact that the large transverse single spin asymmetries observed in hadronic scattering originally inspired the development of TMDs, inclusive hadron production in $p + p$ scattering cannot be cleanly separated into Sivers, Collins, or other contributions as is possible in SIDIS. In recent work Rogers and Mulders (2010)

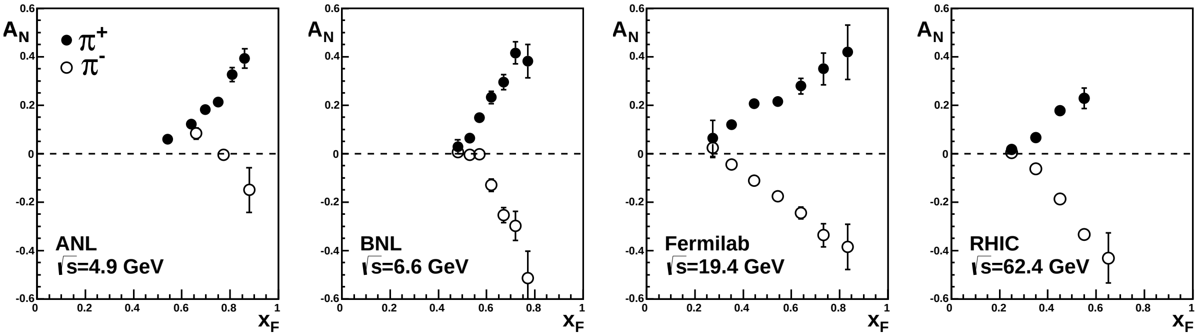

FIG. 21 The transverse single spin asymmetry in forward $\pi^{\pm}$ production as measured in polarized proton-proton collisions across a range of center-of-mass energies. From left to right, the data are from Klem *et al.* (1976), Allgower *et al.* (2002), Adams *et al.* (1991), and Arsene *et al.* (2008).

argue that the TMD framework is not valid in the case of hadroproduction of hadrons, as factorization does not hold. While the short-distance (perturbative) components are still believed to factorize from the long-distance (non-perturbative) ones, the long-distance components become entangled and no longer factorize from one another into independent TMD distributions and/or fragmentation functions. What is particularly interesting is that the factorization breaking effects are relevant in precisely the kinematic regime where a parton description is generally expected to apply. It will be exciting to see this tested experimentally in the upcoming years, exploring long-distance quantum entanglement effects in QCD. In the longer-term future, it may be possible to develop well-defined functions within the framework of pQCD which describe the correlations between the partons in the incoming and/or outgoing hadrons.

In the meantime, single spin asymmetries for forward meson production in $p+p$ collisions have been shown to remain large across a very wide range of center-of-mass energies (Abelev *et al.*, 2008a; Adams *et al.*, 1991, 1996; Allgower *et al.*, 2002; Arsene *et al.*, 2008) and up to the highest measured p_T of ~5 GeV (Koster, 2012). As shown in Fig. 21, the transverse single spin asymmetries in charged pion production as a function of Feynman-x are remarkably similar from $\sqrt{s}$ =4.9 GeV all the way up to 62.4 GeV measured by the BRAHMS experiment at RHIC.

At higher energies and in particular at p_T values large enough to serve as a hard scale, one can try to interpret these phenomena utilizing the tools of pQCD. With no explicitly measured scale sensitive to the partonic transverse momentum in inclusive single spin asymmetries, a more appropriate framework than TMD distributions in which to interpret the asymmetries may be a collinear, twist-3 picture (Efremov and Teryaev, 1982, 1985; Qiu and Sterman, 1999). A relationship between the TMD and the collinear, twist-3 frameworks was laid out in Ji *et al.* (2006).

Surprises continue to emerge from these kinds of measurements, with large asymmetries for negative kaons as well as antiprotons from BRAHMS (Arsene *et al.*, 2008) suggesting that the pion asymmetries are not a valence quark effect as previously believed, and a recent hint from STAR (Adamczyk *et al.*, 2012c) that the asymmetry for eta mesons may be larger than that of neutral pions.

VIII. FUTURE PROJECTS

A new program of dedicated experiments is planned to investigate key open questions in QCD spin physics. We briefly outline these experiments and their prime physics objectives.

Since May 2012 CEBAF is undergoing a major upgrade that will bring the maximum available energy of the electron beam to 12 GeV. The experimental equipment in all three halls will be upgraded (Hall A and C) or completely renewed (Hall B), in order to better match the increased energy and luminosity. A new experimental Hall D is being built. Commissioning of the new accelerator and of the experimental halls is expected for 2014. The future physics program focuses on dedicated studies of large x phenomena, hard exclusive reactions and TMD effects in kinematics where valence quarks dominate the physics (Dudek *et al.*, 2012).

At CERN a proposal by the COMPASS Collaboration (Gautheron *et al.*, 2010) to study TMDs and GPDs in the period 2014–2017 has been approved. The COMPASS data will provide a link between the kinematic domains of HERA on one hand and of HERMES and JLAB on the other. The program will start with the first ever polarized Drell–Yan experiment using a transversely polarized ammonia (proton) target and a negative pion beam. Due to the underlying annihilation of the anti up-quark from the pion and the target up quark, the process is dominated by the up quark distribution in the valence region. An important goal is to check the QCD prediction of a sign change in the naive T-odd TMDs with respect to the DIS case. A study of GPDs in DVCS and hard exclusive meson production with a polarized muon beam will follow in 2015 using a liquid hydrogen target, a dedicated target recoil detector and an additional large-angle electromagnetic calorimeter. An important measurement is the beam charge-and-spin asymmetry, which uses the property of the muon beam that polarization changes sign when going from positive to negative muons. A first result on the correlation of transverse size and longitudinal momentum fraction might already be expected from a 2012 pilot run. In parallel semi-inclusive DIS data will be taken on the pure hydrogen target.

There are proposals to create a polarized fixed-target Drell-Yan program at Fermilab following the SeaQuest experiment, scheduled to complete data taking in 2014. R&D has begun for a suitable polarized target, and a formal proposal to polarize the 120 GeV proton beam in the Main Injector has been submitted to Fermilab management (Courant *et al.*, 2011). One of the primary physics motivations for such a program would be to explore in detail the QCD spin-momentum correlations described by TMD distributions such as the Sivers distribution, in particular the role of color flow in Drell-Yan versus semi-inclusive DIS interactions.

A variety of possibilities for the medium-term future of RHIC is currently under discussion. R&D is ongoing for a polarized ^{3}He source for RHIC (Zelenski *et al.*, 2008), which would allow the neutron spin structure to be studied in collider kinematics for the first time. There are also proposals to significantly extend the detector capabilities at RHIC; see e.g. Aidala *et al.* (2012). Of particular interest to nucleon structure studies are potential upgraded forward spectrometers capable of reconstructing jets, with hadronic particle identification and Drell-Yan measurement capabilities up to pseudorapidities of ~ 4. The ability to perform full jet reconstruction in the forward region where large transverse single spin asymmetries are observed, and in addition to measure and identify hadrons within the jet, would allow separation of effects due to distribution versus fragmentation functions and shed great light on the origin of these significant spin-momentum correlations. An integrated design process for new detectors is underway such that they would be able to take full advantage of electron-proton and electron-ion collisions in the longer-term future should an electron beam be added to RHIC.

Ideas for future polarization measurements are also discussed and investigated in more detail at FAIR (Germany), J-PARC (Japan) and NICA (Russia).

A possible Electron-Ion Collider (EIC) is being discussed in connection with the future of RHIC and JLab. The goal is to achieve highly polarized (greater than 70%) electron and light-nucleus beams with center-of-mass energies ranging from about 20–150 GeV at maximum collision luminosities typically $\sim 10^{34}$ cm^{-2} s^{-1}. Significant R&D is ongoing to realize the technical challenges for reaching this luminosity frontier for colliders and for achieving and maintaining polarization of light nuclei (D and ^{3}He) in a storage ring. An EIC with the above performance would offer unique access to the small-x region where gluons dominate as well as to the intermediate and high x regions at unprecedented high Q^2. One could then study gluon polarization down to x values of about 10^{-4} (Aschenauer *et al.*, 2012). The high luminosity would enable us to measure and map GPDs over a broad range of the kinematic variables and study the QCD evolution of the DVCS process plus TMD distributions in kinematics where sea/glue effects are expected to be important. In addition to being the first *ep* collider exploring the structure of polarized protons, an EIC would also be the first electron-nucleus collider allowing precision studies of the gluon and sea quark structure of nuclei. Unpolarized ion beams from deuterium to the heaviest nuclei – uranium or lead – would also be accelerated. Knowledge about the spatial distribution of quarks and gluons in nuclei is needed for example in the interpretation of heavy-ion collision data and the search for quark-gluon plasma. A comprehensive review of EIC physics opportunities is given in Boer *et al.* (2011).

IX. CONCLUSIONS AND OUTLOOK

The challenge to understand the internal spin structure of the nucleon has inspired a global program of enormous experimental and theoretical work in QCD during the last 25 years.

For longitudinal spin structure, there is a good convergence of spin measurements from CERN, DESY, JLab, RHIC and SLAC taking into account the Q^2 dependence of the data and kinematics of the different experiments. There is also good convergence of theoretical understanding with the data, including QCD inspired models of the nucleon and lattice calculations with disconnected diagrams included. Semi-inclusive measurements in polarized lepton-nucleon and proton-proton collisions have yielded much information about the size of the separate valence, sea and gluon spin contributions to the nucleon's spin. The small value of the nucleon's flavor-singlet axial-charge, about 0.35, extracted from polarized deep inelastic scattering seems to be a valence quark effect. No significant sea-quark polarization is observed in semi-inclusive deep inelastic scattering experiments; the sum of valence spin contributions is in close agreement with the measured total spin contribution $g_A^{(0)}|_{\rm pDIS}$. While gluon polarization Δg at the scale of the experiments may be as much as 50% of the nucleon's spin at the scale of the experiments, the QCD anomaly correction $-3\frac{\alpha_s}{2\pi}\Delta g$ is too small to resolve the difference between $g_A^{(0)}|_{\rm pDIS}$ and the early quark models predictions, about 0.6. Prime theory candidates to explain the small "quark spin content" include transfer of valence quark spin to quark orbital angular momentum through the pion cloud and a possible topological effect whereby some fraction of the valence quarks' "spin" resides at Bjorken $x = 0$, where it is missed by polarized deep inelastic scattering experiments. The proton spin puzzle seems to be telling us about the interplay of valence quarks with chiral dynamics and the complex vacuum structure of QCD. Ongoing and planned experimental activity will improve the precision on the size of gluon and strangeness polarization in the nucleon.

Finite orbital angular momentum of the valence quarks is expected, induced also by confinement which introduces a transverse scale in the physics. Quark orbital angular momentum through spin-orbit coupling is a prime candidate to explain the large transverse single spin asymmetries observed in proton-proton collisions and lepton-nucleon scattering. The desire to understand and measure QCD orbital angular momentum effects in the nucleon has spawned a new program to explore and map the three-dimensional structure of the nucleon – both in spatial co-ordinates (generalized parton distributions) and transverse momentum dependence.

Studies of transverse nucleon structure will drive the experimental program in the near future, with dedicated running or approved programs at COMPASS, the 12 GeV upgrade of JLab, FNAL and RHIC. These experiments will test our understanding of initial and final state interactions in QCD (through comparison of Sivers and Boer-Mulders observables in Drell-Yan and semi-inclusive deep inelastic scattering). Precise measurements of GPDs and TMDs will test QCD evolution in a regime where transverse structure becomes important. The aim for precise information about quark (and gluon) total and orbital angular momentum in the nucleon is also a driving force for much theoretical work. Highlights include models of transverse spin phenomena, lattice calculations and development of QCD fitting technology to extract GPDs and TMDs from the newly measurable observables.

ACKNOWLEDGMENTS

The research of SDB is supported by the Austrian Science Fund, FWF, through grants P20436 and P23753.

We thank M. Diehl, R. Fatemi, A. Korzenev, S. Kuhn, W. Melnitchouk, B. Pasquini, T.C. Rogers, M. Stratmann, S. Taneja, A. W. Thomas, F. Videbaek, R. Windmolders, A. Zelenski and E. Zemlyanichkina for helpful discussions.

REFERENCES

Aaron, F. D., *et al.* (H1 Collaboration) (2008), Phys. Lett. **B659**, 796

Abbon, P., *et al.* (COMPASS Collaboration) (2007), Nucl. Instrum. Meth. **A577**, 455

Abe, K., *et al.* (E154 Collaboration) (1997), Phys. Rev. Lett. **79**, 26

Abe, K., *et al.* (E143 collaboration) (1998), Phys. Rev. **D58**, 112003

Abe, K., *et al.* (Belle Collaboration) (2005), hep-ex/0507063

Abelev, B. I., *et al.* (STAR Collaboration) (2008a), Phys. Rev. Lett. **101**, 222001

Abelev, B. I., *et al.* (STAR Collaboration) (2008b), Phys. Rev. Lett. **100**, 232003

Abelev, B. I., *et al.* (STAR Collaboration) (2009), Phys. Rev. **D80**, 111108

Ackermann, K. H., *et al.* (STAR Collaboration) (2003), Nucl. Instrum. Meth. **A499**, 624

Ackerstaff, K., *et al.* (HERMES Collaboration) (1999a), Phys. Rev. Lett. **82**, 1164

Ackerstaff, K., *et al.* (HERMES Collaboration) (1999b), Phys. Lett. **B464**, 123

Adamczyk, L., *et al.* (STAR Collaboration) (2012a), arXiv:1205.2735 [nucl-ex]

Adamczyk, L., *et al.* (STAR Collaboration) (2012b), arXiv:1206.1928 [nucl-ex]

Adamczyk, L., *et al.* (STAR Collaboration) (2012c), arXiv:1205.6826 [nucl-ex]

Adamczyk, M., *et al.* (BRAHMS Collaboration) (2003), Nucl. Instrum. Meth. **A499**, 437

Adams, D., *et al.* (SMC Collaboration) (2000), Nucl. Instrum. Meth. **A443**, 1

Adams, D. L., *et al.* (FNAL E704 Collaboration) (1991), Phys. Lett. **B264**, 462

Adams, D. L., *et al.* (FNAL E581/704 Collaboration) (1994), Phys. Lett. **B336**, 269

Adams, D. L., *et al.* (FNAL E704 Collaboration) (1996), Phys. Rev. **D53**, 4747

Adare, A., *et al.* (PHENIX Collaboration) (2007), Phys. Rev. **D76**, 051106

Adare, A., *et al.* (PHENIX Collaboration) (2009a), Phys. Rev. **D79**, 012003

Adare, A., *et al.* (PHENIX Collaboration) (2009b), Phys. Rev. Lett. **103**, 012003

Adare, A., *et al.* (PHENIX Collaboration) (2011a), Phys. Rev. **D83**, 032001

Adare, A., *et al.* (PHENIX Collaboration) (2011b), Phys. Rev. Lett. **106**, 062001

Adare, A., *et al.* (PHENIX Collaboration) (2012), arXiv:1202.4020 [hep-ex]

Adcox, K., *et al.* (PHENIX Collaboration) (2003), Nucl. Instrum. Meth. **A499**, 469

Adeva, B., *et al.* (SMC Collaboration) (1993), Phys. Lett. **B302**, 533

Adeva, B., *et al.* (SMC Collaboration) (1994), Nucl. Instrum. Meth. **A343**, 363

Adeva, B., *et al.* (SMC Collaboration) (1996), Phys. Lett. **B369**, 93

Adeva, B., *et al.* (SMC Collaboration) (1998a), Phys. Lett. **B420**, 180

Adeva, B., *et al.* (SMC Collaboration) (1998b), Phys. Rev. **D58**, 112001

Adeva, B., *et al.* (SMC Collaboration) (2004), Phys. Rev. **D70**, 012002

Adolph, C., *et al.* (COMPASS Collaboration) (2012a), arXiv:1205.5121 [hep-ex]

Adolph, C., *et al.* (COMPASS Collaboration) (2012b), arXiv:1205.5122 [hep-ex]

Adolph, C., *et al.* (COMPASS Collaboration) (2012c), arXiv:1202.4064 [hep-ex]

Adolph, C., *et al.* (COMPASS Collaboration) (2012d), Phys. Lett. **B713**, 10

Ageev, E. S., *et al.* (COMPASS Collaboration) (2006), Phys. Lett. **B633**, 25

Ageev, E. S., *et al.* (COMPASS Collaboration) (2007), Nucl. Phys. **B765**, 31

Aggarwal, M. M., *et al.* (STAR Collaboration) (2011), Phys. Rev. Lett. **106**, 062002

Aidala, C., *et al.* (PHENIX Collaboration) (2012), arXiv:1207.6378 [nucl-ex]

Airapetian, A., *et al.* (HERMES Collaboration) (2000a), Phys. Rev. Lett. **84**, 2584

Airapetian, A., *et al.* (HERMES Collaboration) (2000b), Phys. Rev. Lett. **84**, 4047

Airapetian, A., *et al.* (HERMES Collaboration) (2001), Phys. Rev. **D64**, 097101

Airapetian, A., *et al.* (HERMES Collaboration) (2003), Phys. Lett. **B562**, 182

Airapetian, A., *et al.* (HERMES Collaboration) (2004), Phys. Rev. Lett. **92**, 012005

Airapetian, A., *et al.* (HERMES Collaboration) (2005a), Phys. Rev. **D71**, 012003

Airapetian, A., *et al.* (HERMES Collaboration) (2005b), Phys. Rev. Lett. **94**, 012002

Airapetian, A., *et al.* (HERMES Collaboration) (2005c), Nucl. Instrum. Meth. **A540**, 68

Airapetian, A., *et al.* (HERMES Collaboration) (2007a), Phys. Rev. **D75**, 012007

Airapetian, A., *et al.* (HERMES Collaboration) (2007b), Phys. Rev. **D75**, 011103

Airapetian, A., *et al.* (HERMES Collaboration) (2008a), JHEP **0806**, 017

Airapetian, A., *et al.* (HERMES Collaboration) (2008b), JHEP **0806**, 066

Airapetian, A., *et al.* (HERMES Collaboration) (2008c), Phys. Lett. **B666**, 446

Airapetian, A., *et al.* (HERMES Collaboration) (2009a), Phys. Lett. **B679**, 100

Airapetian, A., *et al.* (HERMES Collaboration) (2009b), Phys. Rev. Lett. **103**, 152002

Airapetian, A., *et al.* (HERMES Collaboration) (2009c), JHEP **0911**, 083

Airapetian, A., *et al.* (HERMES Collaboration) (2010a), Phys. Lett. **B693**, 11

Airapetian, A., *et al.* (HERMES Collaboration) (2010b), JHEP **1006**, 019

Airapetian, A., *et al.* (HERMES Collaboration) (2010c), JHEP **1008**, 130

Airapetian, A., *et al.* (HERMES Collaboration) (2010d), Nucl. Phys. **B829**, 1

Airapetian, A., *et al.* (HERMES Collaboration) (2011a), Nucl. Phys. **B842**, 265

Airapetian, A., *et al.* (HERMES Collaboration) (2011b), Phys. Lett. **B704**, 15

Airapetian, A., *et al.* (HERMES Collaboration) (2012a), arXiv:1204.4161 [hep-ex]

Airapetian, A., *et al.* (HERMES Collaboration) (2012b), JHEP **1207**, 032

Airapetian, A., *et al.* (HERMES Collaboration) (2012c), arXiv:1206.5683 [hep-ex]

Alcorn, J., *et al.* (JLab Hall A Collaboration) (2004), Nucl. Instrum. Meth. **A522**, 294

Alekseev, I., *et al.* (2003), Nucl. Instrum. Meth. **A499**, 392

Alekseev, M., *et al.* (COMPASS Collaboration) (2009a), Phys. Lett. **B673**, 127

Alekseev, M., *et al.* (COMPASS Collaboration) (2009b), Phys. Lett. **B680**, 217

Alekseev, M., *et al.* (COMPASS Collaboration) (2009c), Phys. Lett. **B676**, 31

Alekseev, M. G., *et al.* (COMPASS Collaboration) (2010a), Eur.Phys.J. **C70**, 39, arXiv:1007.1562 [hep-ex]

Alekseev, M. G., *et al.* (COMPASS Collaboration) (2010b), Phys. Lett. **B692**, 240

Alekseev, M. G., *et al.* (COMPASS Collaboration) (2010c), Phys. Lett. **B693**, 227

Alekseev, M. G., *et al.* (COMPASS Collaboration) (2010d), Phys. Lett. **B690**, 466

Alexakhin, V. Y., *et al.* (COMPASS Collaboration) (2007), Phys. Lett. **B647**, 8

Alguard, M. J., *et al.* (1976), Phys. Rev. Lett. **37**, 1261

Alguard, M. J., *et al.* (1978), Phys. Rev. Lett. **41**, 70

Allgower, C. E., *et al.* (2002), Phys. Rev. **D65**, 092008

Altarelli, G., R. D. Ball, S. Forte, and G. Ridolfi (1997), Nucl. Phys. **B496**, 337

Altarelli, G., R. D. Ball, S. Forte, and G. Ridolfi (1998), Acta Phys. Polon. **B29**, 1145

Altarelli, G., and G. Parisi (1977), Nucl. Phys. **B126**, 298

Altarelli, G., and G. G. Ross (1988), Phys. Lett. **B212**, 391

Anselmino, M., M. Boglione, U. D'Alesio, A. Kotzinian, S. Melis, *et al.* (2009a), Eur. Phys. J. **A39**, 89

Anselmino, M., M. Boglione, U. D'Alesio, A. Kotzinian, F. Murgia, *et al.* (2005), Phys. Rev. **D71**, 074006

Anselmino, M., M. Boglione, U. D'Alesio, A. Kotzinian, F. Murgia, *et al.* (2007a), Phys. Rev. **D75**, 054032

Anselmino, M., M. Boglione, U. D'Alesio, A. Kotzinian, F. Murgia, *et al.* (2009b), Nucl. Phys. Proc. Suppl. **191**, 98

Anselmino, M., M. Boglione, U. D'Alesio, S. Melis, F. Murgia, *et al.* (2011), arXiv:1107.4446 [hep-ph]

Anselmino, M., M. Boglione, and S. Melis (2012), arXiv:1204.1239 [hep-ph]

Anselmino, M., M. Boglione, A. Prokudin, and C. Turk (2007b), Eur. Phys. J. **A31**, 373

Anselmino, M., A. Efremov, and E. Leader (1995), Phys. Rept. **261**, 1

Anthony, P. L., *et al.* (E142 Collaboration) (1996), Phys. Rev. **D54**, 6620

Anthony, P. L., *et al.* (E155 Collaboration) (1999), Phys. Lett. **B463**, 339

Anthony, P. L., *et al.* (E155 Collaboration) (2000), Phys. Lett. **B493**, 19

Anthony, P. L., *et al.* (E155 Collaboration) (2003), Phys. Lett. **B553**, 18

Antille, J., *et al.* (1980), Phys. Lett. **B94**, 523

Apokin, V. D., *et al.* (1990), Phys. Lett. **B243**, 461

Arsene, I., *et al.* (BRAHMS Collaboration) (2008), Phys. Rev. Lett. **101**, 042001

Artru, X., and M. Mekhfi (1990), Z. Phys. **C45**, 669

Aschenauer, E. C., R. Sassot, and M. Stratmann (2012), arXiv:1206.6014 [hep-ph]

Ashman, J., *et al.* (EMC Collaboration) (1988), Phys. Lett.

B206, 364

Ashman, J., *et al.* (EMC Collaboration) (1989), Nucl. Phys. **B328**, 1

Avakian, H., S. J. Brodsky, A. Deur, and F. Yuan (2007), Phys. Rev. Lett. **99**, 082001

Avakian, H., A. V. Efremov, P. Schweitzer, O. Teryaev, F. Yuan, *et al.* (2009), Mod. Phys. Lett. **A24**, 2995

Avakian, H., *et al.* (CLAS Collaboration) (2010), Phys. Rev. Lett. **105**, 262002

Aybat, S. M., J. C. Collins, J.-W. Qiu, and T. C. Rogers (2012), Phys. Rev. **D85**, 034043

Aybat, S. M., A. Prokudin, and T. C. Rogers (2011), arXiv:1112.4423 [hep-ph]

Aybat, S. M., and T. C. Rogers (2011a), arXiv:1107.3973 [hep-ph]

Aybat, S. M., and T. C. Rogers (2011b), Phys. Rev. **D83**, 114042

Bacchetta, A. (2012), Nuovo Cim. **C035N2**, 19

Bacchetta, A., A. Courtoy, and M. Radici (2011), Phys. Rev. Lett. **107**, 012001

Bacchetta, A., U. D'Alesio, M. Diehl, and C. A. Miller (2004), Phys. Rev. **D70**, 117504

Bacchetta, A., and M. Radici (2011), Phys. Rev. Lett. **107**, 212001

Bacchetta, A., *et al.* (2007), JHEP **02**, 093

Bakker, B. L. G., E. Leader, and T. L. Trueman (2004), Phys. Rev. **D70**, 114001

Bali, G. S., *et al.* (QCDSF Collaboration) (2012), Phys. Rev. Lett. **108**, 222001

Ball, R. D., L. Del Debbio, S. Forte, A. Guffanti, J. I. Latorre, *et al.* (2010), Nucl. Phys. **B838**, 136

Ball, R. D., S. Forte, and G. Ridolfi (1996), Phys. Lett. **B378**, 255

Ball, R. D., *et al.* (NNPDF Collaboration) (2012), Nucl. Phys. **B855**, 153

Barber, D. P., M. Boge, H. D. Bremer, R. Brinkmann, E. Gianfelice-Wendt, *et al.* (1994), Nucl. Instrum. Meth. **A338**, 166

Barber, D. P., H. D. Bremer, M. Boge, R. Brinkmann, W. Bruckner, *et al.* (1993), Nucl. Instrum. Meth. **A329**, 79

Barone, V., F. Bradamante, and A. Martin (2010a), Prog. Part. Nucl. Phys. **65**, 267

Barone, V., A. Drago, and P. G. Ratcliffe (2002), Phys. Rept. **359**, 1

Barone, V., S. Melis, and A. Prokudin (2010b), Phys. Rev. **D81**, 114026

Bass, S. D. (1999a), Eur. Phys. J. **A5**, 17

Bass, S. D. (1999b), Phys. Lett. **B463**, 286

Bass, S. D. (2003), Phys. Rev. **D67**, 097502

Bass, S. D. (2005), Rev. Mod. Phys. **77**, 1257

Bass, S. D. (2007a), Mod. Phys. Lett. **A22**, 1005

Bass, S. D. (2007b), *The Spin structure of the proton* (World Scientific, Singapore)

Bass, S. D., A. Casey, and A. W. Thomas (2011), Phys. Rev. **C83**, 038202

Bass, S. D., R. J. Crewther, F. M. Steffens, and A. W. Thomas (2002), Phys. Rev. **D66**, 031901

Bass, S. D., B. L. Ioffe, N. N. Nikolaev, and A. W. Thomas (1991), J. Moscow. Phys. Soc. **1**, 317

Bass, S. D., and P. V. Landshoff (1994), Phys. Lett. **B336**, 537

Bass, S. D., and A. W. Thomas (1993), J. Phys. G **G19**, 925

Bass, S. D., and A. W. Thomas (2010), Phys. Lett. **B684**, 216

Baum, G., *et al.* (1980), Phys. Rev. Lett. **45**, 2000

Baum, G., *et al.* (1983), Phys. Rev. Lett. **51**, 1135

Bazilevsky, A., *et al.* (2003), AIP Conf. Proc. **675**, 584

Beckmann, M., A. Borissov, S. Brauksiepe, F. Burkart, H. Fischer, *et al.* (2002), Nucl. Instrum. Meth. **A479**, 334

Belitsky, A. V., X. Ji, and F. Yuan (2003), Phys. Rev. Lett. **91**, 092003

Belitsky, A. V., D. Mueller, and A. Kirchner (2002), Nucl. Phys. **B629**, 323

Beringer, J., *et al.* (Particle Data Group) (2012), Phys. Rev. D **86**, 010001

Bianconi, A. (2011), arXiv:1109.0688 [hep-ph]

Bianconi, A., S. Boffi, R. Jakob, and M. Radici (2000), Phys. Rev. **D62**, 034008

Bjorken, J. D. (1966), Phys. Rev. **148**, 1467

Bjorken, J. D. (1970), Phys. Rev. **D1**, 1376

Blümlein, J., and H. Böttcher (2010), Nucl. Phys. **B841**, 205

Bodwin, G. T., and J.-W. Qiu (1990), Phys. Rev. **D41**, 2755

Boer, D., and P. J. Mulders (1998), Phys. Rev. **D57**, 5780

Boer, D., *et al.* (2011), arXiv:1108.1713 [nucl-th]

Bourrely, C., J. Soffer, and F. Buccella (2002), Eur. Phys. J. **C23**, 487

Brodsky, S. J., M. Burkardt, and I. Schmidt (1995), Nucl. Phys. **B441**, 197

Brodsky, S. J., J. R. Ellis, and M. Karliner (1988), Phys. Lett. **B206**, 309

Brodsky, S. J., D. S. Hwang, and I. Schmidt (2002a), Phys. Lett. **B530**, 99

Brodsky, S. J., D. S. Hwang, and I. Schmidt (2002b), Nucl. Phys. **B642**, 344

Brommel, D., *et al.* (QCDSF-UKQCD Collaboration) (2007), PoS **LAT2007**, 158

Bunce, G., N. Saito, J. Soffer, and W. Vogelsang (2000), Ann. Rev. Nucl. Part. Sci. **50**, 525

Buon, J., and K. Steffen (1986), Nucl. Instrum. Meth. **A245**, 248

Burkardt, M. (2003), Int. J. Mod. Phys. **A18**, 173

Burkardt, M., C. A. Miller, and W. D. Nowak (2010), Rept. Prog. Phys. **73**, 016201

Burkhardt, H., and W. N. Cottingham (1970), Annals Phys. **56**, 453

Cahn, R. N. (1978), Phys. Lett. **B78**, 269

Cahn, R. N. (1989), Phys. Rev. **D40**, 3107

Camacho, C. M., *et al.* (JLab Hall A DVCS Collaboration) (2006), Phys. Rev. Lett. **97**, 262002

Cao, F.-G., and A. I. Signal (2001), Eur. Phys. J. **C21**, 105

Carlitz, R. D., J. C. Collins, and A. H. Mueller (1988), Phys. Lett. **B214**, 229

Chekanov, S., *et al.* (ZEUS Collaboration) (2009), JHEP **0905**, 108

Chen, P., and X. Ji (2008), Phys. Lett. **B660**, 193

Chen, S., *et al.* (CLAS Collaboration) (2006), Phys. Rev. Lett. **97**, 072002

Chen, X.-S., X.-F. Lu, W.-M. Sun, F. Wang, and T. Goldman (2008), Phys. Rev. Lett. **100**, 232002

Cheng, H.-Y. (1996), Int. J. Mod. Phys. **A11**, 5109

Close, F. E. (1979), *An Introduction to Quarks and Partons* (Academic, New York)

Close, F. E., and R. G. Milner (1991), Phys. Rev. **D44**, 3691

Close, F. E., and R. G. Roberts (1993), Phys. Lett. **B316**, 165

Close, F. E., and R. G. Roberts (1994), Phys. Lett. **B336**, 257

Close, F. E., and A. W. Thomas (1988),

Phys. Lett. **B212**, 227
Collins, J. (2011), *Foundations of perturbative QCD* (Cambridge University Press, Cambridge, England)
Collins, J. C. (1993), Nucl. Phys. **B396**, 161
Collins, J. C. (2002), Phys. Lett. **B536**, 43
Collins, J. C., S. F. Heppelmann, and G. A. Ladinsky (1994), Nucl. Phys. **B420**, 565
Conway, J. S., *et al.* (FNAL E615 Collaboration) (1989), Phys. Rev. **D39**, 92
Courant, E. D., *et al.* (SPIN-Fermilab Collaboration) (2011), arXiv:1110.3042 [physics.acc-ph]
Courtoy, A., A. Bacchetta, and M. Radici (2012a), arXiv:1206.1836 [hep-ph]
Courtoy, A., A. Bacchetta, M. Radici, and A. Bianconi (2012b), Phys. Rev. **D85**, 114023
Crewther, R. J. (1978), Acta Phys. Austriaca Suppl. **19**, 47
Cudell, J. R., A. Donnachie, and P. V. Landshoff (1999), Phys. Lett. **B448**, 281
Derbenev, Y. S., *et al.* (1978), Part. Accel. **8**, 115
Dharmawardane, K., *et al.* (CLAS Collaboration) (2006), Phys. Lett. **B641**, 11
Diehl, M. (2002), Eur. Phys. J. **C25**, 223
Diehl, M. (2003), Phys. Rept. **388**, 41
Diehl, M., and S. Sapeta (2005), Eur. Phys. J. **C41**, 515
Djawotho, P. (STAR Collaboration) (2011), arXiv:1106.5769 [nucl-ex]
Donnachie, A., and P. V. Landshoff (2011), arXiv:1112.2485 [hep-ph]
Dragoset, W. H., *et al.* (1978), Phys. Rev. **D18**, 3939
Dudek, J., *et al.* (2012), arXiv:1208.1244 [hep-ex]
Efremov, A. V., K. Goeke, and P. Schweitzer (2006), Phys. Rev. **D73**, 094025
Efremov, A. V., and O. V. Teryaev (1982), Sov. J. Nucl. Phys. **36**, 140
Efremov, A. V., and O. V. Teryaev (1985), Phys. Lett. **B150**, 383
Efremov, A. V., and O. V. Teryaev (1988), JINR Report No. E2-88-287
Ellis, J. R., and R. L. Jaffe (1974), Phys. Rev. **D9**, 1444
Ellis, J. R., and M. Karliner (1995), arXiv:hep-ph/9601280 [hep-ph]
Falciano, S., *et al.* (NA10 Collaboration) (1986), Z. Phys. **C31**, 513
Filippone, B. W., and X.-D. Ji (2001), Adv. Nucl. Phys. **26**, 1
de Florian, D., R. Sassot, and M. Stratmann (2007), Phys. Rev. **D75**, 114010
de Florian, D., R. Sassot, M. Stratmann, and W. Vogelsang (2008), Phys. Rev. Lett. **101**, 072001
de Florian, D., R. Sassot, M. Stratmann, and W. Vogelsang (2009), Phys. Rev. **D80**, 034030
Franco, C. (COMPASS Collaboration) (2010), PoS **DIS2010**, 225
Fritzsch, H. (1989), Phys. Lett. **B229**, 122
Garzia, I. (BaBar Collaboration) (2012), arXiv:1201.4678 [hep-ex]
Gautheron, F., *et al.* (COMPASS Collaboration) (2010), COMPASS-II Proposal, CERN-SPSLC-2010-14, CERN-SPSLC-P-340
Gayou, O., *et al.* (Jefferson Lab Hall A Collaboration) (2002), Phys. Rev. Lett. **88**, 092301
Girod, F. X., *et al.* (CLAS Collaboration) (2008), Phys. Rev. Lett. **100**, 162002
Glück, M., E. Reya, M. Stratmann, and W. Vogelsang (2001), Phys. Rev. **D63**, 094005
Göckeler, M., *et al.* (QCDSF Collaboration, UKQCD Collaboration) (2007), Phys. Rev. Lett. **98**, 222001
Goeke, K., M. V. Polyakov, and M. Vanderhaeghen (2001), Prog. Part. Nucl. Phys. **47**, 401
Goldstein, G. R., J. O. Hernandez, and S. Liuti (2011), Phys. Rev. **D84**, 034007
Goloskokov, S. V., and P. Kroll (2008), Eur. Phys. J. **C53**, 367
Goloskokov, S. V., and P. Kroll (2009), Eur. Phys. J. **C59**, 809
Guanziroli, M., *et al.* (NA10 Collaboration) (1988), Z. Phys. **C37**, 545
Guidal, M. (2010), Phys. Lett. **B693**, 17
Hägler, P., B. U. Musch, J. W. Negele, and A. Schäfer (2009), Europhys. Lett. **88**, 61001
Hägler, P., *et al.* (LHPC Collaboration) (2008), Phys. Rev. **D77**, 094502
Hautmann, F., M. Hentschinski, and H. Jung (2012), arXiv:1205.6358 [hep-ph]
Hirai, M., and S. Kumano (AAC Collaboration) (2009), Nucl. Phys. **B813**, 106
't Hooft, G. (1986), Phys. Rept. **142**, 357
't Hooft, G., and M. J. G. Veltman (1972), Nucl. Phys. **B44**, 189
Jaffe, R. L. (1990), Comments Nucl. Part. Phys. **19**, 239
Jaffe, R. L. (2001), AIP Conf. Proc. **588**, 54
Jaffe, R. L., and X.-D. Ji (1992), Nucl. Phys. **B375**, 527
Jaffe, R. L., and A. Manohar (1990), Nucl. Phys. **B337**, 509
Ji, X., J.-W. Qiu, W. Vogelsang, and F. Yuan (2006), Phys. Rev. Lett. **97**, 082002
Ji, X.-D. (1997a), Phys. Rev. **D55**, 7114
Ji, X.-D. (1997b), Phys. Rev. Lett. **78**, 610
Ji, X.-D. (1998), J. Phys. G **G24**, 1181
Ji, X.-D., J. Tang, and P. Hoodbhoy (1996), Phys. Rev. Lett. **76**, 740
Jones, M. K., *et al.* (JLab Hall A Collaboration) (2000), Phys. Rev. Lett. **84**, 1398
Kang, Z.-B., and A. Prokudin (2012), Phys. Rev. **D85**, 074008
Kaplan, D. B., and A. Manohar (1988), Nucl. Phys. **B310**, 527
Kiryluk, J. (STAR Collaboration) (2005), , 718arXiv:hep-ex/0501072 [hep-ex]
Klem, R. D., J. E. Bowers, H. W. Courant, H. Kagan, M. L. Marshak, *et al.* (1976), Phys. Rev. Lett. **36**, 929
Kodaira, J. (1980), Nucl. Phys. **B165**, 129
Koster, J. (2012), Nuovo Cim. **C035N2**, 187
Kotzinian, A. (COMPASS Collaboration) (2007), arXiv:0705.2402 [hep-ex]
Kuhn, S. E., J.-P. Chen, and E. Leader (2009), Prog. Part. Nucl. Phys. **63**, 1
Kulagin, S. A., and W. Melnitchouk (2008a), Phys. Rev. **C77**, 015210
Kulagin, S. A., and W. Melnitchouk (2008b), Phys. Rev. **C78**, 065203
Kumano, S., and M. Miyama (2002), Phys. Rev. **D65**, 034012
Kumericki, K., and D. Mueller (2010), Nucl. Phys. **B841**, 1
Lampe, B., and E. Reya (2000), Phys. Rept. **332**, 1
Larin, S. A., T. van Ritbergen, and J. A. M. Vermaseren (1997), Phys. Lett. **B404**, 153
Leader, E. (2011), Phys. Rev. **D83**, 096012
Leader, E., A. V. Sidorov, and D. B. Stamenov (1998),

Phys. Rev. **D58**, 114028

Leader, E., A. V. Sidorov, and D. B. Stamenov (2006), Phys. Rev. **D73**, 034023

Leader, E., A. V. Sidorov, and D. B. Stamenov (2010), Phys. Rev. **D82**, 114018

Lepage, G. P., and S. J. Brodsky (1980), Phys. Rev. **D22**, 2157

Lorce, C., and B. Pasquini (2011), Phys. Rev. **D84**, 034039

Lu, Z., and I. Schmidt (2010), Phys. Rev. **D81**, 034023

MacKay, W. W., *et al.* (2003) (IEEE) p. 1697, proc. of the 2003 Part. Acc. Conf.

Manion, A. (PHENIX Collaboration) (2011), J. Phys. Conf. Ser. **295**, 012070

Mattingly, A. C., and P. M. Stevenson (1994), Phys. Rev. **D49**, 437

Mazouz, M., *et al.* (JLab Hall A Collaboration) (2007), Phys. Rev. Lett. **99**, 242501

Mecking, B. A., *et al.* (CLAS Collaboration) (2003), Nucl. Instrum. Meth. **A503**, 513

Mertig, R., and W. L. van Neerven (1996), Z. Phys. **C70**, 637

Mueller, D., D. Robaschik, B. Geyer, F. Dittes, and J. Horejsi (1994), Fortsch. Phys. **42**, 101

Mulders, P. J., and R. D. Tangerman (1996), Nucl. Phys. **B461**, 197

Musch, B. U., P. Hägler, M. Engelhardt, J. W. Negele, and A. Schäfer (2012), Phys. Rev. **D85**, 094510

Myhrer, F., and A. W. Thomas (1988), Phys. Rev. **D38**, 1633

Myhrer, F., and A. W. Thomas (2008), Phys. Lett. **B663**, 302

Myhrer, F., and A. W. Thomas (2010), J. Phys. G **G37**, 023101

Nakagawa, I., *et al.* (2008), AIP Conf. Proc. **980**, 380

Narison, S., G. M. Shore, and G. Veneziano (1995), Nucl. Phys. **B433**, 209

Nocera, E. R., S. Forte, G. Ridolfi, and J. Rojo (2012), arXiv:1206.0201 [hep-ph]

Okada, H., I. G. Alekseev, A. Bravar, G. Bunce, S. Dhawan, *et al.* (2006), Phys. Lett. **B638**, 450

Osipenko, M., *et al.* (CLAS Collaboration) (2009), Phys. Rev. **D80**, 032004

Pappalardo, L. L. (2010), Nuovo Cim. **B125N1**, 51

Pappalardo, L. L., and M. Diefenthaler (HERMES Collaboration) (2011), arXiv:1107.4227 [hep-ex]

Parsamyan, B. (2011), J.Phys.Conf.Ser. **295**, 012046

Pasquini, B., and P. Schweitzer (2011), Phys. Rev. **D83**, 114044

Pate, S. F., D. W. McKee, and V. Papavassiliou (2008), Phys. Rev. **C78**, 015207

Peng, J.-C. (2003), Eur. Phys. J. **A18**, 395

Pesaro, G. (COMPASS Collaboration) (2011), J. Phys. Conf. Ser. **295**, 012058

Procureur, S. (COMPASS Collaboration) (2006), arXiv:hep-ex/0605043 [hep-ex]

Qian, X. (JLab Hall A Collaboration) (2012), Mod. Phys. Lett. **A27**, 1230021

Qian, X., *et al.* (JLab Hall A Collaboration) (2011), Phys. Rev. Lett. **107**, 072003

Qiu, J.-W., and G. Sterman (1999), Phys. Rev. **D59**, 014004

Radyushkin, A. V. (1997), Phys. Rev. **D56**, 5524

Ralston, J. P., and D. E. Soper (1979), Nucl. Phys. **B152**, 109

Ratcliffe, P. G. (2004), Czech. J. Phys. **54**, B11

Reimer, P. E. (2007), Eur. Phys. J. **A31**, 593

Roberts, R. G. (1990), *The Structure of the proton: Deep inelastic scattering* (Cambridge University Press, Cambridge, England)

Rogers, T. C., and P. J. Mulders (2010), Phys. Rev. **D81**, 094006

Romalis, M. V., *et al.* (1998), Nucl. Instrum. Meth. **A402**, 260

Saroff, S., *et al.* (1990), Phys. Rev. Lett. **64**, 995

Sbrizzai, G. (COMPASS Collaboration) (2011), J.Phys.Conf.Ser. **295**, 012043

Schreiber, A. W., and A. W. Thomas (1988), Phys. Lett. **B215**, 141

Seidl, R., *et al.* (Belle Collaboration) (2008), Phys. Rev. **D78**, 032011

Shore, G. M. (1998), arXiv:hep-ph/9812355 [hep-ph]

Shore, G. M. (2008), Lect. Notes Phys. **737**, 235

Shore, G. M., and B. E. White (2000), Nucl. Phys. **B581**, 409

Sivers, D. W. (1990), Phys. Rev. **D41**, 83

Soffer, J. (1995), Phys. Rev. Lett. **74**, 1292

Sokolov, A. A., and I. M. Ternov (1964), Sov. Phys. Dokl. **8**, 1203

Steffens, F. M., H. Holtmann, and A. W. Thomas (1995), Phys. Lett. **B358**, 139

Stepanyan, S., *et al.* (CLAS Collaboration) (2001), Phys. Rev. Lett. **87**, 182002

Thomas, A. W. (2008), Phys. Rev. Lett. **101**, 102003

Thomas, A. W., A. Casey, and H. H. Matevosyan (2010), Int. J. Mod. Phys. **A25**, 4149

Towell, R. S., *et al.* (FNAL E866/NuSea Collaboration) (2001), Phys. Rev. **D64**, 052002

Tsushima, K., T. Yamaguchi, Y. Kohyama, and K. Kubodera (1988), Nucl. Phys. **A489**, 557

Vanderhaeghen, M., P. A. M. Guichon, and M. Guidal (1999), Phys. Rev. **D60**, 094017

Vogelsang, W. (1996), Phys. Rev. **D54**, 2023

Vossen, A., *et al.* (Belle Collaboration) (2011), Phys. Rev. Lett. **107**, 072004

Wakamatsu, M. (2003), Phys. Rev. **D67**, 034005

Wakamatsu, M. (2007), Phys. Lett. **B646**, 24

Wakamatsu, M. (2010), Phys. Rev. **D81**, 114010

Walker, A. (2011), arXiv:1107.0917 [hep-ex]

Windmolders, R. (2002), arXiv:hep-ph/0211350 [hep-ph]

Zelenski, A., J. G. Alessi, A. Kponou, and D. Raparia (2008), Conf. Proc. **C0806233**, TUOBM03

Zelenski, A., *et al.* (2002), Rev. Sci. Instrum. **73**, 888

Zelenski, A., *et al.* (2005), Nucl. Instrum. Meth. **A536**, 248

Zhang, B., Z. Lu, B.-Q. Ma, and I. Schmidt (2008), Phys. Rev. **D77**, 054011

Zheng, X., *et al.* (JLab Hall A Collaboration) (2004), Phys. Rev. Lett. **92**, 012004

Zhu, L. Y., *et al.* (FNAL-E866/NuSea Collaboration) (2007), Phys. Rev. Lett. **99**, 082301

Zhu, L. Y., *et al.* (FNAL E866/NuSea Collaboration) (2009), Phys. Rev. Lett. **102**, 182001

Zijlstra, E. B., and W. L. van Neerven (1994), Nucl. Phys. **B417**, 61